

## **Request to admit annex with an unapproved format**



**Reason for request:** I need to attach four scientific papers to my thesis. Three of them have been published in peer-reviewed journals and the PDF format provided by the journals cannot be changed to the approved PDF/A 1a. Therefore, it is not possible to upload an annex with the approved format.

**Other information:** The three published scientific papers have OPEN ACCESS and their publication within the thesis should not be a problem. The fourth paper has been submitted but not published yet. Nonetheless, we are planning to publish it in an OPEN ACCESS way as well. The fourth paper will be published before the thesis.

REPORT

 OPEN ACCESS

## Regulation of 4E-BP1 activity in the mammalian oocyte

Denisa Jansova<sup>a</sup>, Marketa Koncicka<sup>a</sup>, Anna Tetkova<sup>a</sup>, Renata Cerna<sup>a</sup>, Radek Malik <sup>b</sup>, Edgar del Llano<sup>a</sup>, Michal Kubelka <sup>a</sup>, and Andrej Susor<sup>a</sup>

<sup>a</sup>Institute of Animal Physiology and Genetics, ASC, Libečov, Czech Republic; <sup>b</sup>Institute of Molecular Genetics, ASCR, Prague, Czech Republic

### ABSTRACT

Fully grown mammalian oocytes utilize transcripts synthesized and stored during earlier development. RNA localization followed by a local translation is a mechanism responsible for the regulation of spatial and temporal gene expression. Here we show that the mouse oocyte contains 3 forms of cap-dependent translational repressor expressed on the mRNA level: 4E-BP1, 4E-BP2 and 4E-BP3. However, only 4E-BP1 is present as a protein in oocytes, it becomes inactivated by phosphorylation after nuclear envelope breakdown and as such it promotes cap-dependent translation after NEBD. Phosphorylation of 4E-BP1 can be seen in the oocytes after resumption of meiosis but it is not detected in the surrounding cumulus cells, indicating that 4E-BP1 promotes translation at a specific cell cycle stage. Our immunofluorescence analyses of 4E-BP1 in oocytes during meiosis I showed an even localization of global 4E-BP1, as well as of its 4E-BP1 (Thr37/46) phosphorylated form. On the other hand, 4E-BP1 phosphorylated on Ser65 is localized at the spindle poles, and 4E-BP1 phosphorylated on Thr70 localizes on the spindle. We further show that the main positive regulators of 4E-BP1 phosphorylation after NEBD are mTOR and CDK1 kinases, but not PLK1 kinase. CDK1 exerts its activity toward 4E-BP1 phosphorylation via phosphorylation and activation of mTOR. Moreover, both CDK1 and phosphorylated mTOR co-localize with 4E-BP1 phosphorylated on Thr70 on the spindle at the onset of meiotic resumption. Expression of the dominant negative 4E-BP1 mutant adversely affects translation and results in spindle abnormality. Taken together, our results show that the phosphorylation of 4E-BP1 promotes translation at the onset of meiosis to support the spindle assembly and suggest an important role of CDK1 and mTOR kinases in this process. We also show that the mTOR regulatory pathway is present in human oocytes and is likely to function in a similar way as in mouse oocytes.

### ARTICLE HISTORY

Received 10 October 2016  
Revised 31 January 2017  
Accepted 8 February 2017

### KEYWORDS

4E-BP1; CDK1; cumulus cells; kinase; mTOR; mRNA; meiosis; oocyte; spindle; translation

### Introduction

Translational control of specific mRNAs is a widespread mechanism of gene regulation and contributes to diverse biologic processes in many cell types. During the meiotic division of mammalian oocytes (so called oocyte maturation) protein synthesis plays an important role in controlling the progress of meiosis, since the regulation of gene expression on the level of transcription is ceased. At the onset of the first meiotic division, nuclear envelope breakdown (NEBD; G2/M transition) occurs, chromosomes condense and a bipolar spindle forms from the microtubule organizing centers.<sup>1</sup> During meiosis I, the spindle migrates from the center of the oocyte to the cortex, and the oocyte undergoes an asymmetric division resulting in a large egg competent for fertilization and a relatively small polar body. Proper positioning of the spindle during asymmetric cell division ensures correct partitioning of cellular determinants.<sup>2</sup> How these events are orchestrated in detail remains unclear.


The importance of protein synthesis for meiotic and mitotic progression has been shown previously. Those published results revealed that protein synthesis is not required for NEBD in mouse

oocytes, although the formation of the spindle and progression to metaphase II requires active protein synthesis.<sup>3</sup> In contrast, positive regulators of the cap-dependent translational pathway become activated post NEBD and inactivated after fertilization.<sup>4–9</sup>

Regulation of translation occurs mainly at the initiation step, which was shown to be rate limiting for overall protein synthesis.<sup>10</sup> Protein factors that bind to the cap structure at the 5'UTR (untranslated region) and to the 3'UTR-poly(A) sequence of mRNAs have been identified as being essential for this process. Most of the interactions of these proteins are regulated by phosphorylation.<sup>11,12</sup> The best described protein kinase regulating translation initiation is the mTOR/FRAP kinase, the targets of which are the Eukaryotic initiation factor 4E-binding protein 1 (4E-BP1)<sup>13</sup> and the S6 kinase.<sup>14</sup> Hypo-phosphorylated 4E-BP1 binds eIF4E and in such a way inhibits the formation of a translation initiation complex (eIF4F) at the cap structure. EIF4F contains eIF4E (the cap-binding protein), eIF4G1 (the scaffold protein) and eIF4A (an RNA helicase). This complex is probably critical for the translation of mRNAs with extensive secondary structure in their 5'UTR. Upon resumption of meiosis, 4E-BP1

**CONTACT** Andrej Susor  [susor@iapg.cas.cz](mailto:susor@iapg.cas.cz)  Institute of Animal Physiology and Genetics, ASC, Rumburska 89, Libečov, Czech Republic.

Color versions of one or more of the figures in this article can be found online at [www.tandfonline.com/kccy](http://www.tandfonline.com/kccy).

 Supplemental data for this article can be accessed on the [publisher's website](#).

© 2017 Denisa Jansova, Marketa Koncicka, Anna Tetkova, Renata Cerna, Radek Malik, Edgar del Llano, Michal Kubelka, and Andrej Susor. Published with license by Taylor & Francis. This is an Open Access article distributed under the terms of the Creative Commons Attribution License (<http://creativecommons.org/licenses/by/3.0/>), which permits unrestricted use, distribution, and reproduction in any medium, provided the original work is properly cited. The moral rights of the named author(s) have been asserted.

becomes phosphorylated at several sites resulting in its release from eIF4E, allowing eIF4F formation. Phosphorylation at Ser65 and Thr70 modulates the binding of 4E-BP1 to eIF4E directly. Phosphorylation of these sites depends upon 4E-BP1s C-terminal TOR signaling motif that binds Raptor, a component of the mTORC1. Phosphorylation at Thr37/46, which is known to be mediated by mTOR, is required for the modification of Thr70 and Ser65, reflecting the hierarchical phosphorylation of 4E-BP1,<sup>15</sup> and depends upon 4E-BP1s N-terminal RAIP motif.<sup>16</sup> Phosphorylation of Thr37/46 is profoundly inhibited by starving cells of amino acids, which inactivates mTOR signaling.<sup>17</sup> mTORC1 signaling is activated via phosphatidylinositol 3-kinase and protein kinase B (PKB, also termed AKT) and by the Ras/Raf/ERK pathway.<sup>18</sup> AKT plays a substantial role during the progression of meiosis from GV-stage (germinal vesicle – nucleus in the oocytes) to the MI/MII-stage.<sup>19,20</sup> Involvement of the mTOR/4F axis in translational regulation during mitosis might be used as a model case for the meiotic cell. Increased phosphorylation of 4E-BP1 has been detected during the meiotic progression of mammalian oocytes,<sup>4,21,22</sup> and different phosphorylated forms of 4E-BP1 have been shown to co-localize with the meiotic spindle in mouse oocytes.<sup>9,22</sup> Blocking of 4E-BP1 phosphorylation during maturation has also resulted in the irreversible arrest of metaphase I in bovine oocytes,<sup>23</sup> abnormal formation of MII spindles in mouse oocytes<sup>9</sup> or affected asymmetric division.<sup>24</sup>

The aim of this work was to study the metabolic pathways which are involved in 4E-BP1 phosphorylation during in vitro meiotic maturation of mouse oocytes. We discovered that 4E-BP1 becomes phosphorylated in post-NEBD stage oocytes and this phosphorylation remains constant until the MII stage of oocyte maturation and promotes specific translation, which affects spindle assembly. Furthermore, we have uncovered the involvement of different kinases which are potentially involved in the phosphorylation of 4E-BP1.

## Results

### Only 4E-BP1 is present in the mouse oocyte

In mammals 3 genes code 4E-BP1, 2 and 3.<sup>25</sup> Our first objective was to determine which form is dominant during mouse oocyte meiotic maturation from the GV to MII stage on the mRNA level. Quantitative RT-PCR analysis showed the presence of all 3 forms of *4e-bps* but with a slightly higher abundance of *4e-bp3*. The global amount of the mRNAs for the 3 different *4e-bps* remained constant throughout meiosis from GV to MII oocytes (Fig. 1A).

Next, we analyzed the presence of all 3 isoforms on the protein level. Our WB analyses showed an absence of 4E-BP2 and 4E-BP3 proteins in the oocytes, which is in the contrary to the results obtained from WB analyses of brain lysate (Fig. 1B and C). However, 4E-BP1 was highly abundant in mouse oocytes with an increased mobility shift post-NEBD (Fig. 1B). Our data showed higher presence of the 4E-BP1 protein in the oocytes than in the brain sample (Fig. 1B and C; Supplementary Fig. 1A). WB also showed that whole population of 4E-BP1 in MII stage oocytes is present as the upper (presumably phosphorylated) band. Treatment of MII oocyte lysate with lambda protein phosphatase (LPP) resulted in the disappearance of the

upper band and mobility shift toward lower band, similar pattern to that seen in the GV stage oocytes (Fig. 1D). The experiment in the Fig. 1D shows that mobility shift represents phosphorylation of the 4E-BP1. Moreover, the appearance of mobility shift was confirmed by microinjection of oocytes with RNA coding for 4E-BP1 protein tagged with hemagglutinin (HA). The oocytes were kept in the GV stage or matured for 3 h to NEBD and to MII for 12 h and analyzed by WB, using HA antibody. Our data showed no phosphorylation shift in the GV oocytes, appearance of 2 bands in the NEBD oocytes and whole expressed exogenous HA-4E-BP1 was phosphorylated in the MII stage (Supplementary Fig. 1B).

It is well established that phosphorylation of 4E-BP1 plays an important role in the regulation of cap-dependent translation.<sup>25-30</sup> We thus investigated the localization of 4E-BP1 and its phosphorylated forms (Thr37/46/70 and Ser65) during meiosis I. We analyzed different meiotic stages of maturing oocytes; a germinal vesicle (nucleus is present, prophase I) stage was collected directly post isolation; oocytes underwent NEBD following release from the 3-Isobutyl-1-methylxanthine (IBMX) block, oocytes undergone naturally NEBD within 1 h, a group post-NEBD was collected 3 h post IBMX wash (PIW); a metaphase I (MI) stage was collected 7 h PIW and metaphase II (MII) oocytes were collected 12 h PIW. Cell cycle progression was monitored by timing and by immunocytochemistry (ICC) using DNA staining with DAPI. Pan 4E-BP1 antibody was used to analyze the localization of global 4E-BP1 during GV to MII (Fig. 2A). In GV oocytes global 4E-BP1 was evenly distributed throughout the cytoplasm but with a higher signal visible in the nucleoplasm (Fig. 2A and Supplementary Fig. 3), without staining in the nucleolus (marked by asterisk). In the post-NEBD stages the global 4E-BP1 was also spread evenly with just a slight increase at the spindle. ICC experiments using phospho-specific antibody against the Thr37/46 form showed no signal in the GV and a similar localization was seen as total 4E-BP1 protein in the post-NEBD. Antibody recognizing 4E-BP1 phosphorylated at Ser65 showed an increased fluorescence signal in the vicinity of chromosomes, at the spindle assembly area and later at the spindle poles. The pattern of 4E-BP1 phosphorylation at Thr70 showed significant localization at the newly forming spindle post-NEBD or bipolar spindle at MI and MII, and was also present in the extruded polar body. The phospho-specific antibodies did not show a positive signal in the GV stage, which is in a good agreement with our WB data (Fig. 1B and Supplementary Fig. 1A, B). Moreover, double staining of 4E-BP1 phosphorylated at Ser65 or Thr70 with marker of microtubule organizing centers  $\gamma$ -tubulin showed significant enrichment of the 4E-BP1(Ser65) signal in the region with stained  $\gamma$ -tubulin; however, 4E-BP1(Thr70) was distributed along the whole spindle (Fig. 2B).

As 4E-BP1 phosphorylated at the Thr70 was found to be exclusively localized at the forming spindle, we therefore speculated whether this localization was tubulin-dependent. We disrupted the spindle by treatment with 1  $\mu$ M Nocodazole (Noco) for 1h post-NEBD. Although the dissolved spindle changed the 4E-BP1 (Thr70) pattern, the fluorescence signal still persisted at the chromosomal area (Fig. 2C).

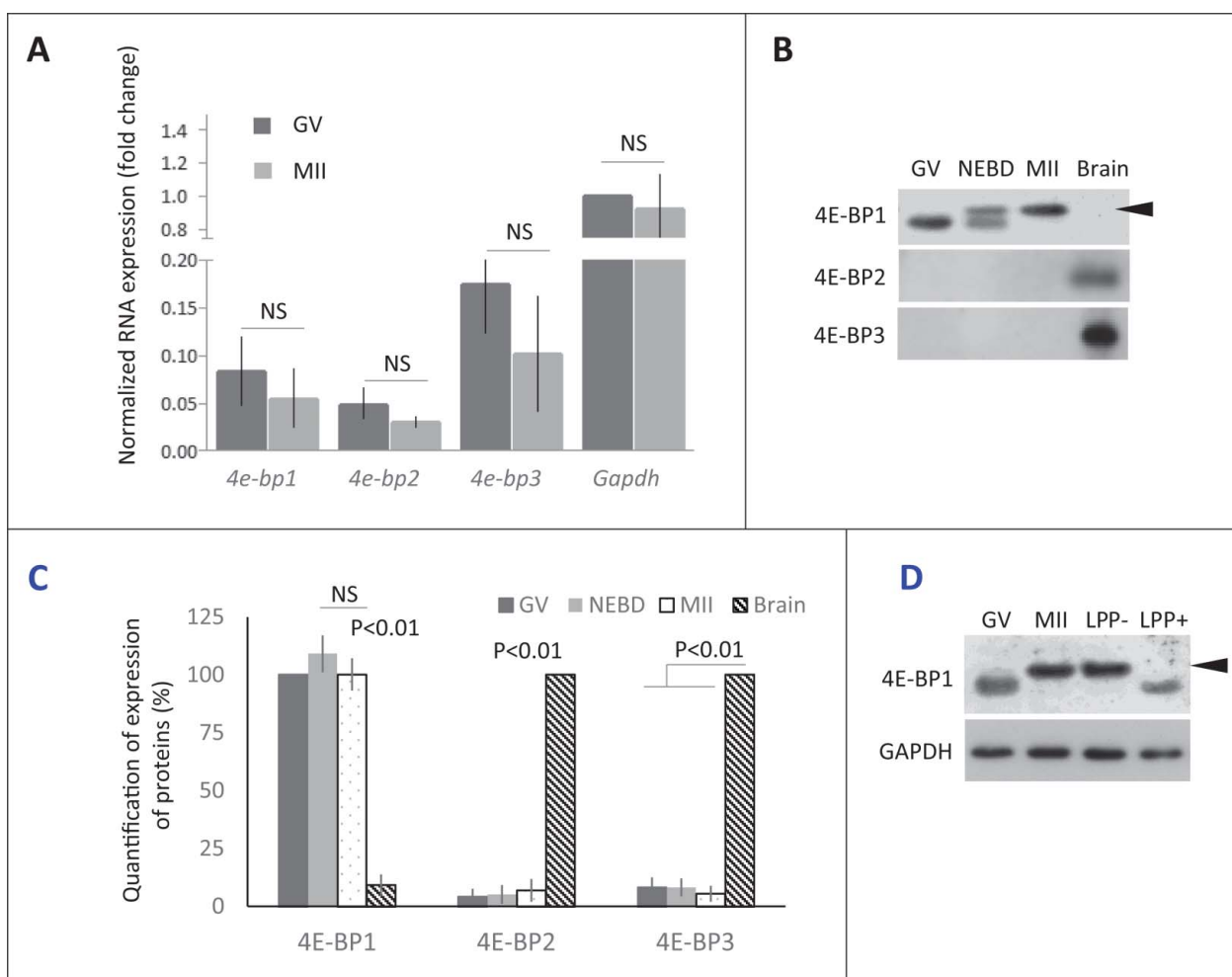


**Figure 1.** Expression of 4E-BP forms in mouse oocytes. (A) Quantitative RT-PCR analysis shows all 3 forms of *4e-bp* mRNA, which are stable during oocyte maturation (NS = non-significant,  $n \geq 3$ ). Results were normalized to the relative internal standard *Gapdh* mRNA in GV. (B) Immunoblotting shows presence of only 4E-BP1 form on the protein level. Both 4E-BP2 and 4E-BP3 are absent in the oocytes, although they are present in the brain. Expression of the 4E-BP1 in the brain sample is significantly lower in comparison with oocytes (See Fig. S1A). 4E-BP1 displays visible phosphorylation shift (arrowhead) post NEBD (a typical experiment from at least 3 replicates is shown). (C) Quantification of protein expression of the 4E-BP1–3 in the oocytes during maturation and brain samples. Data are presented as mean  $\pm$  SD, Student's t-test. (D) Treatment of the lysate from MII oocytes with Lambda Protein Phosphatase (LPP+) suppressed mobility shift of the 4E-BP1 on the WB. Arrowhead points to phospho 4E-BP1 form. See Figure S1A and B.

### Activity of mTOR is increased in the human oocyte post-NEBD

As the mouse oocyte is a model organism for the study of human oocytes, we speculated whether mTOR(Ser2448) in human oocytes would be activated similarly as in the mouse oocyte, with a comparable localization pattern. ICC staining of human oocytes in GV, NEBD and MII stages showed that there was no signal for phospho-specific antibody against mTOR (Ser2448) in the GV stage (Supplementary Fig. 3) but increased fluorescence was visible in the NEBD and MII stage. The MII oocyte produced normally formed spindle stained with anti-tubulin antibody with a strong signal for mid-body structure positive for mTOR(Ser2448) (Supplementary Fig. 3).

### 4E-BP1 phosphorylation requires mTOR and CDK1 activity

The timing of increased phosphorylation of 4E-BP1 positively correlates with increased cap-dependent translation after

NEBD in the mouse, porcine and bovine oocyte.<sup>5,9,21</sup> Also, the timing of the increased phosphorylation of mTOR after NEBD.<sup>9,31</sup> suggests a potential role for mTOR in 4E-BP1 phosphorylation during mammalian meiosis.

Previously we have shown that suppression of mTOR activity using 100 nM mTOR inhibitor Rapamycin (Rapa) significantly represses phosphorylation of 4E-BP1, however, it does not prevent the oocytes to reach MII stage.<sup>18</sup> Phosphorylation of 4E-BP1 by CDK1 kinase<sup>32–34</sup> has been also described in other systems, in which it becomes activated at the onset of both mitosis,<sup>34,35</sup> and meiosis.<sup>36</sup> In mammalian oocytes, CDK1 activity is essential for the major morphological events occurring during meiotic maturation (including NEBD, chromosome congression and condensation, formation of the meiotic spindle) and its inhibition in the beginning of maturation results in the complete block of meiosis with oocytes arresting in the GV stage.<sup>37</sup> We therefore investigated the ability of the CDK1 inhibitor 10  $\mu$ M Roscovitine (Rosco), as well as 100 nM mTOR inhibitor Rapa, to suppress phosphorylation of 4E-BP1 post

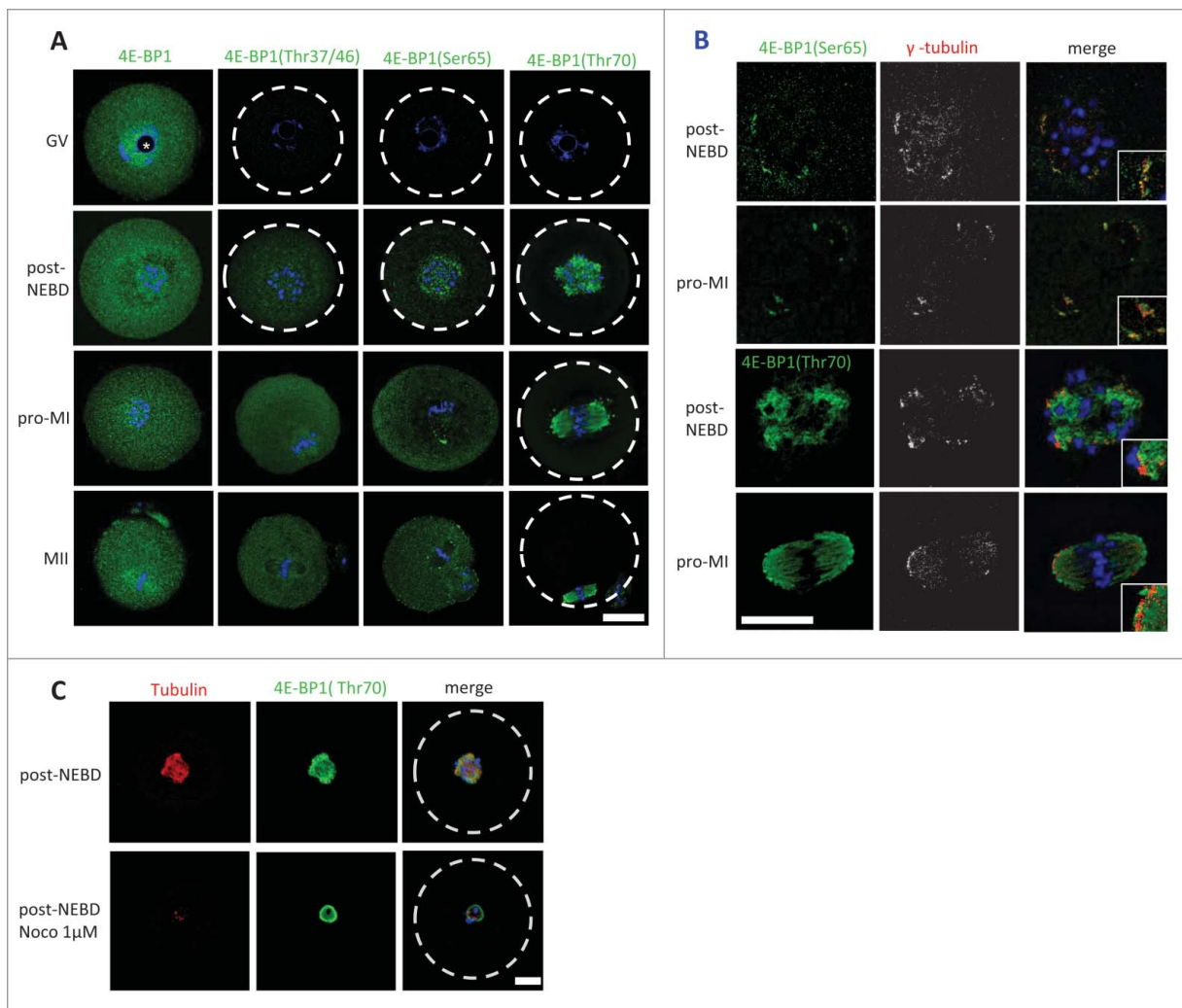


**Figure 2.** Localization of 4E-BP1 and its phosphorylated forms in the oocytes. (A) Confocal images of different meiotic stages GV (germinal vesicle), post-NEBD (3 h post IBMX wash, PIW), pro-MI (7 h PIW) and MII (12 h) stained with phospho-specific antibody (green) and DAPI (blue), white line indicates oocyte edge. Scale bar = 25  $\mu$ m. Nucleolus is depicted by asterisk, from at least 3 replicates and  $n \geq 30$ . (B) Marker of the microtubule-organizing centers, gamma tubulin (pseudo-colored and red) co-localizes with 4E-BP1 (Ser65) and (Thr70). Scale bar = 25  $\mu$ m,  $n = 10$ . Enlarged detail in the right bottom corner. (C) Confocal images of control oocytes and oocytes treated with 1  $\mu$ M Noco for 1 h in the post-NEBD stage ( $n \geq 28$ ), tubulin (red), 4E-BP1 (green) and DNA (blue). Scale bar = 20  $\mu$ m.

NEBD. Rapa or Rosco were added to the culture media 1h PIW. Similarly to Rapa, the inhibition of CDK1 also showed significant suppression of phosphorylation shift (Fig. 3A). Next, based on its activity described in mitotic cells, we decided to determine whether PLK1 is also involved in the phosphorylation of 4E-BP1.<sup>38</sup> We added 100 nM specific PLK1 inhibitor BI2536<sup>39</sup> to the oocytes 1h PIW. However, no effect of BI2536 on 4E-BP1 phosphorylation was seen after 2h of culture (Fig. 3A and B).

Our study supports other published research<sup>32-34</sup> documenting that CDK1/CYCB1 (MPF) kinase is also involved in 4E-BP1 phosphorylation and in the inactivation of its suppressor function. Mitosis is commonly thought to be associated with reduced cap-dependent protein translation, however, our previously published results<sup>4,5,9</sup> show that the main regulators of cap-dependent translation initiation become activated at the onset of meiosis in pig oocytes. Therefore, we elucidated whether MPF had an impact on the activation of mTOR in mouse oocytes. By downregulation of CDK1 using Rosco treatment (added post-NEBD)

we found a significant decrease in phosphorylation of mTOR(Ser2448) (Fig. 3C and D). On the other hand, treatment with Okadaic Acid (OA) substantially increased phosphorylation/activation of mTOR in the treated oocytes, when compared with control oocytes (Fig. 3C and D). Our WB data revealed that MPF influenced the activity of mTOR in the mammalian oocyte after the re-initiation of meiosis. We expected a positive correlation between the localization of the kinases and that of the phosphorylated forms of 4E-BP1. The ICC experiments indeed showed that fluorescence for both mTOR(Ser2448) and CDK1 kinases are present at the newly forming spindle or bipolar spindle (Fig. 3E), which was in good agreement with the localization of phosphorylated 4E-BP1 (Fig. 2).

Reduced cap-dependent protein translation is believed to be connected with mitosis. However, Heesom et al.<sup>32</sup> and Huda et al.<sup>34</sup> have demonstrated that cap-dependent translation is generally sustained during mitosis and 4E-BP1 becomes phosphorylated after entry to mitosis. Thus we isolated cumulus cells (CCs) from GV and MII oocyte-



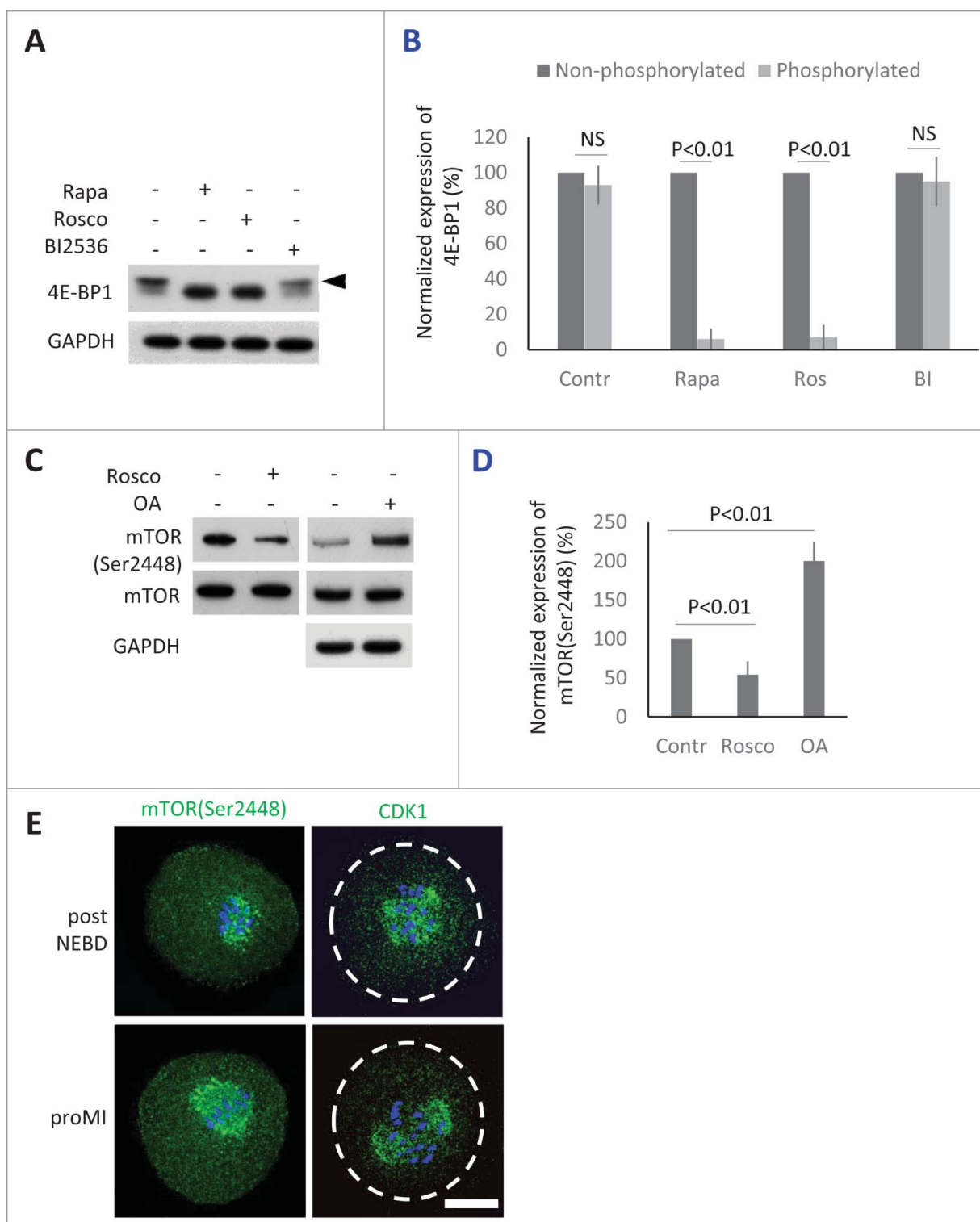


**Figure 3.** Protein kinases phosphorylating 4E-BP1 in the oocytes. (A) Detection of 4E-BP1 by immunoblotting in the oocytes treated with specific inhibitors Rapa (100 nM), Rosco (10  $\mu$ M), or BI2536 (100 nM) post-NEBD. Arrowhead marks the presence of upper band (phosphorylation shift) of 4E-BP1 in the oocytes treated for 2 h post-NEBD, GAPDH was used as a loading control, a typical experiment from at least 3 replicates is shown. (B) Quantification of non-phosphorylated and phosphorylated form of 4E-BP1 in the post NEBD oocytes. Data are presented as mean  $\pm$  SD, Student's t-test, NS = non-significant. (C) CDK1 effect on mTOR phosphorylation in the oocytes treated by Rosco (10  $\mu$ M) or OA (1  $\mu$ M). Immunoblot was probed with mTOR(Ser2448) and control (mTOR and GAPDH) antibodies. Twenty oocytes were used per sample. (D) Presence of mTOR(Ser2448) normalized to the mTOR in the Rosco or OA treated oocytes. Data are presented as mean  $\pm$  SD, Student's t-test. (E) Localization of mTOR(Ser2448) and CDK1 in the post NEBD and pro-MI stage oocytes,  $n \geq 30$ , phospho-specific antibody (green) and DNA (blue). Scale bar = 20  $\mu$ m.

cumulus complexes to investigate the phosphorylated status of 4E-BP1 in other cells that are naturally present in the G0 or G1 stage<sup>40</sup> of the cell cycle. WB data from CCs

lysates revealed that 4E-BP1 was not phosphorylated in the CCs isolated either from GV or from MII CCs (Supplementary Fig. 4A). Oocytes in GV and MII stages were used as a

control of the protein mobility shift. Accordingly, in the ICC experiments there was no 4E-BP1 phosphorylation signal observed for Thr37/46/70 and Ser65 in the CCs, although 4E-BP1 was present in this cell type (Supplementary Fig. 4B).

Altogether, our results suggest that upon exit from prophase the activity of CDK1/CYCB1 (MPF) is required for the phosphorylation of 4E-BP1, most likely via activation of mTOR.

### Expression of a dominant negative 4E-BP1 mutant promotes aberrant spindle formation

4E-BP1 phosphorylation releases eIF4E binding to permit translation initiation; the overall increase in phospho-4E-BP1 in the cytoplasm may facilitate maternal mRNA translational recruitment in the cytoplasm. To down-regulate phosphorylation of 4E-BP1, we expressed RNA coding for 4E-BP1 with all 4 phospho-sites mutated - Thr37/46/70 and

Ser65 (4E-BP1-4Ala; Fig. 4A). Microinjection (Fig. 4B) of the *in vitro* transcribed (IVT) RNA coding for 4E-BP1-wild type (4E-BP1-Wt) or 4E-BP1-4Ala showed that the whole population of endogenous and exogenous 4E-BP1-Wt was phosphorylated in the MII oocytes (Fig. 4C; also see Fig. 1A and D), however, in MII oocytes microinjected with 4E-BP1-4Ala RNA 2 not phosphorylated bands were present (depicted by arrowhead) and upper band of phosphorylated endogenous 4E-BP1 (Fig. 4C). Moreover, ICC detection with 4E-BP1 antibody in the microinjected oocytes showed significant increase of the intensity of the 4E-BP1 protein level for both injected constructs in comparison with no injected group (Supplementary Fig. 5; mean value  $\pm$  29 % in the 4E-BP1-Wt and mean value  $\pm$  23 % in the 4E-BP1-4Ala,  $P < 0.001$  Student's *t*-test). Microinjected oocytes with 4E-BP1-4Ala RNA extruded a polar body, however, ICC analysis showed significant increase in aberrant spindles accompanied by the absence of chromosome alignment to the

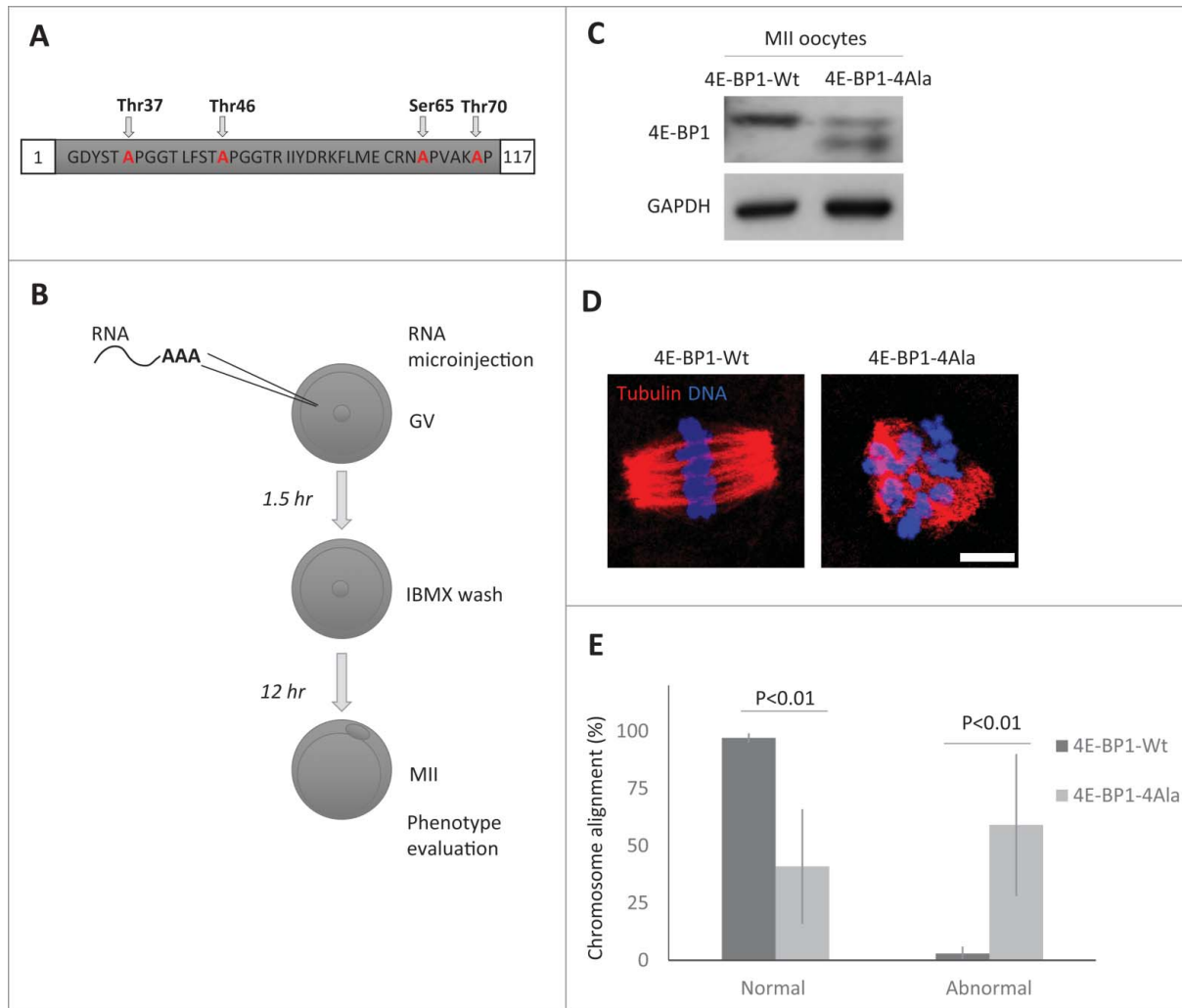


**Figure 4.** Down-regulation of 4E-BP1 phosphorylation in oocytes results in defects in the MII spindle assembly. (A) Scheme of dominant negative mutant construct of 4E-BP1-4Ala used for *in vitro* transcription. (B) Scheme of experimental procedure to express 4E-BP1 RNA constructs in the oocyte. (C) Immunoblotting evaluation of expression of microinjected non-phosphorylatable form (marked by arrowhead) of 4E-BP1 in the matured MII oocytes  $n = 2$ . GAPDH was used as a loading control. See Figure S5. (D) Confocal images of MII spindles of oocytes microinjected with 4E-BP1-Wt or dominant negative mutant 4E-BP1-4Ala, Tubulin (red) and DNA (blue). Scale bar = 10  $\mu$ m. (E) Quantification of chromosome alignment in the metaphase plate, MII oocytes expressing 4E-BP1-Wt or 4E-BP1-Ala RNA. Data are presented as mean  $\pm$  SD, Student's *t*-test,  $n \geq 25$ .

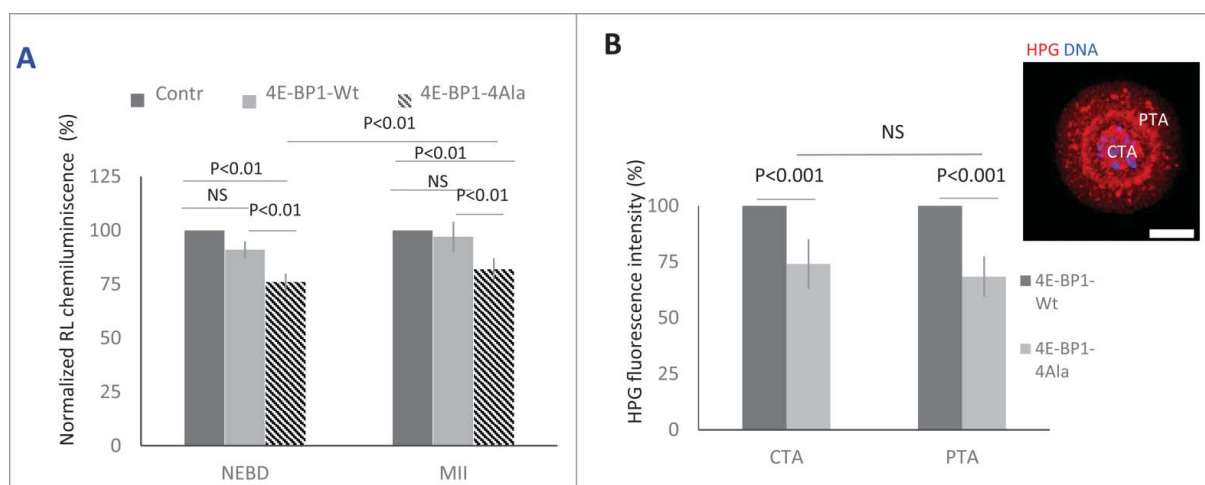


**Figure 5.** 4E-BP1 effects on protein synthesis in the oocytes. (A) Renilla luciferase reporter carrying 5'UTR TOP motive of *Eef2* co-injected with 4E-BP1-Wt or 4E-BP1-4Ala RNA. In the control no 4E-BP1 RNA was used and the IRES motive Firefly Luciferase was used as a loading control. Chemiluminescence was measured in the post NEBD stage (mean value  $\pm$  6 and 4 %, Student's *t*-test, NS = non-significant) and MII stage oocytes (mean values  $\pm$  SD, Student's *t*-test). Data are presented as mean  $\pm$  SD,  $n \geq 10$  replicates. (B) Measurement of *in situ* translation intensity in the chromosomal area (CTA, mean value  $\pm$  SD, Student's *t*-test, NS = non-significant) and perispindular translational area (PTA, mean value  $\pm$  SD, Student's *t*-test) in the post NEBD oocytes, HPG (red) and DNA (blue). Data are presented as mean  $\pm$  SD,  $n \geq 21$ . Scale bar = 20  $\mu$ m.

metaphase plate in 59% of the 4E-BP1-4Ala injected oocytes (mean value  $\pm$  31%;  $P < 0.01$ , Student's *t*-test), whereas only 3% of the 4E-BP1-Wt injected oocytes produced them (mean value  $\pm$  2 %;  $P < 0.01$ , Student's *t*-test, Fig. 4E).

It is accepted that 4E-BP1 is a key player in cap-dependent translation<sup>27</sup> which predominantly utilizes mRNA with TOP motif.<sup>41</sup> To further investigate this, we examined the expression of a dominant negative mutant of 4E-BP1<sup>41</sup> and its influence on the translation of the *Renilla* Luciferase (RL) reporter with canonical TOP motive of the *Eef2*<sup>41</sup>. We performed microinjection of IVT RNA coding 4E-BP1-Wt or 4E-BP1-4Ala with RL reporter RNA and *Firefly* Luciferase (FL) with IRES motif as a microinjection loading control. Analysis of chemiluminescence showed a significant decrease of RL expression in the oocytes expressing 4E-BP1-4Ala in comparison with the control injected with RL and FL (Fig. 5A). Decrease of RL expression was non-significant in 4E-BP1-Wt RNA injected (mean value  $\pm$  6%,  $P > 0.05$ , Student's *t*-test) in the post-NEBD stage in comparison with 24% significant decrease in the 4E-BP1-4Ala RNA injected groups (mean value  $\pm$  4%,  $P < 0.01$ , Student's *t*-test). RL expression in the MII oocytes showed significant (18%) decrease in the oocytes injected with 4E-BP1-4Ala RNA in comparison with the control group (mean value  $\pm$  5%,  $P < 0.01$ , Student's *t*-test). Moreover, we analyzed *in situ* translation (Fig. 5B) in the 2 distinct areas of the oocyte after expression of 4E-BP1-Wt or 4E-BP1-4Ala, one at the area of the newly forming spindle (Chromosomal Translational Area; CTA) and the second at the Perispindular Translational Area (PTA). We detected a significant decrease of translation at the CTA (26 %, mean  $\pm$  11 %;  $P < 0.01$ , Student's *t*-test) and PTA (32 %, mean  $\pm$  9 %;  $P < 0.01$ , Student's *t*-test), however, without significant differences between CTA and PTA ( $P > 0.05$ ; Fig. 5B).

## Discussion

Here we present an analysis of regulation of 4E-BP1 phosphorylation during meiotic division of the mammalian oocyte, a cell

that naturally undergoes NEBD, then enters prometaphase and resumes meiosis further by asymmetric cytokinesis creating a fertilizable egg and a polar body. The progress of oocytes through cell cycle is highly synchronized, with rapid inactivation/phosphorylation of 4E-BP1, which suggests that cap-dependent translation is highly active in this cell type and stage.

In accordance with Mayer et al.<sup>23</sup> we were not able to detect 4E-BP2 and 4E-BP3 proteins suggesting that 4E-BP1 is the only form of eIF4E-binding protein present in mouse and bovine oocytes. However, mRNAs coding all 3 isoforms are present and stable in mouse oocytes during maturation indicating their role post-fertilization during early embryonic development, or alternatively, they might be translated to substitute 4E-BP1 in case of an insufficiency of the 4E-BP1 form.<sup>42</sup>

Here we show that the main effector kinases of 4E-BP1 phosphorylation are mTOR and CDK1, which become highly active after the resumption of meiosis both in mouse, human and, also bovine oocytes (mTOR,<sup>9,23</sup> and MPF<sup>36</sup>), which is similar to mitosis.<sup>43</sup> It has been reported that also PLK1 promotes phosphorylation of 4E-BP1 in mitotic cells,<sup>44</sup> however, inhibition of PLK1 in mammalian oocytes did not show any effect on 4E-BP1 phosphorylation in our model system. Inhibition of mTOR or CDK1, on the other hand, strongly affects 4E-BP1 phosphorylation in a very similar manner. These findings suggest the existence of a different mechanism of 4E-BP1 phosphorylation in the meiotic cell. We further show that inhibition of CDK1 kinase activity results in inhibition of mTOR phosphorylation on the site activation (Ser2448), suggesting that CDK1 exerts its effect on 4E-BP1 phosphorylation via activation of mTOR, although we cannot exclude the possibility that CDK1 phosphorylates 4E-BP1 directly. So, in accordance with Heesom et al.<sup>32</sup> we show that the main regulator of 4E-BP1 phosphorylation in mouse oocytes is mTOR, on the other hand, CDK1 activity is in our system required for the full mTOR activation rather than for direct 4E-BP1 phosphorylation. It is known that mTOR is phosphorylated and activated in mitotic cells by AKT,<sup>45</sup> however, according to our results, it



seems that during mammalian meiosis this pathway is not sufficient for full mTOR activation, which is likely to be mediated by CDK1.

An increase in 4E-BP1 phosphorylation has been previously seen in porcine, bovine and mouse oocytes,<sup>4,8,9,21,22</sup> however, only recently the localization of the differently phosphorylated forms of 4E-BP1 has been described in mouse oocytes.<sup>38</sup> The nature and role of Ser65 and Thr70 phosphorylation for spindle localization is unclear at the present time, although it should be noted that cap-dependent translation becomes elevated at the onset of meiosis and is inactivated later when it exits meiosis (fertilization).<sup>6</sup> Romasko et al.<sup>22</sup> show that 4E-BP1(Ser112) has similar localization as 4E-BP1(Ser65) in our study. Regulation of 4E-BP1 phosphorylation at the spindle is likely to be temporally and mechanistically distinct from its regulation in the rest of the oocyte. The dynamic spatial and temporal pattern of localization of phosphorylated 4E-BP1 that forms at the spindle is indicative of a novel mechanism promoting localized protein production related to transcripts localized at the spindle. Depolymerization of the newly forming spindle by Noco treatment changed the 4E-BP1(Thr70) pattern, however, phosphorylation still persisted at the chromosomal area. This suggests the existence of a mechanism, which maintains phosphorylation at this position, most likely involving Lamin A/C and/or endoplasmic reticulum structures surrounding the spindle assembly area. Such a mechanism would promote the accumulation of specific proteins by microtubule-independent machinery, involving some sort of semipermeable membrane<sup>46</sup> formed from microfilaments,<sup>47,48</sup> ER,<sup>49-51</sup> LMN<sup>9</sup> and possibly other constituents.

A number of studies,<sup>22,52-57</sup> have reported the enrichment of specific mRNAs at the spindle, which may contribute to the local proteome. Beside the enrichment of global translation at the oocyte spindle,<sup>9</sup> Romasko et al.<sup>22</sup> has also shown that *Mis18a* mRNA coding MIS18 Kinetochores Protein A is localized at the oocyte spindle, which is required for metaphase alignment and proper chromosome segregation.<sup>58</sup> Another example of localized translation has been documented by Bomar et al.<sup>52</sup> who identified the localization of *Akap95* (A kinase-anchoring protein) mRNA at the MII spindle without protein expression at this stage, but the mRNA was then translated after fertilization and the protein was present in the female pronucleus causing an unequal distribution between maternal and paternal nuclei in the zygote. Local transcriptome coupled with its translation suggests the role of translational machineries, where mTOR, CDK1 and 4E-BP1 are key players, the mechanism that is used by meiotic and mitotic cells of various species. However, differences between the cell types suggest there are distinct modes of regulation.

There are various factors involved in spindle formation. Apart from the specific transport of mRNA to the spindle, a population of RNA might already be present in the nucleus,<sup>9,56,59,60</sup> which indicates a significant contribution of the local transcriptome to the formation of spindle directly post-NEBD. In accordance with this, 4E-BP1 is enriched in the nucleus in its non-phosphorylated state. 4E-BP1 in the nucleus might be bound to the 5'UTR of mRNAs, where it probably functions as a translational repressor. Consequently, after its hyperphosphorylation following NEBD, it becomes inactivated and in such a way promotes the

translation of specific mRNAs at the newly forming spindle. These results suggest that the function of mRNA retention in the nucleus may be to sustain translational repression, and that their subsequent translation can be regulated in a spatiotemporally restricted manner in response to cell cycle events.

We propose that meiotic phosphorylation of 4E-BP1 on Ser65 and Thr70 by mTOR acts to stimulate cap-dependent translation as the oocyte proceeds through meiosis (particularly after NEBD) and that specific localization of the key cap-dependent translation regulatory factors,<sup>22,61</sup> is essential for the translation of specific mRNAs at the spindle area to ensure errorless meiotic progression. We identify the 2 kinases mTOR and CDK1 involved in the inactivation of the 4E-BP1 at the spindle where all the important regulators are present. Using PLK1 inhibitor BI2536 we show that PLK1 kinase is not involved in 4E-BP1 phosphorylation in mouse oocytes and also, that CDK1 exerts its influence via the phosphorylation (and as such further activation) of mTOR, which as a result is likely to phosphorylate Ser65 and Thr70 of 4E-BP1. However, we cannot exclude the possibility that CDK1 phosphorylates at least one of these sites directly, as was previously reported by Heesom et al.<sup>32</sup> and Shuda et al.<sup>34</sup> Since the effect of CDK1 inhibition on the level of 4E-BP1 phosphorylation is less pronounced in later stages of meiosis (data not shown) it is tempting to speculate that the increased activation of mTOR mediated by CDK1 might be temporally and possibly also spatially restricted to the most critical process during early meiosis, i.e. formation of the meiotic spindle. Such hypothesis is supported also by the data obtained by us and other studies<sup>38</sup> showing the increased presence of 4E-BP1 phosphorylated forms at the spindle and in the chromosomal area. It is also interesting to note that CDK1 has been shown to directly phosphorylate the key mTOR binding partner Raptor during mitosis.<sup>62</sup> This reinforces our conclusions and those from other studies suggesting that mTOR activity is highly regulated by cell cycle progression. A number of other proteins involved in the regulation of translation have also been described previously. Papst<sup>63</sup> reported that Ribosomal Protein S6 Kinase is a substrate for CDK1/CYCB1 in mitosis and Elongation factor-1<sup>64</sup> in the *Xenopus* oocytes during meiotic cell division is a physiologic substrate of CDK1/CYCB1 in mitosis.

After fertilization when the nuclear envelope is reformed again at the end of meiosis, phosphorylation of 4E-BP1 disappears.<sup>5,9</sup> This indicates a specific/exclusive role of this pathway in meiotic maturation, which is also supported by our findings showing that no phosphorylated 4E-BP1 is present in the CCs, naturally occurring in the G0 or G1 stage. We might conclude that phosphorylation of 4E-BP1 follows exit from prophase of the cell cycle. It has been reported previously that overall protein synthesis becomes reduced during meiosis.<sup>4,9,65</sup> However, studies in synchronized HeLa cells have shown that this inhibition ceases by late telophase<sup>66</sup> and that overall protein synthesis increases rapidly as cells enter G1-phase.<sup>67</sup>

Here we show that the presence of a non-phosphorylated 4E-BP1 population in an oocyte that progresses through meiosis results in aberrant morphology of the metaphase II spindle that is most likely the result of impaired translation of a subset of RNAs. Previously, we have described the effect of mTOR/4F

pathway downregulation on in situ translation at the chromosomal area.<sup>9</sup> Our current finding shows that a non-phosphorylated mutant does not display significant differences in the level of translation between the chromosomal and perispindular areas. This might be explained by the fact that exogenous 4E-BP1, which is loaded to the cytoplasm in the form of RNA, and its consequent 4E-BP1 protein, lacks endogenous localization in this large cell and so influences both translational areas within the cell. On the other hand, the expression of a mutant in the cytoplasm which is unable to be phosphorylated leads to downregulation of translation in the cytoplasm and at the chromosomal area.

4E-BP1 null mice are viable and fertile.<sup>42</sup> However, we have observed aberrant spindle formation in the MII oocytes expressing a non-phosphorylatable 4E-BP1 form, which might suggest that the role of 4E-BP1 is rather in the fine tuning of meiotic progression. Regulation of 4E-BP1 in the oocyte might be affected by cell stress or by the age of the female. Moreover, insulin stimulates the mTOR signaling pathway<sup>68</sup> and insulin signaling promotes the production of high-quality oocytes.<sup>69</sup> Consistently, oocytes from diabetic mice display spindle abnormalities, which can be reversed by pancreatic islet transplantation.<sup>70</sup> Our findings showing localization of phosphorylated/inactivated 4E-BP1 at the spindle also suggest the existence of a mechanism that links maternal age and environmental exposures to diminished oocyte quality arising from defective spindle formation and function. We show that mTOR becomes also activated post NEBD in the human oocyte, with strong signal at midbody in the MII oocyte, suggesting its similar role in the human oocyte meiosis in specific translational regulation, as it plays in the mouse oocyte. Here, mTOR pathway might contribute to the age related chromosome segregation errors in the woman oocytes, similarly as it has been documented in the mouse model,<sup>9</sup> as well as in mammalian and yeast cells.<sup>71</sup> Lapasset et al.<sup>7</sup> showed that the treatment with Rapamycin resulted in the prevention of extrusion of second polar body in starfish oocytes. They present the absence of eIF4E dissociation from 4E-BP in the presence of Rapamycin without the effect on translation of Cyclin B1 or Mos. Taken together, mTOR involvement is indispensable for inactivation of translational repressor 4E-BP1, which prevents the synthesis of essential proteins necessary for a correct completion of the meiotic and mitotic divisions. In addition to translational initiation factors, Ribosomal protein S3 (RPS3) is present at the mitotic<sup>72</sup> or newly forming meiotic spindle.<sup>73</sup> RPS3 knockdown causes arrest in mitotic metaphase,<sup>72</sup> which resembles the effect of mTOR inhibition<sup>23</sup> in the bovine oocyte. The influence of known effector kinases in the inactivation of the translational repressor 4E-BP1 might be essential for the temporal and spatial translation of specific mRNAs at the spindle area to ensure errorless meiotic progression.

In this study we propose that localized translational regulation at the oocyte spindle regulated through an mTOR/CDK1 pathway might represent a mechanism which links spindle formation and function with the temporal and spatial regulation of the local transcriptome in the particular subcellular areas, which affects oocyte quality. There is still much to learn about

the dynamics of distribution of mRNA and translational regulatory components, as well as how exactly these are regulated in the different cellular compartments. Further elucidation of the relationship between cytoskeletal elements and translation machinery may help to explain the logistics of translational control of spindle assembly and chromosome segregation.

## Material and methods

### Oocytes isolation and maturation

Mouse ovaries were obtained from CD1 mice at least 6 weeks old which were stimulated to by intraperitoneal injection of 5 UI of pregnant mare serum gonadotropin (PMSG; Folligon, Merck Animal Health) 46 h before collection. GV oocytes were isolated into transfer medium Tetkova et al.<sup>74</sup> supplemented with 100  $\mu$ M of 3-isobutyl-1-methylxanthine (IBMX) used to prevent spontaneous resumption of meiosis. Selected oocytes were stripped of the cumulus cells and cultured in M16 medium (Millipore) without IBMX at 37°C, 5% CO<sub>2</sub>. After 70 min post IBMX wash (PIW) at least 90% of oocytes underwent nuclear envelope breakdown (NEBD, resumption of meiosis; G2/M transition) and oocytes arrested in the GV were discarded. Pro-metaphase I (pro-MI) and metaphase I (MI) stage oocytes were collected after post IBMX wash at 3 h (post-NEBD), 7 h (pro-MI) and 12 h (MII). All animal work was conducted according to Act No 246/1992 on the protection of animals against cruelty. Human oocytes, not used in human reproduction, were obtained from the Obstetrics and Gynecology Clinic of the General University Hospital in Prague. The project was accredited (#30/12) by the Ethical Committee of the General Hospital, Prague.

### Oocyte treatments

Mouse oocytes were treated with 100nM BI2536 for 2 hours post NEBD (Axon Medchem), 1  $\mu$ M Nocodazole for 1 h (M1404, Sigma-Aldrich), 100 nM Rapamycin (#9904, CST) or 10  $\mu$ M Roscovitine (R7772, Sigma-Aldrich); 1  $\mu$ M Okadaic acid (OA, CAS 459616, Millipore) for 2 h after NEBD. For nascent protein synthesis specific stage NEBD-2 h, oocytes were cultured in methionine-free medium (Gibco) supplemented with 1% dialyzed fetal bovine serum (10,000MW; Sigma) and 50 mM L-homopropargylglycine (HPG) for 30 min. HPG was detected by using a Click-iT Cell Reaction Kit (Life Technologies). *In situ* translation detection showed increased incorporation of HPG in the chromosomal area (CTA) and perispindular area (PTA)<sup>9</sup>

### RNA isolation and quantitative RT-PCR

RNA was extracted with RNeasy Plus Micro kit (Qiagen) according to manufacturer's instructions. Genomic DNA was depleted using guide columns. H<sub>2</sub>O for qRT-PCR was used for RNA elution in amount of 25  $\mu$ L for 25 oocytes. Samples were stored at -80°C until expression analysis. mRNA equivalent for 1 oocyte was amplified by a One-step RT-PCR kit (Qiagen) with real-time detection using SybrGreenI fluorescent dye on a Rotor Gene 3000 instrument (Corbett Research, Australia). The qRT-PCR reactions were prepared in duplicates in one

run. Reaction conditions were: reverse transcription at 50°C for 30 min, initial activation at 95°C for 15 min, cycling: denaturation at 95°C for 20 sec, annealing at a temperature specific for each set of primers (see Table S1) for 20 sec, extension at 7°C for 30 sec. Products were verified by melting analysis and gel electrophoresis on 1.2% agarose gel with ethidium bromide staining. The relative concentration of templates in different samples was determined using comparative analysis software (Corbett Research). The results for individual target genes were normalized according to the relative internal standard GAPDH. The data are presented from at least 3 biologic replicates. The significant differences between GV and MII were evaluated using *t*-test (PrismaGraph5).

### Immunocytochemistry

Mouse and human oocytes were fixed for 20 min in 4% PFA in phosphate saline buffer (PBS). Oocytes were permeabilized for 10 min in 0.2% Triton X-100 in PBS, then washed with PVA/PBS. Oocytes were incubated with primary antibodies at 4°C overnight. We are using human 4E-BP1 nomenclature to unify the text discussing human and mouse systems. The human 4E-BP1 sequence of amino acid numbers is greater by one. The following antibodies were used in 1:100 dilution: rabbit anti-4E-BP1 (#9452, CST), rabbit anti-phospho-4E-BP1(Thr70) (#13396, CST), rabbit anti-phospho-4E-BP1(T37/46) (#9459, CST), rabbit anti-phospho-4E-BP1(Ser65) (#9451, CST), rabbit anti-CDK1 (#9112, CST), mouse anti-tubulin (#T6793, Sigma) and  $\gamma$ -tubulin (#T6557, Sigma), rabbit anti-phospho-mTOR(Ser2448, #2971, CST) and mouse anti-LMNA/C (SAB4200236, Sigma Aldrich). After washing in PBS, detection of the primary antibodies was performed by cultivation of the oocytes with relevant Alexa Fluor 488, 594 or 647 conjugates (diluted 1: 250) for 1 h at room temperature. Oocytes were then washed 2 times for 15 min in PVA/PBS and mounted using Vectashield Mounting Medium with DAPI (H-1200, Vector Laboratories). Samples were visualized using a Leica SP5 inverted confocal microscope (Leica Microsystems) in 16 bit depth. Images were assembled in LEICA LasAFX (Leica Microsystems) software and equatorial sections were quantified by Image J software (<http://rsbweb.nih.gov/ij/>).

### Western blot

Oocytes were lysed with 6  $\mu$ l of Millipore H<sub>2</sub>O and 2, 5  $\mu$ l of 4x lithium dodecyl sulfate, sample buffer NP 0007 and 1  $\mu$ l reduction buffer NP 0004 (Novex, Thermo Fisher Scientific) and boiled at 100°C for 5 min. If not stated otherwise, sample of 50 oocytes per sample was used. To detect phosphorylation shift, oocytes were dissolved in the 20  $\mu$ l of the 1x NEBuffer with 800 U of LPP enzyme (P0753, New England BioLabs) and incubated overnight at 30°C, LPP was omitted in the control sample (LPP-). Lysates were separated using a 4–12% gradient polyacrylamide gel SDS (NP323BOX, Life Technologies) page and transferred to an immobilon P membrane (PVDF; Millipore) using semidry blotting system (Biometra GmbH). Membranes were blocked for 1 h, in 1–5% skimmed milk dissolved in Tween-Tris-buffer saline (TTBS, pH 7,4) according to antibody (list of primary antibodies and dilutions is below). After 3 cycles for 10 min washing in TTBS, membranes were incubated

at 4°C overnight in 1% milk/TTBS with the following primary antibodies: GAPDH (rabbit, G9545, Sigma-Aldrich) and Tubulin (mouse, T6793, Sigma-Aldrich) antibodies were diluted 1:30 000 and 4E-BP1 (rabbit, 9452, CST), 4E-BP1(T69) (rabbit, 9455S, CST), 4E-BP1(T36/45) (rabbit, 9459, CST), 4E-BP1(S64) (rabbit, 9451S, CST), anti HA (rabbit, 3724, CST) antibodies were diluted 1:500; mTOR(Ser2448) (rabbit, 2971S, CST), mTOR (rabbit, 2972, CST) antibodies were diluted 1:8 000 and 1:2 000 respectively. After 3 cycles of 10 min washing in TTBS the membrane was incubated for 1 h with secondary antibody Peroxidase Anti-Rabbit Donkey (711–035–152, Jackson immunoresearch) or Peroxidase Anti-mouse Donkey (715–035–151, Jackson immunoresearch) in 1:7.500 dilution in 1% milk/TTBS 1 h at room temperature. Immunodetected proteins were visualized by ECL (Amersham, GE Healthcare life science), films were scanned using a GS-800 calibrated densitometer (Bio-Rad) and quantified using Image J software (<http://rsbweb.nih.gov/ij/>).

### Microinjection

GV stage mouse oocytes were microinjected in transfer medium with IBMX on an inverted microscope Leica DMI 6000B with Transferman NK2 and Femtojet (Eppendorf). Oocytes were injected with *in vitro* transcribed RNA (mMessage, Ambion) from mutant plasmid pCW57.1–4E-BP1–4Ala<sup>41</sup> and pCMV3-N-HA-4E-BP1 (generous gift of professor Nahum Sonenberg, McGill University, Montreal, Canada; Gingras et al.<sup>27</sup>). Approximately 5  $\mu$ l of RNA solutions of 4E-BP1-Ala or 4E-BP1-Wt diluted in RNase free water, to concentration 50 ng/ $\mu$ l were microinjected into oocytes.

### Dual-luciferase assay

Oocytes were injected in the presence of IBMX with 50 ng/ $\mu$ l of IVT RNA (mMessage, Ambion) from *Renilla Luciferase* constructs (*Eef2*-5'UTR - RL; #38235; Addgene) with combination of injection amount control *Firefly Luciferase* (FL; #18964; Addgene<sup>75</sup>) and RNA for 4E-BP1-Wt or 4E-BP1–4Ala in the presence of IBMX. Oocytes were cultured for 5 h without IBMX. At least 5 oocytes were lysed in 5  $\mu$ l of Passive Lysis Buffer and stored at –80°C until measurement of chemiluminescence by Dual-Luciferase Assay System (Promega) according to the manufacturer's instructions. Signal intensities were measured using a Glomax Luminometer (Promega). Activity of RL was normalized to the FL luciferase.

### Statistical analysis

Experiments were repeated at least 3 times unless stated. Mean and SD values were calculated using MS Excel, statistical significance of the differences between the groups was tested using Student's *t*-test (PrismaGraph5) and *P*<0.05 was considered as statistically significant.

### Abbreviations

Akap95	Kinase (PRKA) anchor protein 8
CCs	Cumulus cells

CDK1	Cyclin dependent kinase 1
CTA	Chromosomal translational area
CYCB1	Cyclin B1
DAPI	4', 6-diamidino-2-phenylindole
ER	Endoplasmic reticulum
eIF4E	Eukaryotic initiation factor 4E
eIF4G1	Eukaryotic initiation factor 4G1
eIF4A	Eukaryotic initiation factor 4A
FL	Firefly Luciferase
FRAP kinase	FKBP-12-rapamycin-associated protein
G1-phase	Gap 1 phase
GV	Germinal vesical stage
HPG	L-homopropargylglycine
HA	Hemagglutinin
IBMX	3-Isobutyl-1-methylxanthine
IRES	Internal ribosome entry site
IVT	<i>In vitro</i> transcribed
LMN	Lamin A/C
Mis18a	MIS18 kinetochore protein A
mTOR	Mammalian target of rapamycin
MI	Metaphase of first meiotic maturation
MII	Metaphase of second meiotic maturation
MPF	Maturation promoting factor
Noco	Nocodazole
NEBD	Nuclear envelope breakdown
OA	Okadaic acid
PTA	Perispindular translational area
PVA	Polyvinyl alcohol
PIW	Post IBMX wash
PLK1	Polo-like kinase1
PKB/ AKT	Protein kinase B/ serine/threonine-specific protein kinase
PBE	Polar body extrusion.
Ras/Raf/ERK pathway	Mitogen-activated protein kinases pathway
Rosco	Roscovotine
RL	Renilla Luciferase
Rapa	Rapamycin
S6 kinase	Ribosomal s6 kinase
TOP	Terminal oligopyrimidine motif
3UTR	Three prime untranslated region
4E-BP1	Eukaryotic translation initiation factor 4E-binding protein 1
4E-BP2	Eukaryotic translation initiation factor 4E-binding protein 2
4E-BP3	Eukaryotic translation initiation factor 4E-binding protein 3
5UTR	Five prime untranslated region

## Disclosure of potential conflicts of interest

No potential conflicts of interest were disclosed.

## Acknowledgments

We thank Jaroslava Supolikova and Marketa Hancova for their exceptional assistance with experiments and Nahum Sonenberg and his laboratory for kindly providing the pCMV3-N-HA- 4E-BP1 plasmid.

## Funding

This work was supported by GACR13–12291S, GACR15–22765S, EXCELLENCE CZ.02.1.01/0.0/0.0/15\_003/0000460 OP RDE and Institutional Research Concept RVO67985904.

## ORCID

Radek Malik  <http://orcid.org/0000-0002-6783-1146>

Michal Kubelka  <http://orcid.org/0000-0002-2264-5884>

## References

- [1] Schuh M, Ellenberg J. Self-organization of MTOCs replaces centrosome function during acentrosomal spindle assembly in live mouse Oocytes. *Cell* 2007; 130:484-98
- [2] Kusch J, Liakopoulos D, Barral Y. Spindle asymmetry: a compass for the cell. *Trends Cell Biol* 2003; 13:562-9
- [3] Hashimoto N, Kishimoto T. Regulation of meiotic metaphase by a cytoplasmic maturation-promoting factor during mouse oocyte maturation. *Dev Biol* 1988; 126:242-52; PMID:3350209
- [4] Ellederová Z, Kovarova H, Melo-Sterza F, Livingstone M, Tomek W, Kubelka M. Suppression of translation during in vitro maturation of pig oocytes despite enhanced formation of cap-binding protein complex eIF4F and 4E-BP1 hyperphosphorylation. *Mol Reprod Dev* 2006; 73:68-76; PMID:16211600
- [5] Ellederová Z, Cais O, Susor A, Uhlířová K, Kovářová H, Jelínková L, Tomek W, Kubelka M. ERK1/2 map kinase metabolic pathway is responsible for phosphorylation of translation initiation factor eIF4E during in vitro maturation of pig oocytes. *Mol Reprod Dev* 2008; 75:309-17; PMID:17290414
- [6] Susor A, Jelínková L, Karabínová P, Torner H, Tomek W, Kovářová H, Kubelka M. Regulation of cap-dependent translation initiation in the early stage porcine parthenotes. *Mol Reprod Dev* 2008; 75:1716-25; PMID:18386287
- [7] Lapasset L, Pradet-Balade B, Vergé V, Lozano J-C, Oulhen N, Cormier P, Peaucellier G. Cyclin B synthesis and rapamycin-sensitive regulation of protein synthesis during starfish oocyte meiotic divisions. *Mol Reprod Dev* 2008; 75:1617-26; PMID:18361417
- [8] Tomek W, Torner H, Kanitz W. Comparative analysis of protein synthesis, transcription and cytoplasmic polyadenylation of mRNA during maturation of bovine oocytes in vitro. *Reprod Domest Anim Zuchthyg* 2002; 37:86-91
- [9] Susor A, Jansova D, Cerna R, Danylevska A, Anger M, Toralova T, Malik R, Supolikova J, Cook MS, Oh JS, et al. Temporal and spatial regulation of translation in the mammalian oocyte via the mTOR-eIF4F pathway. *Nat Commun* 2015; 6:6078; PMID:25629602
- [10] Jackson RJ, Hellen CUT, Pestova TV. The mechanism of eukaryotic translation initiation and principles of its regulation. *Nat Rev Mol Cell Biol* 2010; 11:113-27; PMID:20094052
- [11] Gingras AC, Gygi SP, Raught B, Polakiewicz RD, Abraham RT, Hoekstra MF, Aebersold R, Sonenberg N. Regulation of 4E-BP1 phosphorylation: a novel two-step mechanism. *Genes Dev* 1999; 13:1422-37; PMID:10364159
- [12] Gingras AC, Raught B, Sonenberg N. Regulation of translation initiation by FRAP/mTOR. *Genes Dev* 2001; 15:807-26; PMID:11297505
- [13] Raught B, Gingras AC, Sonenberg N. The target of rapamycin (TOR) proteins. *Proc Natl Acad Sci U S A* 2001; 98:7037-44; PMID:11416184
- [14] Tavares MR, Pavan ICB, Amaral CL, Meneguello L, Luchessi AD, Simabuco FM. The S6K protein family in health and disease. *Life Sci* 2015; 131:1-10; PMID:25818187
- [15] Gingras AC, Raught B, Gygi SP, Niedzwiecka A, Miron M, Burley SK, Polakiewicz RD, Wyslouch-Cieszynska A, Aebersold R, Sonenberg N. Hierarchical phosphorylation of the translation inhibitor 4E-BP1. *Genes Dev* 2001; 15:2852-64; PMID:11691836
- [16] Tee AR, Proud CG. Caspase cleavage of initiation factor 4E-binding protein 1 yields a dominant inhibitor of cap-dependent translation and reveals a novel regulatory motif. *Mol Cell Biol*



- 2002; 22:1674-83; PMID:11865047; <http://dx.doi.org/10.1128/MCB.22.6.1674-1683.2002>
- [17] Wang X, Beugnet A, Murakami M, Yamanaka S, Proud CG. Distinct signaling events downstream of mTOR cooperate to mediate the effects of amino acids and insulin on initiation factor 4E-binding proteins. *Mol Cell Biol* 2005; 25:2558-72; PMID:15767663; <http://dx.doi.org/10.1128/MCB.25.7.2558-2572.2005>
- [18] Corradetti MN, Guan K-L. Upstream of the mammalian target of rapamycin: do all roads pass through mTOR? *Oncogene* 2006; 25:6347-60; PMID:17041621; <http://dx.doi.org/10.1038/sj.onc.1209885>
- [19] Kalous J, Kubelka M, Solc P, Susor A, Motlík J. AKT (protein kinase B) is implicated in meiotic maturation of porcine oocytes. *Reprod Camb Engl* 2009; 138:645-54
- [20] Tomek W, Smiljakovic T. Activation of Akt (protein kinase B) stimulates metaphase I to metaphase II transition in bovine oocytes. *Reprod Camb Engl* 2005; 130:423-30
- [21] Tomek W, Melo Sterza FA, Kubelka M, Wollenhaupt K, Torner H, Anger M, Kanitz W. Regulation of translation during in vitro maturation of bovine oocytes: the role of MAP kinase, eIF4E (cap binding protein) phosphorylation, and eIF4E-BP1. *Biol Reprod* 2002; 66:1274-82; PMID:11967187; <http://dx.doi.org/10.1095/biolreprod66.5.1274>
- [22] Romasko EJ, Amarnath D, Midic U, Latham KE. Association of maternal mRNA and phosphorylated EIF4EBP1 variants with the spindle in mouse oocytes: localized translational control supporting female meiosis in mammals. *Genetics* 2013; 195:349-58; PMID:23852387; <http://dx.doi.org/10.1534/genetics.113.154005>
- [23] Mayer S, Wrenzycki C, Tomek W. Inactivation of mTOR arrests bovine oocytes in the metaphase-I stage, despite reversible inhibition of 4E-BP1 phosphorylation. *Mol Reprod Dev* 2014; 81:363-75; PMID:24459013; <http://dx.doi.org/10.1002/mrd.22305>
- [24] Lee S-E, Sun S-C, Choi H-Y, Uhm S-J, Kim N-H. mTOR is required for asymmetric division through small GTPases in mouse oocytes. *Mol Reprod Dev* 2012; 79:356-66; PMID:22407942; <http://dx.doi.org/10.1002/mrd.22035>
- [25] Poulin F, Gingras A-C, Olsen H, Chevalier S, Sonenberg N. 4E-BP3, a New Member of the Eukaryotic Initiation Factor 4E-binding Protein Family. *J Biol Chem* 1998; 273:14002-7; PMID:9593750; <http://dx.doi.org/10.1074/jbc.273.22.14002>
- [26] Pause A, Belsham GJ, Gingras AC, Donzé O, Lin TA, Lawrence JC, Sonenberg N. Insulin-dependent stimulation of protein synthesis by phosphorylation of a regulator of 5'-cap function. *Nature* 1994; 371:762-7; PMID:7935836; <http://dx.doi.org/10.1038/371762a0>
- [27] Gingras AC, Raught B, Sonenberg N. eIF4 initiation factors: effectors of mRNA recruitment to ribosomes and regulators of translation. *Annu Rev Biochem* 1999; 68:913-63; PMID:10872469; <http://dx.doi.org/10.1146/annurev.biochem.68.1.913>
- [28] Mader S, Lee H, Pause A, Sonenberg N. The translation initiation factor eIF-4E binds to a common motif shared by the translation factor eIF-4 gamma and the translational repressors 4E-binding proteins. *Mol Cell Biol* 1995; 15:4990-7; PMID:7651417; <http://dx.doi.org/10.1128/MCB.15.9.4990>
- [29] Tsukiyama-Kohara K, Vidal SM, Gingras AC, Glover TW, Hanash SM, Heng H, Sonenberg N. Tissue distribution, genomic structure, and chromosome mapping of mouse and human eukaryotic initiation factor 4E-binding proteins 1 and 2. *Genomics* 1996; 38:353-63; PMID:8975712; <http://dx.doi.org/10.1006/geno.1996.0638>
- [30] Fadden P, Haystead TA, Lawrence JC. Identification of phosphorylation sites in the translational regulator, PHAS-I, that are controlled by insulin and rapamycin in rat adipocytes. *J Biol Chem* 1997; 272:10240-7; PMID:9092573; <http://dx.doi.org/10.1074/jbc.272.15.10240>
- [31] Kogasaka Y, Hoshino Y, Hiradate Y, Tanemura K, Sato E. Distribution and association of mTOR with its cofactors, raptor and rictor, in cumulus cells and oocytes during meiotic maturation in mice. *Mol Reprod Dev* 2013; 80:334-48; PMID:23440873; <http://dx.doi.org/10.1002/mrd.22166>
- [32] Heesom KJ, Gampel A, Mellor H, Denton RM. Cell cycle-dependent phosphorylation of the translational repressor eIF-4E binding protein-1 (4E-BP1). *Curr Biol* 2001; 11:1374-9; PMID:11553333; [http://dx.doi.org/10.1016/S0960-9822\(01\)00422-5](http://dx.doi.org/10.1016/S0960-9822(01)00422-5)
- [33] Greenberg VL, Zimmer SG. Paclitaxel induces the phosphorylation of the eukaryotic translation initiation factor 4E-binding protein 1 through a Cdk1-dependent mechanism. *Oncogene* 2005; 24:4851-60; PMID:15897904; <http://dx.doi.org/10.1038/sj.onc.1208624>
- [34] Shuda M, Velásquez C, Cheng E, Cordek DG, Kwun HJ, Chang Y, Moore PS. CDK1 substitutes for mTOR kinase to activate mitotic cap-dependent protein translation. *Proc Natl Acad Sci U S A* 2015; 112:5875-82; PMID:25883264; <http://dx.doi.org/10.1073/pnas.1505787112>
- [35] Velásquez C, Cheng E, Shuda M, Lee-Oesterreich PJ, Pogge von Strandmann L, Gritsenko MA, Jacobs JM, Moore PS, Chang Y. Mitotic protein kinase CDK1 phosphorylation of mRNA translation regulator 4E-BP1 Ser83 may contribute to cell transformation. *Proc Natl Acad Sci U S A* 2016; 113:8466-71; PMID:27402756; <http://dx.doi.org/10.1073/pnas.1607768113>
- [36] Hampl A, Eppig JJ. Analysis of the mechanism(s) of metaphase I arrest in maturing mouse oocytes. *Development* 1995; 121:925-33; PMID:7743936
- [37] Wang X, Swain JE, Bollen M, Liu X-T, Ohl DA, Smith GD. Endogenous regulators of protein phosphatase-1 during mouse oocyte development and meiosis. *Reproduction* 2004; 128:493-502; PMID:15509695; <http://dx.doi.org/10.1530/rep.1.00173>
- [38] Shang ZF, Yu L, Li B, Tu WZ, Wang Y, Liu XD, Guan H, Huang B, Rang WQ, Zhou PK. 4E-BP1 participates in maintaining spindle integrity and genomic stability via interacting with PLK1. *Cell Cycle* 2012; 11:3463-71; PMID:22918237; <http://dx.doi.org/10.4161/cc.21770>
- [39] Lénárt P, Petronczki M, Steegmaier M, Di Fiore B, Lipp JJ, Hoffmann M, Rettig WJ, Kraut N, Peters J-M. The small-molecule inhibitor BI 2536 reveals novel insights into mitotic roles of polo-like kinase 1. *Curr Biol CB* 2007; 17:304-15; PMID:17291761; <http://dx.doi.org/10.1016/j.cub.2006.12.046>
- [40] Katska L, Bochenek M, Kania G, Ryńska B, Smorag Z. Flow cytometric cell cycle analysis of somatic cells primary cultures established for bovine cloning. *Theriogenology* 2002; 58:1733-44; PMID:12472143; [http://dx.doi.org/10.1016/S0093-691X\(02\)01043-9](http://dx.doi.org/10.1016/S0093-691X(02)01043-9)
- [41] Thoreen CC, Chantranupong L, Keys HR, Wang T, Gray NS, Sabatini DM. A unifying model for mTORC1-mediated regulation of mRNA translation. *Nature* 2012; 485:109-13; PMID:22552098; <http://dx.doi.org/10.1038/nature11083>
- [42] Tsukiyama-Kohara K, Poulin F, Kohara M, DeMaria CT, Cheng A, Wu Z, Gingras AC, Katsume A, Elchebly M, Spiegelman BM, et al. Adipose tissue reduction in mice lacking the translational inhibitor 4E-BP1. *Nat Med* 2001; 7:1128-32; PMID:11590436; <http://dx.doi.org/10.1038/nm1001-1128>
- [43] Vazquez-Martin A, Oliveras-Ferraras C, Bernadó L, López-Bonet E, Menendez JA. The serine 2481-autophosphorylated form of mammalian Target Of Rapamycin (mTOR) is localized to midzone and midbody in dividing cancer cells. *Biochem Biophys Res Commun* 2009; 380:638-43; PMID:19285014; <http://dx.doi.org/10.1016/j.bbrc.2009.01.153>
- [44] He Z, Wu J, Dang H, Lin H, Zheng H, Zhong D. Polo-like kinase 1 contributes to the tumorigenicity of BEL-7402 hepatoma cells via regulation of Survivin expression. *Cancer Lett* 2011; 303:92-8; PMID:21330050; <http://dx.doi.org/10.1016/j.canlet.2011.01.007>
- [45] Makker A, Goel MM, Mahdi AA. PI3K/PTEN/Akt and TSC/mTOR signaling pathways, ovarian dysfunction, and infertility: an update. *J Mol Endocrinol* 2014; 53:R103-118; PMID:25312969; <http://dx.doi.org/10.1530/JME-14-0220>
- [46] Schweizer N, Pawar N, Weiss M, Maiato H. An organelle-exclusion envelope assists mitosis and underlies distinct molecular crowding in the spindle region. *J Cell Biol* 2015; 210:695-704; PMID:26304726; <http://dx.doi.org/10.1083/jcb.201506107>
- [47] Yu Y, Dumollard R, Rossbach A, Lai FA, Swann K. Redistribution of mitochondria leads to bursts of ATP production during spontaneous mouse oocyte maturation. *J Cell Physiol* 2010; 224:672-80; PMID:20578238; <http://dx.doi.org/10.1002/jcp.22171>
- [48] Yi K, Rubinstein B, Unruh JR, Guo F, Slaughter BD, Li R. Sequential actin-based pushing forces drive meiosis I chromosome migration



- and symmetry breaking in oocytes. *J Cell Biol* 2013; 200:567-76; PMID:23439682; <http://dx.doi.org/10.1083/jcb.201211068>
- [49] FitzHarris G, Marangos P, Carroll J. Changes in endoplasmic reticulum structure during mouse oocyte maturation are controlled by the cytoskeleton and cytoplasmic dynein. *Dev Biol* 2007; 305:133-44; PMID:17368610; <http://dx.doi.org/10.1016/j.ydbio.2007.02.006>
- [50] Dalton CM, Carroll J. Biased inheritance of mitochondria during asymmetric cell division in the mouse oocyte. *J Cell Sci* 2013; 126:2955-64; PMID:23659999; <http://dx.doi.org/10.1242/jcs.128744>
- [51] Schlaitz A-L, Thompson J, Wong CCL, Yates JR, Heald R. REEP3/4 ensure endoplasmic reticulum clearance from metaphase chromatin and proper nuclear envelope architecture. *Dev Cell* 2013; 26:315-23; PMID:23911198; <http://dx.doi.org/10.1016/j.devcel.2013.06.016>
- [52] Bomar J, Moreira P, Balise JJ, Collas P. Differential regulation of maternal and paternal chromosome condensation in mitotic zygotes. *J Cell Sci* 2002; 115:2931-40; PMID:12082153
- [53] Blower MD, Feric E, Weis K, Heald R. Genome-wide analysis demonstrates conserved localization of messenger RNAs to mitotic microtubules. *J Cell Biol* 2007; 179:1365-73; PMID:18166649; <http://dx.doi.org/10.1083/jcb.200705163>
- [54] Eliscovich C, Peset I, Vernos I, Méndez R. Spindle-localized CPE-mediated translation controls meiotic chromosome segregation. *Nat Cell Biol* 2008; 10:858-65; PMID:18536713; <http://dx.doi.org/10.1038/ncb1746>
- [55] Mili S, Macara IG. RNA localization and polarity: from A(PC) to Z (BP). *Trends Cell Biol* 2009; 19:156-64; PMID:19251418; <http://dx.doi.org/10.1016/j.tcb.2009.02.001>
- [56] Lécuyer E, Yoshida H, Parthasarathy N, Alm C, Babak T, Cerovina T, Hughes TR, Tomancak P, Krause HM. Global Analysis of mRNA localization reveals a prominent role in organizing cellular architecture and function. *Cell* 2007; 131:174-87; PMID:17923096; <http://dx.doi.org/10.1016/j.cell.2007.08.003>
- [57] Bolton EM, Tuzova AV, Walsh AL, Lynch T, Perry AS. Noncoding RNAs in prostate cancer: the long and the short of it. *Clin Cancer Res Off J Am Assoc Cancer Res* 2014; 20:35-43; <http://dx.doi.org/10.1158/1078-0432.CCR-13-1989>
- [58] Fujita Y, Hayashi T, Kiyomitsu T, Toyoda Y, Kokubu A, Obuse C, Yanagida M. Priming of centromere for CENP-A recruitment by human hMis18alpha, hMis18beta, and M18BP1. *Dev Cell* 2007; 12:17-30; PMID:17199038; <http://dx.doi.org/10.1016/j.devcel.2006.11.002>
- [59] Jambor H, Surendranath V, Kalinka AT, Mejsstrik P, Saalfeld S, Tomancak P. Systematic imaging reveals features and changing localization of mRNAs in *Drosophila* development. *Elife* 2015; 4:e05003; PMID:25838129; <http://dx.doi.org/10.1080/15384101.2017.1295178>
- [60] Susor A, Jansova D, Anger M, Kubelka M. Translation in the mammalian oocyte in space and time. *Cell Tissue Res* 2016; 363:69-84; PMID:26340983; <http://dx.doi.org/10.1007/s00441-015-2269-6>
- [61] Guertin DA, Sabatini DM. Defining the role of mTOR in cancer. *Cancer Cell* 2007; 12:9-22; PMID:17613433; <http://dx.doi.org/10.1016/j.ccr.2007.05.008>
- [62] Gwinn DM, Asara JM, Shaw RJ. Raptor is phosphorylated by cdc2 during mitosis. *PLoS One* 2010; 5:e9197; PMID:20169205; <http://dx.doi.org/10.1371/journal.pone.0009197>
- [63] Papst PJ, Sugiyama H, Nagasawa M, Lucas JJ, Maller JL, Terada N. Cdc2-Cyclin B Phosphorylates p70 S6 Kinase on Ser411 at Mitosis. *J Biol Chem* 1998; 273:15077-84; PMID:9614117; <http://dx.doi.org/10.1074/jbc.273.24.15077>
- [64] Bellé R, Minella O, Cormier P, Morales J, Poulhe R, Mulner-Lorillon O. Phosphorylation of elongation factor-1 (EF-1) by cdc2 kinase [Internet]. In: Meijer L, Guidet S, Tung HYL, editors. *Progress in Cell Cycle Research*. Boston, MA: Springer US; 1995 [cited 2016 Aug 2]. 265-70. Available from: [http://link.springer.com/10.1007/978-1-4615-1809-9\\_21](http://link.springer.com/10.1007/978-1-4615-1809-9_21)
- [65] Schultz RM, LaMarca MJ, Wassarman PM. Absolute rates of protein synthesis during meiotic maturation of mammalian oocytes in vitro. *Proc Natl Acad Sci* 1978; 75:4160-4; PMID:279905; <http://dx.doi.org/10.1073/pnas.75.9.4160>
- [66] King DW, Barnhisel ML. Synthesis of RNA in mammalian cells during mitosis and interphase. *J Cell Biol* 1967; 33:265-72; PMID:6039370; <http://dx.doi.org/10.1083/jcb.33.2.265>
- [67] Pyronnet S, Pradayrol L, Sonenberg N. A cell cycle-dependent internal ribosome entry site. *Mol Cell* 2000; 5:607-16; PMID:10882097; [http://dx.doi.org/10.1016/S1097-2765\(00\)80240-3](http://dx.doi.org/10.1016/S1097-2765(00)80240-3)
- [68] Vander Haar E, Lee S-I, Bandhakavi S, Griffin TJ, Kim D-H. Insulin signalling to mTOR mediated by the Akt/PKB substrate PRAS40. *Nat Cell Biol* 2007; 9:316-23; PMID:17277771; <http://dx.doi.org/10.1038/ncb1547>
- [69] Wang Q, Ratchford AM, Chi MM-Y, Schoeller E, Frolova A, Schedl T, Moley KH. Maternal diabetes causes mitochondrial dysfunction and meiotic defects in murine oocytes. *Mol Endocrinol* 2009; 23:1603-12; PMID:19574447; <http://dx.doi.org/10.1210/me.2009-0033>
- [70] Chen J, Chen S, Chen Y, Zhang C, Wang J, Zhang W, Liu G, Zhao B, Chen Y. Circulating endothelial progenitor cells and cellular membrane microparticles in db/db diabetic mouse: possible implications in cerebral ischemic damage. *Am J Physiol Endocrinol Metab* 2011; 301:E62-71; PMID:21505143; <http://dx.doi.org/10.1152/ajpendo.00026.2011>
- [71] Bonatti S, Simili M, Galli A, Bagnato P, Pigullo S, Schiestl RH, Abbondandolo A. Inhibition of the Mr 70,000 S6 kinase pathway by rapamycin results in chromosome malsegregation in yeast and mammalian cells. *Chromosoma* 1998; 107:498-506; PMID:9914383; <http://dx.doi.org/10.1007/s004120050335>
- [72] Jang C-Y, Kim HD, Zhang X, Chang J-S, Kim J. Ribosomal protein S3 localizes on the mitotic spindle and functions as a microtubule associated protein in mitosis. *Biochem Biophys Res Commun* 2012; 429:57-62; PMID:23131551; <http://dx.doi.org/10.1016/j.bbrc.2012.10.093>
- [73] Susor A, Kubelka M. Translational regulation in the mammalian oocyte. In: *Oocytes - Maternal information and functions. Results and problems in cell differentiation*. Boston, MA: Springer US; 2017.
- [74] Tetkova A, Hancova M. *Mouse Oocyte Isolation, Cultivation and RNA Microinjection —BIO-PROTOCOL*; 6:e1729; <https://dx.doi.org/10.21769/BioProtoc.1729>
- [75] Safran M, Kim WY, O'Connell F, Flippin L, Günzler V, Horner JW, Depinho RA, Kaelin WG. Mouse model for noninvasive imaging of HIF prolyl hydroxylase activity: assessment of an oral agent that stimulates erythropoietin production. *Proc Natl Acad Sci U S A* 2006; 103:105-10; PMID:16373502; <http://dx.doi.org/10.1073/pnas.0509459103>



Article

# Increased Expression of Maturation Promoting Factor Components Speeds Up Meiosis in Oocytes from Aged Females

Marketa Koncicka <sup>1,2</sup> , Anna Tetkova <sup>1,2</sup> , Denisa Jansova <sup>1</sup> , Edgar Del Llano <sup>1,2,3</sup> , Lenka Gahurova <sup>1,4</sup> , Jana Kracmarova <sup>1</sup>, Sarka Prokesova <sup>1</sup>, Tomas Masek <sup>3</sup>, Martin Pospisek <sup>3</sup>, Alexander W. Bruce <sup>4</sup> , Michal Kubelka <sup>1</sup> and Andrej Susor <sup>1,\*</sup>

<sup>1</sup> Laboratory of Biochemistry and Molecular Biology of Germ Cells, Institute of Animal Physiology and Genetics, CAS, Rumburska 89, 277 21 Libechov, Czech Republic; Koncicka@iapg.cas.cz (M.K.); tetkova@iapg.cas.cz (A.T.); jansova@iapg.cas.cz (D.J.); Llano@iapg.cas.cz (E.D.L.); lveselovska@prf.jcu.cz (L.G.); kracmarova@iapg.cas.cz (J.K.); prokesovas@af.czu.cz (S.P.); kubelka@iapg.cas.cz (M.K.)

<sup>2</sup> Department of Cell Biology, Faculty of Science, Charles University in Prague, Albertov 6, 128 43 Prague, Czech Republic

<sup>3</sup> Department of Genetics and Microbiology, Faculty of Science, Charles University in Prague, Albertov 6, 128 43 Prague, Czech Republic; masek@natur.cuni.cz (T.M.); martin.pospisek@natur.cuni.cz (M.P.)

<sup>4</sup> Laboratory of early mammalian development, Department of Molecular Biology and Genetics, Faculty of Science, University of South Bohemia, Branisovska 1760, 370 05 Ceske Budejovice, Czech Republic; awbruce@prf.jcu.cz

\* Correspondence: susor@iapg.cas.cz

Received: 17 August 2018; Accepted: 17 September 2018; Published: 19 September 2018



**Abstract:** The rate of chromosome segregation errors that emerge during meiosis I in the mammalian female germ line are known to increase with maternal age; however, little is known about the underlying molecular mechanism. The objective of this study was to analyze meiotic progression of mouse oocytes in relation to maternal age. Using the mouse as a model system, we analyzed the timing of nuclear envelope breakdown and the morphology of the nuclear lamina of oocytes obtained from young (2 months old) and aged females (12 months old). Oocytes obtained from older females display a significantly faster progression through meiosis I compared to the ones obtained from younger females. Furthermore, in oocytes from aged females, lamin A/C structures exhibit rapid phosphorylation and dissociation. Additionally, we also found an increased abundance of MPF components and increased translation of factors controlling translational activity in the oocytes of aged females. In conclusion, the elevated MPF activity observed in aged female oocytes affects precocious meiotic processes that can multifactorially contribute to chromosomal errors in meiosis I.

**Keywords:** aging; oocyte; MPF; meiosis; translation; lamin A/C

## 1. Introduction

The development of female germ cells (oocytes) is essential for sexual reproduction. Oocytes, arrested in meiotic prophase, undergo a major growth phase during their development in ovarian follicles. During this phase, they actively transcribe their genome; however, most derived mRNAs are stored in ribonucleoprotein particles to be used much later during the final stages of meiosis and early embryonic development. A unique property of the oocyte is that the final stages of meiosis (after prophase I) occur in the absence of de novo transcription. Consequently, regulation of mRNA stability and translation serves as the main driving forces behind oogenesis and early embryogenesis [1].

Mammalian oocytes undergo two successive cell divisions without an intermediate replicative phase. This brief period is called “meiotic maturation” and is crucial for the formation of an egg capable of being fertilized and for the generation of viable and euploid offspring. At the onset of meiosis I, the nuclear lamina is phosphorylated (namely lamin A/C; LMN A/C) and disassembled, leading to nuclear envelope break down (NEBD), chromosome condensation, and progressive reorganization of microtubules into a bipolar spindle [2]. At the end of meiosis I, the first asymmetric division occurs.

Human and mouse oocytes are vulnerable to aging as the incidence of chromosome segregation errors (aneuploidy) reaches high levels in females/mothers of advanced age [3–5]. For example, in 20-year-old women, aneuploidy occurs in ~2% of matured oocytes; however, after 35 years of age aneuploidy increases to 35% [6,7]. Similarly, oocytes from aged mice display a significant increase in the incidence of aneuploidy. In three-month-old mice, aneuploidy occurs in 5% of cases; however, by 12 months of age this figure increases to 30–50% [4,8,9]. The majority of chromosome segregation errors are known to arise during the first meiotic cytokinesis [6,10]; however, the reasons why female meiosis shows this peculiar vulnerability to aging remains unclear.

In this study, we present evidence for the aberrant timing of meiosis I in the oocytes derived from female mice of advanced age. Such age-associated abnormalities present as aberrations in nuclear envelope morphology as well as the precocious timing of NEBD and the formation of kinetochore-microtubule (K-MT) attachments, resulting in accelerated first polar body extrusion (PBE). Furthermore, we reveal that it is the overexpression of metaphase promoting factor (MPF) components associated with impaired translational machinery that leads to this phenotype.

## 2. Results

### 2.1. Meiosis I Is Accelerated in Oocytes from Females of Advanced Age

It is well known that increased maternal age negatively affects oocyte quality [3,5]. We isolated oocytes from antral follicles and obtained an average of 22 fully grown GV oocytes per young mouse (YF; 2 months old) compared to 3 oocytes per aged female (AF; 12 months old). Following removal of IBMX from the culture medium, to restart meiosis I, 98.75% of selected oocytes from young females and 98.53% oocytes from aged females resumed meiosis (NEBD; Student's *t*-test  $p = 0.9985$ ). Of the cells that resumed meiosis, 84% of the young oocytes extruded polar body and reached MII in the 12 h period compared to 94% of AF oocytes (Student's *t*-test  $p = 0.010809$ ). Measurement of oocyte diameter did not show any differences between age groups ( $71.73 \pm 1.5$  and  $72.31 \pm 1.6$   $\mu\text{m}$ , respectively, Student's *t*-test  $p = 0.99743$ ). To analyze the effect of maternal age on the progress of meiosis I, we compared the maturation of mouse oocytes from young females (YF; 2 months old) and aged females (AF; 12 months old). Time-lapse microscopy revealed that the oocytes from AF progress through meiosis I significantly 30 min faster than oocytes from YF ( $p < 0.05$ ; Figure 1a,b). The oocytes in the AF group initiate nuclear envelope breakdown (NEBD) earlier (Figure 1a) and consequently polar body extrusion (PBE) also occurs earlier than in the YF group ( $p < 0.05$ ; Figure 1b); manifest as a shortening of time between NEBD and PBE (Figure 1b). Next, we scored the attachment of individual cold-stable microtubules (MT) with end-on kinetochores in both age groups. We found that, during metaphase I, 6 h after releasing oocytes from prophase I (6 h post-IBMX-wash), the AF group had a higher number of stably attached kinetochores (95.5%) than the YF group (75.8%,  $p < 0.01$ ) (Figure 1c,d). The larger number of stably end-on attached kinetochores in the AF group demonstrates that the progression through meiosis I was accelerated in the oocytes from the AF group.

### 2.2. Dissociation of Nuclear Envelope Is Accelerated in the Oocytes from Aged Females

The abundant components of the nuclear envelope are lamin A and C (LMN A/C) [11]. Phosphorylation of these lamins at Serine-22 (Ser22) triggers the disassembly of the nuclear lamina, which is a prerequisite for nuclear envelope breakdown [12]. Therefore, we analyzed the phosphorylation of LMN A/C (Ser22) as a marker of meiotic progression. Oocytes from both age

groups were analyzed by Western blotting at various time points relative to their initial isolation (i.e., after 0, 1, 3, 6, and 12 h). We found that the AF group had a significantly increased level of phosphorylated LMN A/C 1 h post-IBMX-wash ( $p < 0.05$ ; Figure 2a,b). On the contrary, the YF group only had an abundant level of phosphorylated LMN A/C 3 h post-IBMX-wash (Figure 2a,b). Despite the observed different timing of LMN A/C phosphorylation between these two groups, the total/eventual level of LMN A/C remained constant (Figure 2a,c).

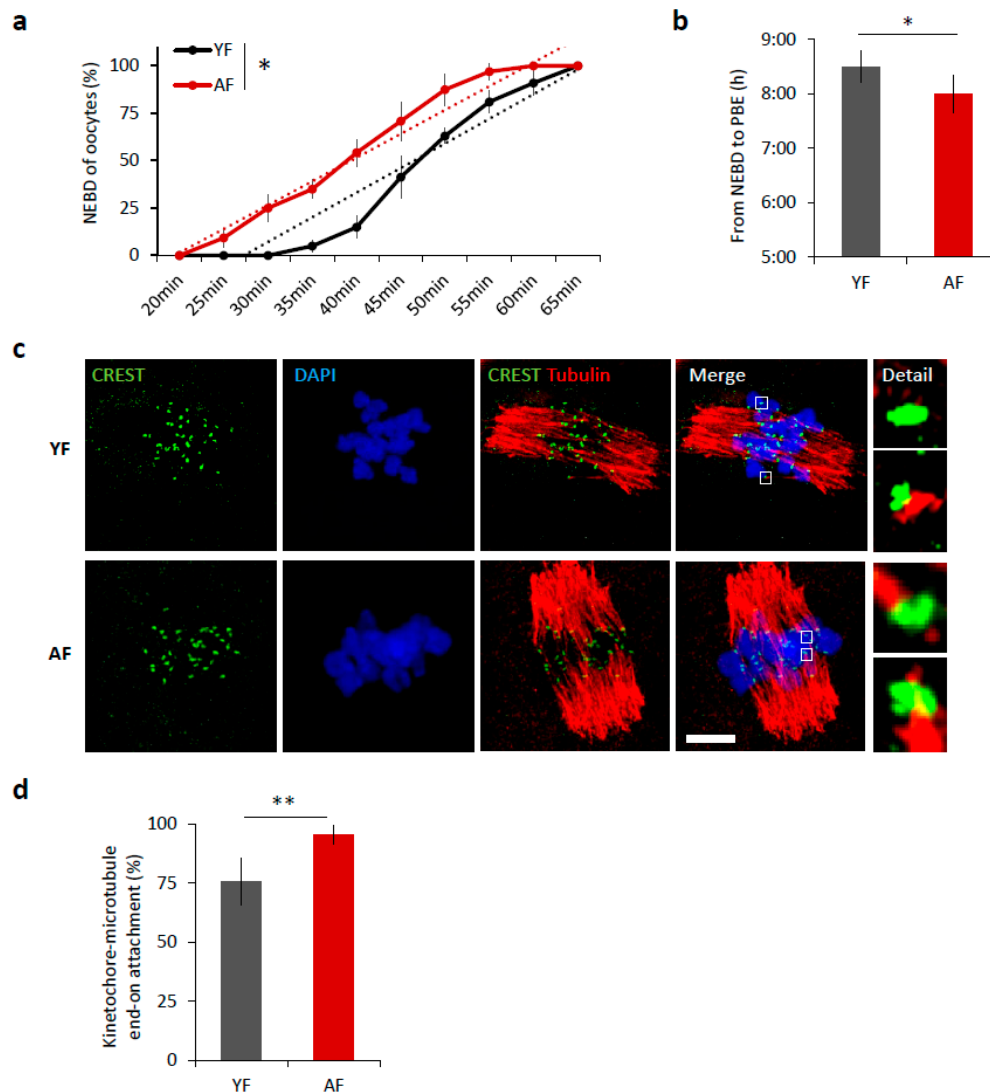


**Figure 1.** Meiosis I is accelerated in oocytes from females of advanced age. **(a)** Timing of nuclear envelope breakdown (NEBD) of oocytes isolated from young females (YF,  $n = 80$ ; black line) and aged females (AF,  $n = 68$ ; red line). Trend line is depicted by dot line. Data represent mean  $\pm$  SD,  $n = 6$ ,  $* p < 0.05$ , Student's  $t$ -test. **(b)** Time from NEBD to polar body extrusion (PBE) in oocytes from YF ( $n = 80$ ;  $t = 8:30$  h) and AF ( $n = 68$ ;  $t = 8$  h). Data represent mean  $\pm$  SD and data are from at least three experiments of biologically different samples.  $* p < 0.05$ , Student's  $t$ -test. **(c)** Representative Z-projections from the assessment of cold stable attachments of kinetochore (KT) to microtubule (MT) imaged by confocal microscopy using CREST (green) and Tubulin (red) antibodies. Representative images from three experiments of biologically different samples are presented (scale bar, 10  $\mu$ m). **(d)** The percentage of cold stable end-on MT to KT attachments in each age group averaged over multiple cells ( $n \geq 15$ ) 6 h post-IBMX-wash. Kinetochore-MT end-on attachments were quantified. The morphology of kinetochores analyzed is specified in detail. Data represent mean  $\pm$  SD.  $** p < 0.01$ , Student's  $t$ -test.

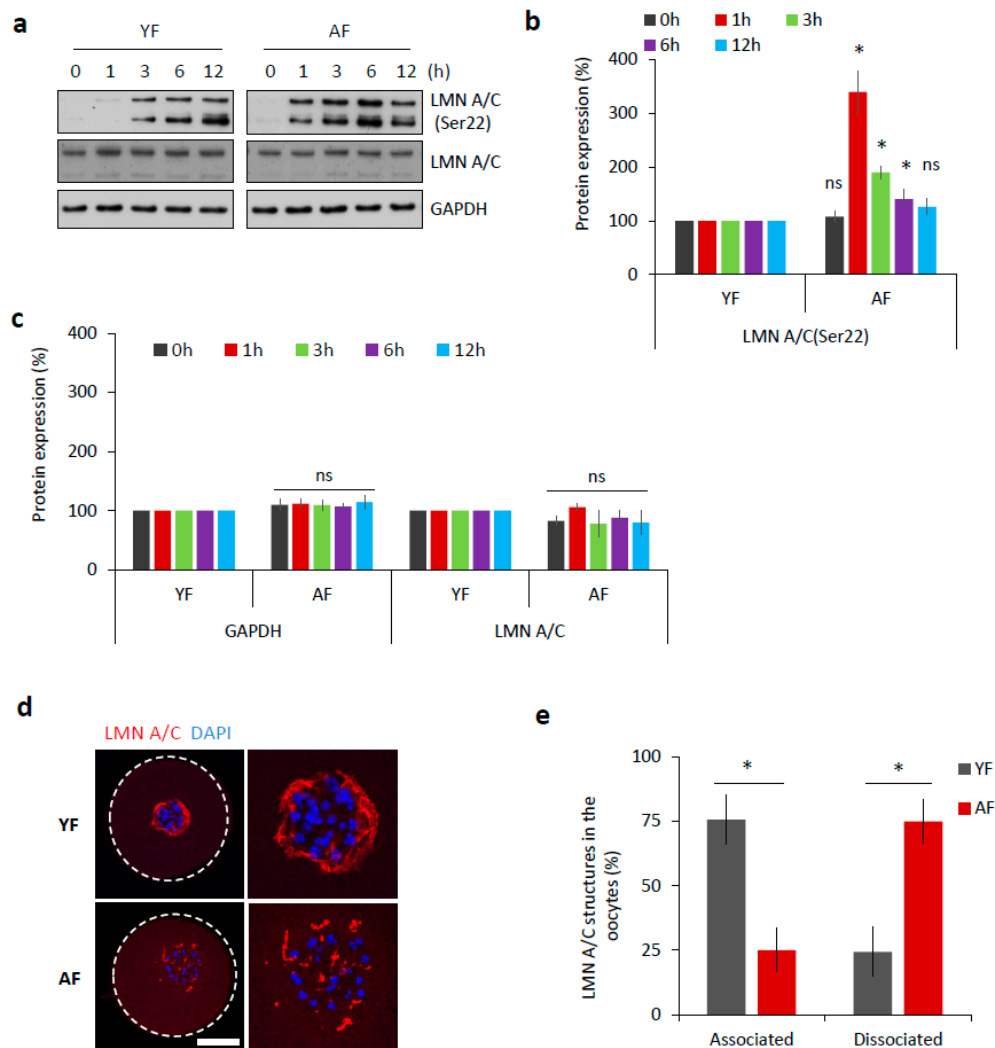


**Figure 2.** Dissociation of nuclear lamina is accelerated in the oocytes from the AF group. (a) Western blot analysis of phosphorylation status of LMN A/C (Ser22) at different time points during meiotic progression (0 h, GV; 1 h, post-NEBD; 3 h, post-NEBD; 6 h, post-NEBD/metaphase I; 12 h, post-NEBD/metaphase II). Antibodies against LMN A/C and GAPDH were used as loading controls. Representative images are from three experiments of biologically different samples. (b) Quantification of LMN A/C phosphorylation (Ser22) at different time points during meiotic maturation. Data are from three experiments of biologically different samples. Values obtained for the YF group were set as 100%. AF values from each antibody was compared between groups and same oocyte stage. Data represent mean  $\pm$  SD. \*  $p < 0.05$ , bars with ns are non-significant, Student's *t*-test. (c) Quantification of GAPDH and LMN A/C protein expression at different time points during meiotic maturation. Data are from three experiments of biologically different samples. Values obtained for the YF group were set as 100%. AF values from each antibody was compared between groups and same oocyte stage. Data represent mean  $\pm$  SD. \*  $p < 0.05$ , bars with ns are non-significant, Student's *t*-test. (d) Representative images of LMN A/C structures 3 h post-IBMX-wash (post-NEBD, scale bar 20  $\mu$ m). The cortex of the oocyte indicated by the white dashed line. See Figure S1 for the LMN A/C localization and phosphorylation during oocyte meiotic progression and Figure S2 for electron microscopy images of the nuclear lamina. (e) Quantification of LMN A/C structures in the oocytes from different age groups post-NEBD ( $n \geq 33$  and three independent biological replicates). Data represent mean  $\pm$  SD. \*  $p < 0.05$ , Student's *t*-test.

It has been previously documented [13,14] that nuclear lamina structures can be still present at least a few hours after NEBD in mouse oocytes. By immunocytochemistry (ICC), we visualized LMN A/C structures during oocyte meiotic maturation (Figure S1a,b). Using specific antibodies,



both total LMN A/C as well as phosphorylated LMN A/C (Ser22) were detected within the disrupted nuclear lamina structures in NEBD stage oocytes, 3 h post-IBMX-wash (Figure S1a,b). The observed lamina structures surrounded the chromosomal area, where the new spindle was due to be assembled (Figure S1c), but disappeared as meiosis progressed (Figure S1). When we compared 3 h post-IBMX-wash oocytes from both age groups, we found that the dissociation of the described LMN A/C structures was completed significantly faster in the AF group, at a time-point at which they still persisted in the YF oocytes ( $p < 0.05$ ; Figure 2d,e).

Additionally, we imaged GV stage oocytes (oocytes with intact nucleus designated as germinal vesicle, GV) from both age groups by transmission electron microscopy and we were able to distinguish visible differences in the structure of the nuclear envelope in both groups. The nuclear membrane of AF oocytes presented an unique characteristic series of invaginations and decreased compactness (Figure S2a,b). The distinct morphology of the nuclear envelope in the AF oocyte group resulted in a significant increase in the circumference of the nuclear envelope ( $p < 0.01$ ; Figure S2b). Moreover, the observed ultrastructural morphology of the nuclear lamina in AF oocytes resembled that reported in the nuclear phenotypes of other aged cells [15,16].

To conclude, in addition to the above-mentioned precocious timing in meiosis, observed in AF oocytes, we also observed a comparatively earlier phosphorylation of LMN A/C that was associated with a faster disassembly of nuclear lamina, thus affecting the timing of nuclear membrane breakdown, when compared to oocytes from the YF group.

### 2.3. CDK1 Activity Is Responsible for NEBD in Mouse Oocytes

NEBD is reported to be driven by CDK1 (MPF) activity via phosphorylation of lamin proteins and subsequent lamina disassembly at the onset of meiotic resumption or mitosis [17,18]. To test whether LMN A/C were phosphorylated in a CDK1-dependent manner, we treated mouse oocytes with 20  $\mu$ M Roscovitine (Rosco), a potent inhibitor of CDK1 activity, for 2 h after NEBD. We found significantly decreased levels of LMN A/C (Ser22) phosphorylation in oocytes treated with Rosco ( $p < 0.05$ ; Figure 3a,b) versus controls, a result that is consistent with findings of [17].

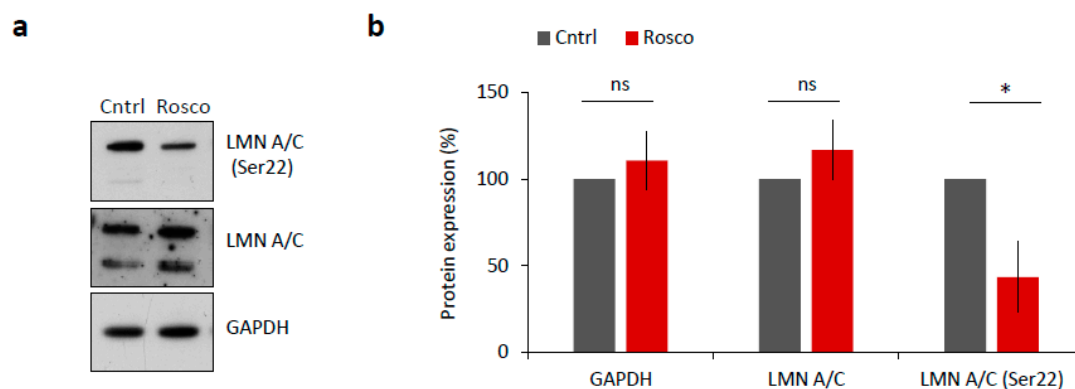


**Figure 3.** CDK1 is responsible for LMN A/C phosphorylation in mouse oocyte. (a) Western blot analysis of oocyte samples treated for 2 h after NEBD with 20  $\mu$ M CDK1 inhibitor, Roscovitine (Rosco). Phosphorylation status of LMN A/C (Ser22) was detected using a specific antibody. Antibodies against LMN A/C and GAPDH were used as a loading control. (b) Quantification of total and phosphorylated LMN A/C after Roscovitine (Rosco) treatment. Protein levels were normalized in a way that non-treated controls are 100%. Data was derived from three experiments containing biologically different samples. Columns represent mean,  $\pm$  SD; ns non-significant; \*  $p < 0.05$ , Student's *t*-test.

Thus, our data confirm the functional involvement of the activated MPF in nuclear lamina disassembly through regulation of LMN A/C phosphorylation status.

#### 2.4. CDK1 Activity Is Increased in Mouse Oocytes from Aged Females

We next examined, whether the expression of MPF components, that directly affect meiotic progression [19], differs between the YF and AF groups of mouse oocytes. Firstly, we isolated total RNA from transcriptionally silent GV staged oocytes from each group and performed quantitative RT-PCR mRNA expression analysis of the MPF component genes *Cdk1* and the B-type *Cyclins*. We found significantly increased levels of both *Cdk1* and *Cyclin B* transcripts in the oocytes from the AF group (Figure 4a) that were not reflected in the total RNA content (Figure S3a) nor in the expression level of *Gapdh* mRNA (Figure 4a). Next we analyzed the expression of MPF components at the protein level via Western blotting, and again we discovered a significant increase in the expression levels of CCNB and CDK1 proteins, specifically in the AF group of oocytes (Figure 4b,c). In addition to the use of a pan-CDK1 antibody, we also probed the oocyte samples with an antibody that specifically recognized phosphorylated (Thr161) CDK1, the enzymatically active form of the protein that is required for a functional MPF activity [19–22]. Again, we found increased phosphorylation status of CDK1 in the AF group versus the YF group of oocytes (Figure 4d,e). Consistently, an analysis of MPF activity, using a standard kinase assay, also revealed a significant increase in CDK1 activity at 1 h in the AF oocytes compared with the YF oocytes, at the time of NEBD (Figure 4d,e).

Taking these results together, we conclude that the activation of the MPF is significantly accelerated in the oocytes from aged females.

#### 2.5. Translation of Positive Regulators of Translation Is Increased in the Oocytes from Aged Females

De novo transcription in fully grown oocytes ceased, so we wondered whether the elevated levels of CCNB and CDK1 proteins in the oocytes from aged females were only due to higher transcript abundance or could also be related to higher translational activity. To experimentally address this question, we compared the incorporation of <sup>35</sup>S-Methionine into nascently translated proteins in both the YF and AF groups of oocytes during maturation (Figure S3b), but we found no significant difference in the levels of global translation (Figure S3b,c). However, we also derived an RNA-seq dataset of mRNA polyribosomal occupancy that allowed us to detect and identify actively translated mRNAs in the two studied age groups of oocytes. Whilst the polysome occupancy was unchanged for mRNAs encoding GAPDH, CDK1, and CCNB1, we did intriguingly identify *Ccnb2*-derived transcripts enriched over 11-fold in polysomal fractions from AF compared to YF oocytes (Figure 5a). A further GO-term (gene ontology) enrichment analysis of polysome-bound mRNAs indicated a significant enrichment of mRNA coding for protein factors belonging to GO functional categories associated with translation initiation and regulation, specifically in the AF oocyte group ( $p$ -value =  $4.76\text{--}6.34 \times 10^{-6}$  for 38 individual mRNAs) (Figure 5b). Generally, this enrichment was higher and the respective categories contained more mRNAs in the AF group over the YF oocytes. We therefore systematically examined the polysome-bound mRNAs whose products are involved in the regulation of translation and revealed increased levels of mRNA coding for positive translation regulators, namely, eukaryotic translation initiation factors (eIF2D, eIF3E, eIF4B, eIF4E3, and eIF4G1), polyadenylation factors (PABPN1L and PABPN1), elongation factor (eEF2), and the number of ribosomal proteins (60S-RPL6, RPL10, RPL10A, RPL17, RPL19, RPL23A, RPL24, RPL37, RPL38; 40S-RPS6, RPS8, RPS9, RPS13, RPS16, and RPS25) in the AF group of oocytes (Figure 5c). Contrarily, we detected a decreased level of mRNA-polysome association for the elongation factor kinase (eEF2K), which is known to act as a suppressor of translational elongation (Figure 5c).

Overall, these results suggest that the translation of individual MPF components and of specific translational factors is elevated in AF oocytes, which is likely to result in changes in the physiology of oocytes from aged female mice.

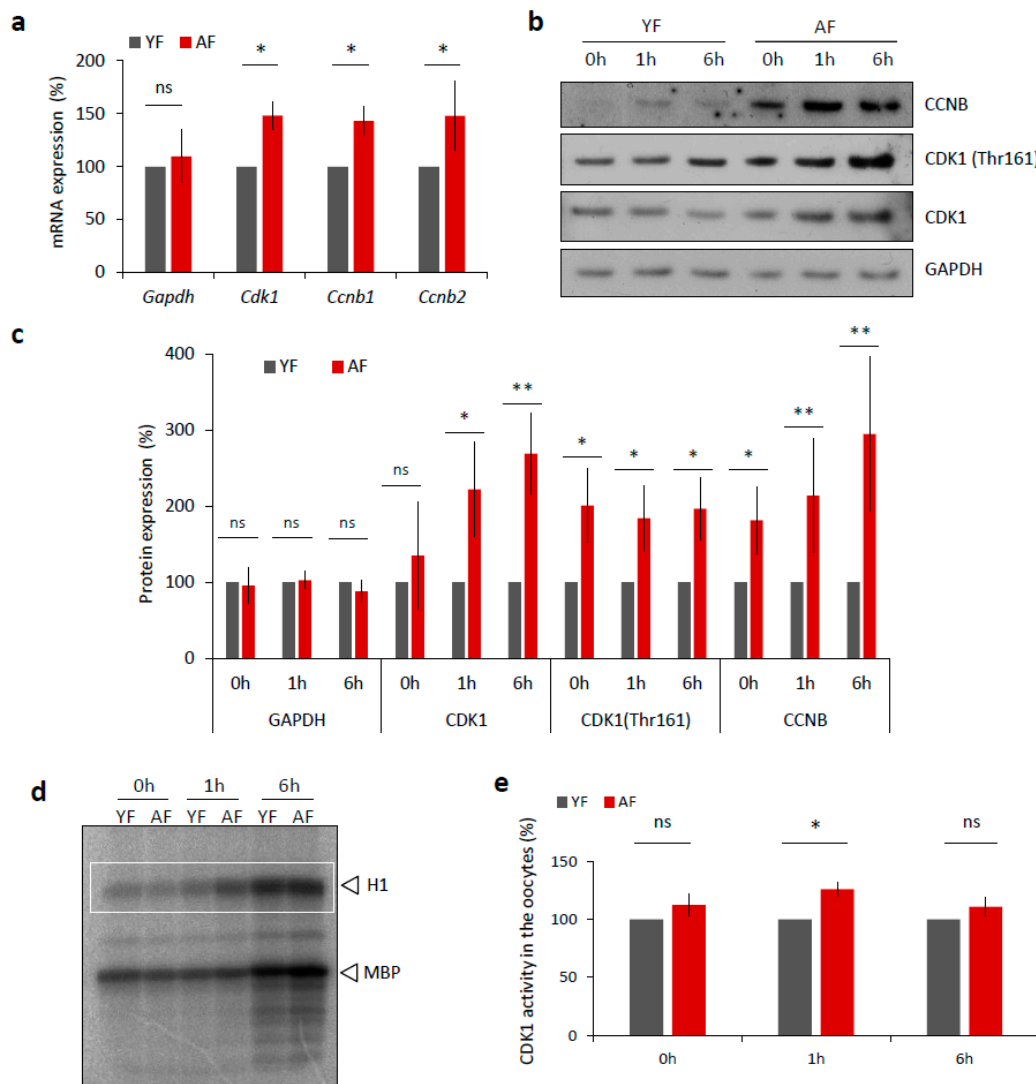


**Figure 4.** Expression of MPF components and its activity is increased in the oocytes from aged females. (a) RT-PCR quantification of mRNA coding for CDK1 and B-type cyclins, as well as loading control *Gapdh* in the GV oocytes (0 h) from different age groups. For quantification of total RNA content in oocytes from YF and AF groups see Figure S3a. Values obtained for the YF group were set as 100%. Data was derived from at least four experiments of biologically different samples. Columns represent mean; error bars  $\pm$  SD; ns non-significant; \*  $p < 0.05$ , Student's *t*-test. (b) Western blot analysis of CDK1, CDK1 (Thr161) and CCNB during oocyte maturation (0 h, 1 h and 6 h) in the both age groups. See Figure S3b,c for the assessment of global translation in oocytes from YF and AF groups. (c) Quantification of MPF components, CDK1, its phosphorylation (Thr161), CCNB and GAPDH as a loading control. Values obtained for the YF group were set as 100%. From at least three experiments of biologically different samples. Columns represent mean  $\pm$  SD; \*  $p < 0.05$ ; \*\*  $p < 0.01$ ; bars with ns are non-significant; Student's *t*-test. (d) Representative image of analysis of CDK1 activity (H1) in the oocytes after isolation (0 h), NEBD (1 h) and at metaphase I (6 h). Kinase assay was done with oocytes of both female age groups. CDK1 activity was measured towards histone H1 as external substrate, marked by white rectangle. (e) Quantification of CDK1 (H1 substrate) activity during oocyte maturation from YF and AF groups. Measurements originated from four experiments of biologically different samples. Values obtained for the YF group were set as 100%. Columns represent mean; error bars  $\pm$  SD; ns non-significant; \*  $p < 0.05$ ; Student's *t*-test.

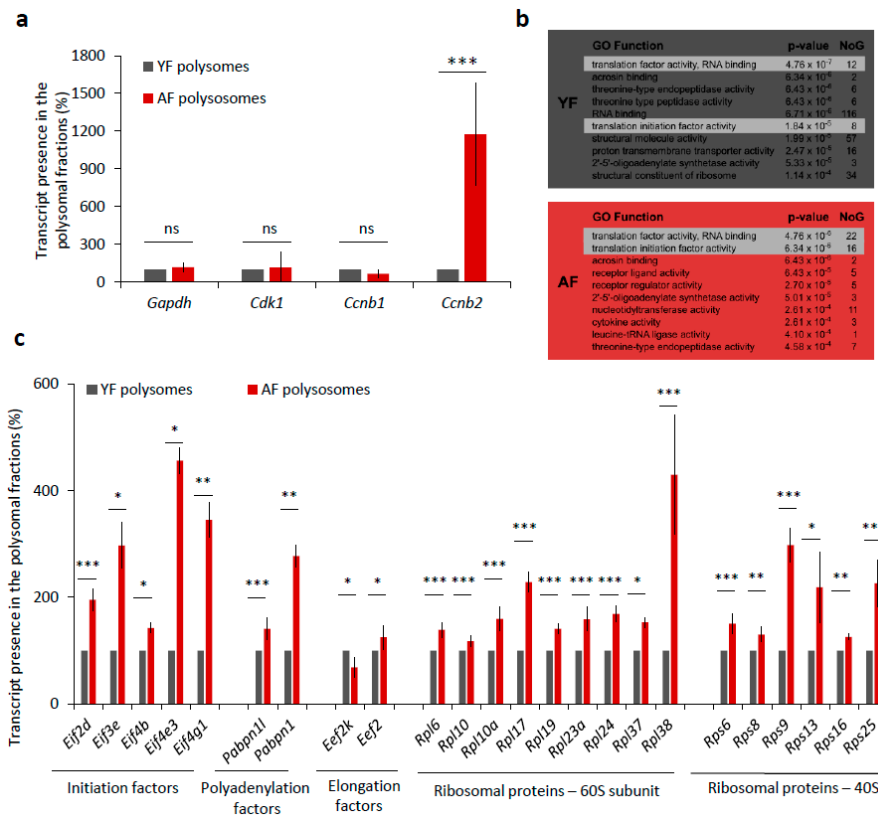


**Figure 5.** Translation of a number of translational factor components is increased in the oocytes from aged females. (a) mRNA abundance of MPF components, *Cdk1* and *Cyclins B* as well as *Gapdh* used as the control in the polyribosomal fractions. Percentage of reads from RNA-Seq. See Figure S3a for quantification of total RNA in oocytes from YF and AF groups. Three independent experimental datasets from biologically different samples. Values obtained for the YF group were set as 100%. Data columns represent mean; error bars,  $\pm$  SEM; ns non-significant; \*\*\*  $p < 0.001$ ; Student's *t*-test. (b) Top 10 most enriched GO Function categories in polysome-bound mRNAs in YF (grey) and AF (red) oocytes determined by Gorilla. NoG (Number of Genes) denotes the number of genes in enriched categories. Highlighted lines represent translational functional categories. (c) Translational regulation of mRNA coding for different translational factors from polysomal fractions of YF and AF oocytes. Values obtained for the YF group were set as 100%. Data represent mean  $\pm$  SEM; \*  $p < 0.05$ ; \*\*  $p < 0.01$ ; \*\*\*  $p < 0.001$ ; Student's *t*-test.

## 2.6. Elevated CDK1 Activity Is Responsible for Faster Meiosis I in Mouse Oocytes

It is known that the expression of CCNB is the limiting factor for the activation of MPF in oocytes prior to resumption of meiosis I [23,24]. It has been reported [25] that the slow increase in CDK1 activity during meiosis I acts as an intrinsic timing mechanism that ensures the appropriate stabilization of kinetochore attachments and thus guards the oocyte against chromosomal segregation errors. We examined whether the overexpression of CCNB affects the timing of meiotic progression. We overexpressed CCNB by microinjecting a cRNA encoding GFP-fused to CCNB into YF oocytes at the GV (0 h) stage (Figure S4). We also microinjected other GV oocytes with *Gfp* cRNA as a negative control. We found that, when experimenting with oocytes derived from the YF cohort, there was a significant increase ( $p < 0.05$ ) in the levels of phosphorylated LMN A/C (Ser22) and phosphorylated CDK1 (Thr161) when microinjected with *Ccnb:gfp* cRNA, as measured 3 h post-IBMX-wash compared to the control group (Figure 6a,b). Live cell imaging of meiotic progression/maturation of such oocytes revealed that the increased expression of CCNB was also able to significantly accelerate overall meiotic progression, as evaluated by the timing of the NEBD and PBE ( $p < 0.05$ ; Figure 6c,d). Specifically, oocytes injected with *Ccnb:gfp* extruded the polar body significantly earlier compared to the control

group (Figure 6c). Thus, they mimicked the phenotype observed in the AF oocytes (Figure 1). Moreover, we also visualized cold-stable kinetochore-microtubule end-on attachments [25,26] and found that the oocytes overexpressing CCNB had a significantly higher rate of the kinetochore-microtubule end-on attachment than the controls at the 6 h post-IBMX-wash ( $p < 0.05$ ; Figure 6e,f). These results suggest that artificially increasing MPF activity leads to a notably more rapid progression through meiosis I as exemplified by the production of stable kinetochore-microtubule attachments.

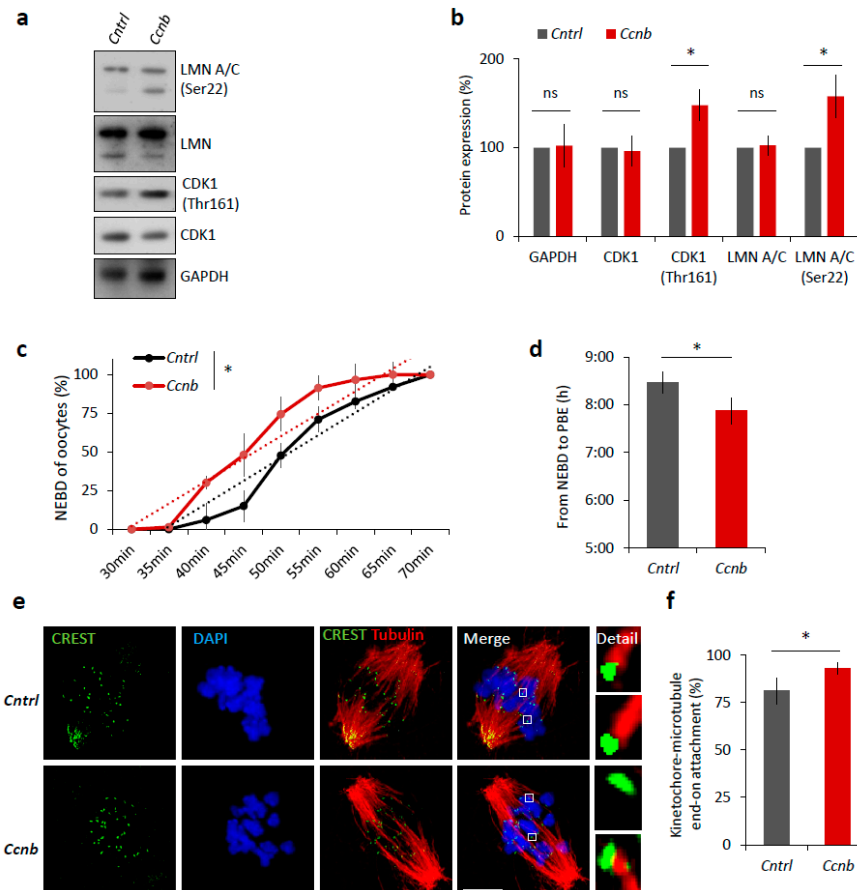


**Figure 6.** Elevated MPF activity is responsible for meiosis I acceleration in oocytes. **(a)** Western blot analysis of LMN A/C (Ser22), LMN A/C, CDK1 (Thr161), CDK1, and GAPDH in the post-NEBD oocytes (3 h) injected with *Ccnb* RNA or control *Gfp* RNA (*Cntrl*). See Figure S4 for the over-expression of CCNB in oocytes. Representative images from at least three experiments of biologically different samples. **(b)** Quantification of protein expression, LMN A/C, and CDK1 phosphorylation. From three experiments of biologically different samples. Values obtained for the YF group were set as 100%. Data represent mean  $\pm$  SD; ns non-significant; \*  $p < 0.05$ ; Student's *t*-test. **(c)** Timing of NEBD of YF oocytes microinjected with *Gfp* ( $n = 46$ ; black line) and *Ccnb* cRNA ( $n = 51$ ; red line). From three experimental data sets of biologically different samples. Trend line is depicted by dot lines. Data represent mean  $\pm$  SD. \*  $p < 0.05$ , Student's *t*-test. **(d)** Time from NEBD to PBE in oocytes from YF injected with RNA coding for *Gfp* ( $n = 46$ ;  $t = 8:25$  h) and *Ccnb* ( $n = 51$ ;  $t = 7:52$  h). Data represent mean  $\pm$  SD and data are from at least three experiments of biologically different samples. Student's *t*-test. **(e)** Representative Z-projections from the assessment of cold stable attachments of kinetochores (KT, CREST, green) to microtubule (MT, tubulin, red) of oocytes microinjected with control *Gfp* and *Ccnb* cRNA. Representative images are from three experiments of biologically different samples (scale bar, 10  $\mu$ m). **(f)** The percentage of cold stable end-on MT to KT attachments in each group averaged over multiple cells ( $n \geq 28$ ) 6 h post-IBMX-wash. Kinetochore-MT end-on attachments were quantified. The morphology of kinetochores analyzed is specified in detail. Data represent mean  $\pm$  SD. \*  $p < 0.05$ , Student's *t*-test.



Taken together, these experiments show we were able to mimic the faster meiotic progression observed in the AF oocytes, that itself stems from higher MPF activity.

### 3. Discussion

Here we have addressed the question of how meiosis I differs in oocytes from females of advanced reproductive age versus those originating from young females. The precise timing of the cell cycle is a prerequisite for the appropriate propagation of genomes. It is well accepted that, in human and mouse oocytes, the incidence of genomic instability and aneuploidy increases with maternal age [5,7,27–30]. Age-associated increase in aneuploidy [27–30] has been attributed, at least in part, to a faster progression through the first meiotic division in oocytes from aged females, which would affect the time available for proper chromosome congression prior to chromosome segregation [27]. The mouse is a useful model in which to study the effect of age on egg quality, including the molecular basis for observed age-associated increase in aneuploidy.

We have found that oocytes from aged females resume meiosis and progress through meiosis I faster than the oocytes from young females. Our finding is consistent with findings of others [5,27,31–33] but opposes other findings reporting a lack of timing in oocytes from aged females [34,35]. In addition, we found that oocytes from aged females are significantly more meiotically competent than from young females, a further consistent observation [36]. The underlying reasons for the reported discrepancies related to the length of meiosis I in aged oocytes are not clear; however, they may have their origin in the methodologies employed to select meiotically competent GV oocytes and/or further differences in oocyte manipulation (e.g., the removal of cumulus cells and microinjection). Relating to our own data, we conclude that an increase in MPF activity during meiosis I temporarily regulates acceleration of NEBD, the attachment of chromosomes, and cytokinesis events in aged oocytes. Moreover, our results are in agreement with previous findings [25] in which it is reported that premature increases of CDK1 kinase activity, induced by cyclin-B microinjection, are responsible for the precocious formation of stable kinetochore-microtubule attachments and lagging chromosomes during anaphase I, a condition that leads to aneuploidy. Thus, the increased presence of MPF components, as observed in our AF oocyte cohort, could clearly act in a similar manner to result in chromosome segregation errors during meiosis I.

Surprisingly, we have also found that transcripts coding for MPF components are significantly overexpressed in the oocytes from aged females. However, it is important to recognize that the abundance of mRNA only represents one part of the regulation of gene expression and that selective translational regulation of transcripts can play a pivotal role. It has been previously reported that CCNB2 has a functional role during the prophase/metaphase transition of mouse oocyte maturation [37], and these data support our findings showing that the increased translational rate of CCNB2 transcripts in the oocytes from aged females might be associated with faster meiotic progression. Consistent with this prevailing view, we have also demonstrated elevated phosphorylation levels of CDK1 (Thr161), that in turn contributes to its MPF activity [38], in AF oocytes. Notwithstanding this observation, the upregulation of Cyclin B clearly plays a positive role in reinforcing CDK1/MPF activity and thus driving meiotic cycle progression. As such, our study correlates the resumption of meiosis with the synthesis of the regulatory subunit of MPF, namely cyclin B1/2, as supported by the fact that the level of MPF activity is known to depend on the amount of cyclin B present [22,39,40]. Thus, the fact that the MPF components in aged GV oocytes are apparently more expressed (but not necessarily fully active) and that they are then rapidly activated during their maturation (in AF versus YF oocytes) contributes to the observed acceleration of the AF oocytes meiotic progression.

We show that both cyclins B are expressed and differentially occupy polyribosomes in the AF group. In addition to the increased expression of MPF components, which leads to accelerated meiotic progression, we also demonstrate that the key components of the translational machinery are more translated (associated with polysome fractions), which in turn is likely to positively affect general translation in AF oocytes. Indeed, our findings are in good agreement with published

data describing increased numbers of ribosomes in oocytes from older females [41]. However, in connection to increased number of ribosomes, we have not observed increased rates of global translation. Nonetheless, our results suggest that there is increased translation of specific mRNAs related to specific translational machinery activity in AF oocytes, which may contribute to amplifying the roles of specific regulators [13,42]; mechanisms that could target specific mRNAs for translation and consequently affect meiotic progression rates. In addition to the increased number of ribosomes and translational regulators in oocytes from females of advanced age, it has also been reported [43,44] that the number of mitochondria is also increased in the oocytes and embryos derived from aged mouse and human subjects.

We have also shown that the GV oocytes from female mice of advanced age have aberrantly formed nuclear envelopes, which strongly resemble the morphology of those in aged somatic cells [15,45]. In association with described precocious meiotic progression and increased MPF activity, we have shown that the nuclear lamina is also precociously dispersed in aged oocytes. We have previously reported that LMN A/C structures surround oocyte chromosomes post-NEBD, resembling an organelle-exclusion “spindle envelope” that acts as a diffusion barrier structure [46–48]. Such spindle envelopes are thought to confine spindle assembly and their mechanical disruption is reported to compromise precise and appropriate chromosome segregation in mitosis [47]. It is therefore possible that the lack of such a functioning spindle envelope in AF-derived oocytes contributes to increased aneuploidy rates observed.

Taken together, our results can provide at least a partial explanation for the commonly recognized multifactorial phenomenon of age-related increase in oocyte aneuploidy on a molecular level. In addition, our study significantly contributes to the overall knowledge base concerning the molecular physiology of aged cells, including but not restricted to oocytes, and provides a solid foundation for further work related to the observed translational discrepancies between young and aged oocytes identified herein, and their functional interplay with meiotic progression/maturation.

## 4. Material and Methods

### 4.1. Oocyte Cultivation, Treatment, and Microinjection

GV oocytes were obtained from CD1 mice 46 h after injection by 5 IU pregnant mare serum gonadotropin (PMSG, HOR 272, ProSpec, Rehovot, Israel). Oocytes were obtained from females in two distinct age categories: young females (YF) group (2 months old) and aged females (AF) group (12 months old). Oocytes were isolated in germinal vesicle stage (GV; 0 h) in transfer medium [49] supplemented with 100  $\mu$ M 3-isobutyl-1-methylxanthine (IBMX, I5879, Sigma-Aldrich, Darmstadt, Germany) to prevent NEBD. Selected fully grown GV oocytes were denuded by pipetting and cultured in M16 medium (M7292, Sigma-Aldrich, Darmstadt, Germany) without IBMX at 37 °C, 5% CO<sub>2</sub>. Post-IBMX-wash (PIW) oocytes undergo nuclear envelope breakdown (NEBD) within 1 h; they reach metaphase I in 6 h and metaphase II in 12 h. For oocytes treatment, 20  $\mu$ M roscovitin (186692-46-6, Cayman Chemical, Ann Arbor, MI, USA) was added 1 h PIW. GV oocytes were microinjected in the presence of the IBMX on inverted microscope Leica DMI 6000B (Leica Microsystems, Wetzlar, Germany) using TransferMan NK2 (Eppendorf, Hamburg, Germany) and FemtoJet (Eppendorf). Oocytes were injected with 20 ng/ $\mu$ L of in vitro transcribed (mMessage, Ambion, Thermo Fisher Scientific, Waltham, MA, USA) RNAs from plasmids (GFP, [50]; CCNB1, Dr. Martin Anger, Laboratory of Cell Division Control, IAPG, CAS) diluted in RNase free water. Approximately 5 pL of RNA solution were injected into one oocyte. Microinjected oocytes were used for time-lapse microscopy, cold tubulin stability testing, and immunoblotting. All animal work was conducted according to Act No 246/1992 for the protection of animals against cruelty; from 25.09.2014 number CZ02389, issued by Ministry of agriculture.

#### 4.2. Time-Lapse Microscopy

Oocytes were scanned with an inverted wide field microscope, Leica DMI 6000B (Leica Microsystems, Wetzlar, Germany), equipped with a chamber system (Pecon, Erbach, Germany), a Tempcontroller 2000-2 (Pecon), and a CO<sub>2</sub> controller (Pecon). Cover-glass-based 4-well chambers (94.6190.402, Sarstedt, Nümbrecht, Germany) were used for live oocytes imaging. Oocytes were put into a 10 µL drop of M16 medium without IBMX and covered by approximately 1 mL of mineral oil (M8410, Sigma-Aldrich). The chamber was pre-tempered to 37 °C and 5% CO<sub>2</sub>. Images were captured every 5 min. Timing of the NEBD and polar body extrusion (PBE) were evaluated through time lapse movies.

#### 4.3. Immunoblotting

Oocytes were washed in phosphate buffer saline (PBS, Sigma-Aldrich) with polyvinyl alcohol (PVA, Sigma-Aldrich) and frozen to −80 °C. An exact number of oocytes (15–30) were lysed in 10 µL of 1× Reducing SDS Loading Buffer (lithium dodecyl sulfate sample buffer NP 0007 and reduction buffer NP 0004, Thermo Fisher Scientific, Waltham, MA, USA) and heated at 100 °C for 5 min. Proteins were separated by gradient precast 4–12% SDS–PAGE gel (NP 0323, Thermo Fisher Scientific) and transferred to Immobilon P membrane (IPVD 00010, Millipore, Merck group, Darmstadt, Germany) using a semidry blotting system (Biometra GmbH, Analytik Jena, Jena, Germany) for 25 min at 5 mA cm<sup>−2</sup>. Membranes were blocked by 5% skimmed milk dissolved in 0.05% Tween-Tris buffer saline (TTBS), pH 7.4 for 1 h. After a brief washing in TTBS, membranes were incubated at 4 °C overnight with the primary antibodies diluted in 1% milk/TTBS (see Table S1). Secondary antibody Peroxidase Anti-Rabbit Donkey (711-035-152) or Peroxidase Anti-Mouse Donkey (715-035-151, Jackson ImmunoResearch, West Grove, PA, USA) was diluted 1:7500 in 1% milk/TTBS. The membranes were incubated in the secondary antibodies for 1 h at room temperature. Immunodetected proteins were visualized on films using ECL (Amersham, GE Healthcare Life Sciences, Barcelona, Spain). Films were scanned using a GS-800 calibrated densitometer (Bio-Rad Laboratories, CA, USA) and quantified using ImageJ (<http://rsbweb.nih.gov/ij/>).

#### 4.4. Measurement of Overall Protein Synthesis

To measure the overall protein synthesis, 50 µCi of <sup>35</sup>S-methionine (Hartmann Analytics, Braunschweig, Germany) was added to methionine-free culture medium. Ten oocytes per sample were labeled for 2 h, then lysed in SDS-buffer, and loaded to SDS-polyacrylamide gel electrophoresis and transferred to an Immobilon P membrane using the semidry blotting system for 25 min at 5 mA cm<sup>−2</sup> (the same materials as in Immunoblotting). The labeled proteins were visualized by autoradiography on FujiFilm (incubated at least 14 days in −80 °C), scanned using BAS-2500 Photo Scanner (FujiFilm Life Science, Tokyo, Japan) and quantified by ImageJ. GAPDH antibody was used as a loading control.

#### 4.5. Immunocytochemistry and Cold-Stable MT Assay

After cultivation, oocytes were fixed for 15 min in 4% paraformaldehyde (PFA, Alfa Aesar, Thermo Fisher Scientific, Waltham, MA, USA) in PBS/PVA. Oocytes were permeabilized in 0.1% Triton (X-100, Sigma-Aldrich) in PBS/PVA for 10 min, washed in PBS/PVA, and incubated overnight at 4 °C with primary antibodies (see Table S1). After washing in PBS/PVA, detection of the primary antibodies was performed by cultivation of the oocytes with relevant Highly Cross-Adsorbed Secondary Antibodies, Alexa Fluor 488, 594 or 647 conjugates (Thermo Fisher Scientific) diluted 1:250 for 1 h at room temperature. Oocytes were then washed two times for 15 min in PBS/PVA and mounted using a Vectashield Mounting Medium with DAPI (H-1200, Vector Laboratories, Burlingame, CA, USA). For the cold-stable MT assay, oocytes were matured for 6 h post-IBMX-wash and then were incubated for 15 min in 4 °C, fixed in 4% PFA/PVA, and stained for tubulin and CREST according to the immunocytochemistry protocol. Confocal images were collected as Z stacks at 0.3 µm intervals

to visualize the entire meiotic spindle region. Samples were visualized using a Leica SP5 inverted confocal microscope (Leica Microsystems, Wetzlar, Germany). To classify kinetochore attachment status, images were scored around the same Z plane using the merged two-color confocal stack of CREST and MT images. Images were assembled in software LAS X (Leica Microsystems).

#### 4.6. Transmission Electron Microscopy

Mouse oocytes in GV were washed three times in PBS/PVA and one time in 0.1 M Sorenson's phosphate buffer (pH = 7.2) with PVA. Oocytes were fixed in 2.5% glutaraldehyde (G5882, Sigma-Aldrich) in 0.1 M Sorenson's phosphate buffer for 1 h at room temperature. Fixed oocytes were transported to the Electron Microscopy facility at the Microscopy Centre of the Institute of Molecular Genetics, CAS. Fixative was removed and oocytes were centrifuged ( $5000\times g/5$  min) in 1% low-temperature melting agarose. Oocytes were embedded to Epon blocks and sliced by UltraCut6 (Leica Microsystems) to ultra-thin sections. Oocyte sections were imaged at 80 kV using FEI Morgagni 268 Transmission Electron Microscope with Olympus Megaview III Digital Camera EM (FEI Company, Hillsboro, OR, USA).

#### 4.7. RNA Isolation and RT-PCR

RNA was extracted using a RNeasy Plus Micro kit (74034, Qiagen, Hilden, Germany) and genomic DNA was depleted using gDNA Eliminator columns. The quality and quantity of the isolated RNA was analyzed using the Bioanalyzer 2100 (Agilent, Santa Clara, CA, USA) system employing the RNA 6000 Pico kit (5067-1513, Agilent). RT-PCR was then carried out using the Rotor-Gene 3000 (Biocompare, South San Francisco, CA, USA) and the OneStep RT-PCR Kit (210210, Qiagen) and SybrGreen I (S7563, Thermo Fisher Scientific) according to manufacturers' provided protocols. Gene/transcript specific RT-PCR primers were designed with an annealing temperature of 58 °C (see Table S2). The reaction condition for reverse transcription was as follows: 50 °C/30 min, then initial activation at 95 °C/15 min, followed by 40 PCR amplification cycles (95 °C/15 s, 58 °C/20 s, 72 °C/30 s) and 72 °C/10 min. Quantification analyses were performed using a dynamic amplification efficiency determination for each amplification run as provided in the comparative quantification function with the Rotor-Gene RG-3000 software. The exact amplification efficiencies were assessed in each tube, and a mathematic model was applied for the derived calculation of the relative gene expression in the control (YF).

#### 4.8. Polysome Fractionation and RNA Extraction

Prior to oocyte collection, 100 µg/mL of cycloheximide (CHX, 01810, Sigma-Aldrich) was added for 10 min. Next, 200 oocytes (per sample) were washed three times in PBS/PVA supplemented with CHX and frozen at -80 °C in low-binding tube (Eppendorf). To disrupt the zona pellucida and lysate the oocytes, 250 µL of zirconia-silica beads (11079110z, BioSpec, Bartlesville, OK, USA) were added to the tube with frozen oocytes together with 350 µL of lysis buffer (10 mM Hepes, pH 7.5; 62.5 mM KCl; 5 mM MgCl<sub>2</sub>; 2 mM DTT; 1% TritonX-100; 100 µg/mL of CHX supplemented with Complete-EDTA-free Protease Inhibitor (05 056 489 001 3, Roche Diagnostics GmbH, Mannheim, Germany) and Ribolock 20 U/mL (EO0381, Thermo Fisher Scientific)). Oocytes were disrupted in the mixer mill apparatus MM301 (shake frequency 30, total time 45 s, Retsch, Haan, Germany). Lysates were clarified by centrifugation at  $8000\times g$  for 5 min at 4 °C. Supernatants were loaded onto 10–50% linear sucrose gradients containing 10 mM Hepes, pH 7.5; 100 mM KCl; 5 mM MgCl<sub>2</sub>; 2 mM DTT; 100 µg/mL CHX; Complete EDTA-free (1 tablet/100 mL); and 5 U/mL Ribolock. Centrifugation was carried out using Optima L-90 ultracentrifuge (Beckman Coulter, Brea, CA, USA) at  $35,000\times g$  for 65 min at 4 °C. Polysome profiles were recorded using ISCO UA-5 UV absorbance reader. We monitored the overall quality of the polysome fractionation experiment by an inclusion of a parallel HEK293 cells sample. Ten equal fractions were recovered from each sample and subjected to RNA isolation by Trizol reagent (Sigma-Aldrich). Each fraction was then tested by qPCR with 18S and 28S rRNA-specific primers in

LightCycler480 (Roche) to reconstruct a distribution of non-polysomal and polysomal RNA complexes in each oocyte—specific profile.

#### 4.9. Library Preparation, RNA Sequencing and Data Analysis

Fractions corresponding to polysomal and non-polysomal part, respectively, were pulled together. These sub-samples were concentrated to 16  $\mu$ L of Clean & Concentrator-5 (R1014, Zymo Research, Irvine, CA, USA) and ribosomal RNA was removed from them by Ribozero-Gold (MRZG12324, Illumina, San Diego, CA, USA). Afterwards, RNA was turned into cDNA and amplified by using the REPLI-g WTA Single Cell Kit (150063, Qiagen). Finally, cDNA was tagged and libraries were prepared using the Nextera DNA Library Prep Kit (FC-121-1030, Illumina). Sequencing was performed in Centro Nacional de Analisis Genomico facility (CNAG, Barcelona, Spain). Samples were sequenced by HiSeq 2500 (Illumina) as 150 bp paired-end. Reads were trimmed using Trim Galore! v0.4.1 and mapped to the mouse GRCm38 genome assembly using Hisat2 v2.0.5. Gene expression was quantified as fragments per kilobase per million (FPKM) values in Seqmonk v1.40.0. Functional annotation was performed using GOrilla [51,52] with ranked lists of genes detected in polysomal fractions (FPKM > 0.1).

#### 4.10. Kinase Assay

Kinase activities of CDK1 (H1) and MAPK (MBP) were determined in a single assay via their capacity to phosphorylate external substrates histone H1 and myelin basic protein (MBP), respectively [53]. Fifteen oocytes per sample were collected and lysed in 5  $\mu$ L of lysis buffer (10  $\mu$ g/mL leupeptin, 10  $\mu$ g/mL aprotinin, 10 mM p-nitrophenyl phosphate, 20 mM  $\beta$ -glycerophosphate, 0.1 mM  $\text{Na}_3\text{VO}_4$ , 5 mM EGTA, 1 mM benzamidine, 1 mM AEBSF) by three cycles of freezing/thawing. Next, 5  $\mu$ L of double kinase buffer (60  $\mu$ g/mL leupeptin, 60  $\mu$ g/mL aprotinin, 24 mM p-nitrophenyl phosphate, 90 mM  $\beta$ -glycerophosphate, 4.6 mM  $\text{Na}_3\text{VO}_4$ , 24 mM EGTA, 2 mM benzamidine, 2 mM AEBSF, 24 mM  $\text{MgCl}_2$ , 0.2 mM EDTA, 4 mM NaF, 1.6 mM DTT, 0.2% (*w/v*) polyvinyl alcohol, 40 mM MOPS pH 7.2, 2.2  $\mu$ M protein kinase inhibitor (P0300, Sigma-Aldrich), 1 mg/mL MBP (M1891, Sigma-Aldrich), 0.5 mg/mL histone H1 (10223549001, Roche), 0.6 mM ATP, 1 mCi/mL [ $\gamma$ - $^{32}\text{P}$ ] ATP (Hartmann Analytic, Braunschweig, Germany) was incubated with the lysed sample for 30 min at 30 °C. The reaction was terminated by addition of 12.5  $\mu$ L of double-strength concentrated reducing sample buffer [54]. The phosphorylated substrates were resolved on 15% SDS-PAGE gel, the gel was stained with Coomassie Brilliant Blue R250 (27816, Sigma-Aldrich), dried and exposed to an intensifying screen in the exposure cassette for 20 h. Phosphorylated substrates were visualized using a FujiFilm BAS-2500 Photo Scanner and the kinase activity was quantified using Aida Image Analyzer software (Elysia Raytest, Angleur, Belgium).

#### 4.11. Statistical Analysis

Mean and standard deviation ( $\pm$ SD) values were calculated using MS Excel. Statistical significance of the differences between the groups was tested using Student's *t*-test (PrismaGraph5) and  $p < 0.05$  was considered as statistically significant (marked by asterisks: \*  $p < 0.05$ ; \*\*  $p < 0.01$ ; \*\*\*  $p < 0.001$ ).

**Supplementary Materials:** Supplementary materials can be found at <http://www.mdpi.com/1422-0067/19/9/2841/s1>. Figure S1. Localization of LMN A/C during oocyte maturation. (a) Representative confocal images from immunocytochemistry (ICC) showed localization of LMN A/C (red) and phosphorylated LMN A/C Ser22 (green) during oocyte maturation (GV 0 h; NEBD 3 h; MI 6 h, MII 12 h). Cortex of oocytes is depicted by white dashed line. DNA, blue and scale bar, 10  $\mu$ m. (b) Co-localization of LMN A/C (Ser22) (green) and the spindle (tubulin, red). DNA, blue and scale bar 10  $\mu$ m. (c) Localization of LMN A/C (red) during oocyte meiotic maturation. DNA, blue and scale bar 10  $\mu$ m. Arrowhead marks polar body. Figure S2. Transmission electron microscopy of oocyte nuclei from females of different age. (a) Representative images of the nucleus from YF and AF oocytes. The images in the right panels show nuclear membrane highlighted with red line. Scale bar 10  $\mu$ m. (b) Measurement of nuclear membrane circumference of oocytes from the YF and the AF group. From two experiments of biologically different samples ( $n \geq 8$ ). Data represent mean  $\pm$  SD. \*\*  $p < 0.01$ , Student's *t*-test. (c) Detail of nuclear lamina from AF and YF oocytes. Representative images are from two experiments from biologically different samples (bar, 1  $\mu$ m).



The images in the right panels show nuclear membrane highlighted with red line. Figure S3. Total RNA amount and global translational activity is not different between YF and AF groups. (a) Quantification of total RNA by Agilent 2100 Bioanalyzer in the oocytes from different age groups. From 10 experiments of biologically different samples. Data represent mean  $\pm$  SD. ns, non-significant, Student's *t*-test. (b) <sup>35</sup>S-Methionine incorporation during meiotic progression of oocytes from YF and AF groups. Representative images are from three experiments of biologically different samples. (c) Quantification of <sup>35</sup>S-Methionine incorporation in the oocytes from different groups. From three experiments of biologically different samples. Values obtained for the YF group were set as 100%. Data represent mean  $\pm$  SD, ns, non-significant, Student's *t*-test. Figure S4. Induced expression of the CCNB in the oocytes. Oocytes injected with control *Gfp* (*Ctrl*) and *Ccnb* RNA. See Figure 6a for the effect of the overexpression. WB analysis of samples using CCNB antibody. Arrowhead depicts endogenous CCNB and arrow GFP tagged CCNB protein. GAPDH was used as a loading control. From three experiments of biologically different samples. Table S1. Primary antibodies used for WB and ICC in the study. Table S2. Primers used in the study for RT-PCR.

**Author Contributions:** A.S. designed research; M.K. (Marketa Koncicka), A.T., S.P., D.J., J.K., T.M., M.P., L.G., and A.S. performed research; A.S., M.K. (Marketa Koncicka), L.G., A.W.B., D.J., E.D.L., T.M. and M.P. analyzed data; A.S., A.W.B., M.K. (Marketa Koncicka) and M.K. (Michal Kubelka) wrote the paper.

**Funding:** This research was funded by MSMT (EXCELLENCE CZ.02.1.01/0.0/0.0/15\_003/0000460 OP RDE) and GACR (18-19395S) and GACR (15-22765S) and MC (EIF-708,255; to L.G.) and GACR (18-02891S; to A.W.B.) and Institutional Research Concept RVO67985904 and Development, and Innovations Infrastructures" (CESNET LM2015042).

**Acknowledgments:** We thank Jaroslava Supolikova and Marketa Hancova for their exceptional assistance with experiments and Martin Anger for kindly providing the GFP and CCNB plasmid.

**Conflicts of Interest:** The authors declare no conflict of interest.

## References

1. Colegrove-Otero, L.J.; Devaux, A.; Standart, N. The Xenopus ELAV protein ElrB represses Vg1 mRNA translation during oogenesis. *Mol. Cell. Biol.* **2005**, *25*, 9028–9039. [[CrossRef](#)] [[PubMed](#)]
2. Schuh, M.; Ellenberg, J. Self-organization of MTOCs replaces centrosome function during acentrosomal spindle assembly in live mouse oocytes. *Cell* **2007**, *130*, 484–498. [[CrossRef](#)] [[PubMed](#)]
3. Hassold, T.; Jacobs, P.; Kline, J.; Stein, Z.; Warburton, D. Effect of maternal age on autosomal trisomies. *Ann. Hum. Genet.* **1980**, *44*, 29–36. [[CrossRef](#)] [[PubMed](#)]
4. Pan, H.; Ma, P.; Zhu, W.; Schultz, R.M. Age-associated increase in aneuploidy and changes in gene expression in mouse eggs. *Dev. Biol.* **2008**, *316*, 397–407. [[CrossRef](#)] [[PubMed](#)]
5. Sebestova, J.; Danylevska, A.; Novakova, L.; Kubelka, M.; Anger, M. Lack of response to unaligned chromosomes in mammalian female gametes. *Cell Cycle* **2012**, *11*, 3011–3018. [[CrossRef](#)] [[PubMed](#)]
6. Hassold, T.; Hunt, P. To err (meiotically) is human: The genesis of human aneuploidy. *Nat. Rev. Genet.* **2001**, *2*, 280–291. [[CrossRef](#)] [[PubMed](#)]
7. Hunt, P. Oocyte Biology: Do the Wheels Fall Off with Age? *Curr. Biol.* **2017**, *27*, R266–R269. [[CrossRef](#)] [[PubMed](#)]
8. Chiang, T.; Duncan, F.E.; Schindler, K.; Schultz, R.M.; Lampson, M.A. Evidence that weakened centromere cohesion is a leading cause of age-related aneuploidy in oocytes. *Curr. Biol.* **2010**, *20*, 1522–1528. [[CrossRef](#)] [[PubMed](#)]
9. Merriman, J.A.; Jennings, P.C.; McLaughlin, E.A.; Jones, K.T. Effect of aging on superovulation efficiency, aneuploidy rates, and sister chromatid cohesion in mice aged up to 15 months. *Biol. Reprod.* **2012**, *86*. [[CrossRef](#)] [[PubMed](#)]
10. Chiang, T.; Schultz, R.M.; Lampson, M.A. Meiotic Origins of Maternal Age-Related Aneuploidy. *Biol. Reprod.* **2012**, *86*. [[CrossRef](#)] [[PubMed](#)]
11. Dechat, T.; Pflieger, K.; Sengupta, K.; Shimi, T.; Shumaker, D.K.; Solimando, L.; Goldman, R.D. Nuclear lamins: Major factors in the structural organization and function of the nucleus and chromatin. *Genes Dev.* **2008**, *22*, 832–853. [[CrossRef](#)] [[PubMed](#)]
12. Heald, R.; McKeon, F. Mutations of phosphorylation sites in lamin A that prevent nuclear lamina disassembly in mitosis. *Cell* **1990**, *61*, 579–589. [[CrossRef](#)]
13. Susor, A.; Jansova, D.; Cerna, R.; Danylevska, A.; Anger, M.; Toralova, T.; Malik, R.; Supolikova, J.; Cook, M.S.; Oh, J.S.; et al. Temporal and spatial regulation of translation in the mammalian oocyte via the mTOR-eIF4F pathway. *Nat. Commun.* **2015**, *6*. [[CrossRef](#)] [[PubMed](#)]

14. Sanfins, A.; Plancha, C.E.; Overstrom, E.W.; Albertini, D.F. Meiotic spindle morphogenesis in in vivo and in vitro matured mouse oocytes: Insights into the relationship between nuclear and cytoplasmic quality. *Hum. Reprod.* **2004**, *19*, 2889–2899. [[CrossRef](#)] [[PubMed](#)]
15. Haithcock, E.; Dayani, Y.; Neufeld, E.; Zahand, A.J.; Feinstein, N.; Mattout, A.; Gruenbaum, Y.; Liu, J. Age-related changes of nuclear architecture in *Caenorhabditis elegans*. *Proc. Natl. Acad. Sci. USA* **2005**, *102*, 16690–16695. [[CrossRef](#)] [[PubMed](#)]
16. Righolt, C.H.; van 't Hoff, M.L.R.; Vermolen, B.J.; Young, I.T.; Raz, V. Robust nuclear lamina-based cell classification of aging and senescent cells. *Aging* **2011**, *3*, 1192–1201. [[CrossRef](#)] [[PubMed](#)]
17. Adhikari, D.; Zheng, W.; Shen, Y.; Gorre, N.; Ning, Y.; Halet, G.; Kaldis, P.; Liu, K. Cdk1, but not Cdk2, is the sole Cdk that is essential and sufficient to drive resumption of meiosis in mouse oocytes. *Hum. Mol. Genet.* **2012**, *21*, 2476–2484. [[CrossRef](#)] [[PubMed](#)]
18. Peter, M.; Nakagawa, J.; Dorée, M.; Labbé, J.C.; Nigg, E.A. In vitro disassembly of the nuclear lamina and M phase-specific phosphorylation of lamins by cdc2 kinase. *Cell* **1990**, *61*, 591–602. [[CrossRef](#)]
19. Jones, K.T. Turning it on and off: M-phase promoting factor during meiotic maturation and fertilization. *Mol. Hum. Reprod.* **2004**, *10*, 1–5. [[CrossRef](#)] [[PubMed](#)]
20. Morgan, D.O. Principles of CDK regulation. *Nature* **1995**, *374*, 131–134. [[CrossRef](#)] [[PubMed](#)]
21. Ducommun, B.; Brambilla, P.; Félix, M.A.; Franza, B.R.; Karsenti, E.; Draetta, G. cdc2 phosphorylation is required for its interaction with cyclin. *EMBO J.* **1991**, *10*, 3311–3319. [[CrossRef](#)] [[PubMed](#)]
22. Solomon, M.J. Activation of the various cyclin/cdc2 protein kinases. *Curr. Opin. Cell Biol.* **1993**, *5*, 180–186. [[CrossRef](#)]
23. Hampl, A.; Eppig, J.J. Translational regulation of the gradual increase in histone H1 kinase activity in maturing mouse oocytes. *Mol. Reprod. Dev.* **1995**, *40*, 9–15. [[CrossRef](#)] [[PubMed](#)]
24. Lévesque, J.T.; Sirard, M.A. Resumption of meiosis is initiated by the accumulation of cyclin B in bovine oocytes. *Biol. Reprod.* **1996**, *55*, 1427–1436. [[CrossRef](#)] [[PubMed](#)]
25. Davydenko, O.; Schultz, R.M.; Lampson, M.A. Increased CDK1 activity determines the timing of kinetochore-microtubule attachments in meiosis I. *J. Cell Biol.* **2013**, *202*, 221–229. [[CrossRef](#)] [[PubMed](#)]
26. Rieder, C.L. The structure of the cold-stable kinetochore fiber in metaphase PtK1 cells. *Chromosoma* **1981**, *84*, 145–158. [[CrossRef](#)] [[PubMed](#)]
27. Eichenlaub-Ritter, U.; Boll, I. Age-related non-disjunction, spindle formation and progression through maturation of mammalian oocytes. *Prog. Clin. Biol. Res.* **1989**, *318*, 259–269. [[PubMed](#)]
28. Zuccotti, M.; Boiani, M.; Garagna, S.; Redi, C.A. Analysis of aneuploidy rate in antral and ovulated mouse oocytes during female aging. *Mol. Reprod. Dev.* **1998**, *50*, 305–312. [[CrossRef](#)]
29. Liu, L.; Keefe, D.L. Ageing-associated aberration in meiosis of oocytes from senescence-accelerated mice. *Hum. Reprod.* **2002**, *17*, 2678–2685. [[CrossRef](#)] [[PubMed](#)]
30. Cukurcam, S.; Betzendahl, I.; Michel, G.; Vogt, E.; Hegele-Hartung, C.; Lindenthal, B.; Eichenlaub-Ritter, U. Influence of follicular fluid meiosis-activating sterol on aneuploidy rate and precocious chromatid segregation in aged mouse oocytes. *Hum. Reprod.* **2007**, *22*, 815–828. [[CrossRef](#)] [[PubMed](#)]
31. Chiang, T.; Schultz, R.M.; Lampson, M.A. Age-Dependent Susceptibility of Chromosome Cohesion to Premature Separase Activation in Mouse Oocytes. *Biol. Reprod.* **2011**, *85*, 1279–1283. [[CrossRef](#)] [[PubMed](#)]
32. Eichenlaub-Ritter, U.; Chandley, A.C.; Gosden, R.G. The CBA mouse as a model for age-related aneuploidy in man: Studies of oocyte maturation, spindle formation and chromosome alignment during meiosis. *Chromosoma* **1988**, *96*, 220–226. [[CrossRef](#)] [[PubMed](#)]
33. Eichenlaub-Ritter, U.; Boll, I. Nocodazole sensitivity, age-related aneuploidy, and alterations in the cell cycle during maturation of mouse oocytes. *Cytogenet. Genome Res.* **1989**, *52*, 170–176. [[CrossRef](#)] [[PubMed](#)]
34. Duncan, F.E.; Chiang, T.; Schultz, R.M.; Lampson, M.A. Evidence That a Defective Spindle Assembly Checkpoint Is Not the Primary Cause of Maternal Age-Associated Aneuploidy in Mouse Eggs1. *Biol. Reprod.* **2009**, *81*, 768–776. [[CrossRef](#)] [[PubMed](#)]
35. Lister, L.M.; Kouznetsova, A.; Hyslop, L.A.; Kalleas, D.; Pace, S.L.; Barel, J.C.; Nathan, A.; Floros, V.; Adelfalk, C.; Watanabe, Y.; et al. Age-Related Meiotic Segregation Errors in Mammalian Oocytes Are Preceded by Depletion of Cohesin and Sgo2. *Curr. Biol.* **2010**, *20*, 1511–1521. [[CrossRef](#)] [[PubMed](#)]
36. Cui, L.-B.; Zhou, X.-Y.; Zhao, Z.-J.; Li, Q.; Huang, X.-Y.; Sun, F.-Z. The Kunming mouse: As a model for age-related decline in female fertility in human. *Zygote* **2013**, *21*, 367–376. [[CrossRef](#)] [[PubMed](#)]

37. Gui, L.; Homer, H. Hec1-dependent cyclin B2 stabilization regulates the G2-M transition and early prometaphase in mouse oocytes. *Dev. Cell* **2013**, *25*, 43–54. [[CrossRef](#)] [[PubMed](#)]
38. De Smedt, V.; Poulhe, R.; Cayla, X.; Dessauge, F.; Karaiskou, A.; Jesus, C.; Ozon, R. Thr-161 phosphorylation of monomeric Cdc2. Regulation by protein phosphatase 2C in *Xenopus* oocytes. *J. Biol. Chem.* **2002**, *277*, 28592–28600. [[CrossRef](#)] [[PubMed](#)]
39. Félix, M.A.; Cohen, P.; Karsenti, E. Cdc2 H1 kinase is negatively regulated by a type 2A phosphatase in the *Xenopus* early embryonic cell cycle: Evidence from the effects of okadaic acid. *EMBO J.* **1990**, *9*, 675–683. [[CrossRef](#)] [[PubMed](#)]
40. Li, J.; Tang, J.-X.; Cheng, J.-M.; Hu, B.; Wang, Y.-Q.; Aalia, B.; Li, X.-Y.; Jin, C.; Wang, X.-X.; Deng, S.-L.; et al. Cyclin B2 can compensate for Cyclin B1 in oocyte meiosis I. *J. Cell Biol.* **2018**. [[CrossRef](#)] [[PubMed](#)]
41. Duncan, F.E.; Jasti, S.; Paulson, A.; Kelsh, J.M.; Fegley, B.; Gerton, J.L. Age-associated dysregulation of protein metabolism in the mammalian oocyte. *Aging Cell* **2017**, *16*, 1381–1393. [[CrossRef](#)] [[PubMed](#)]
42. Xue, S.; Barna, M. Specialized ribosomes: A new frontier in gene regulation and organismal biology. *Nat. Rev. Mol. Cell Biol.* **2012**, *13*, 355–369. [[CrossRef](#)] [[PubMed](#)]
43. Tao, X.; Landis, J.N.; Krisher, R.L.; Duncan, F.E.; Silva, E.; Lonczak, A.; Scott, R.T.; Zhan, Y.; Chu, T.; Scott, R.T.; et al. Mitochondrial DNA content is associated with ploidy status, maternal age, and oocyte maturation methods in mouse blastocysts. *J. Assist. Reprod. Genet.* **2017**, *34*, 1587–1594. [[CrossRef](#)] [[PubMed](#)]
44. Fragouli, E.; Spath, K.; Alfarawati, S.; Kaper, F.; Craig, A.; Michel, C.-E.; Kokocinski, F.; Cohen, J.; Munne, S.; Wells, D. Altered Levels of Mitochondrial DNA Are Associated with Female Age, Aneuploidy, and Provide an Independent Measure of Embryonic Implantation Potential. *PLoS Genet.* **2015**, *11*. [[CrossRef](#)] [[PubMed](#)]
45. Raz, V.; Vermolen, B.J.; Garini, Y.; Onderwater, J.J.M.; Mommaas-Kienhuis, M.A.; Koster, A.J.; Young, I.T.; Tanke, H.; Dirks, R.W. The nuclear lamina promotes telomere aggregation and centromere peripheral localization during senescence of human mesenchymal stem cells. *J. Cell. Sci.* **2008**, *121*, 4018–4028. [[CrossRef](#)] [[PubMed](#)]
46. Maiato, H.; Hergert, P.J.; Moutinho-Pereira, S.; Dong, Y.; Vandenbeldt, K.J.; Rieder, C.L.; McEwen, B.F. The ultrastructure of the kinetochore and kinetochore fiber in *Drosophila* somatic cells. *Chromosoma* **2006**, *115*, 469–480. [[CrossRef](#)] [[PubMed](#)]
47. Schweizer, N.; Pawar, N.; Weiss, M.; Maiato, H. An organelle-exclusion envelope assists mitosis and underlies distinct molecular crowding in the spindle region. *J. Cell Biol.* **2015**, *210*, 695–704. [[CrossRef](#)] [[PubMed](#)]
48. Katsani, K.R.; Karess, R.E.; Dostatni, N.; Doye, V. In vivo dynamics of *Drosophila* nuclear envelope components. *Mol. Biol. Cell* **2008**, *19*, 3652–3666. [[CrossRef](#)] [[PubMed](#)]
49. Tetkova, A.; Hancova, M. Mouse Oocyte Isolation, Cultivation and RNA Microinjection. *Bio-Protocol* **2016**, *6*. [[CrossRef](#)]
50. McGuinness, B.E.; Anger, M.; Kouznetsova, A.; Gil-Bernabé, A.M.; Helmhart, W.; Kudo, N.R.; Wuensche, A.; Taylor, S.; Hoog, C.; Novak, B.; et al. Regulation of APC/C activity in oocytes by a Bub1-dependent spindle assembly checkpoint. *Curr. Biol.* **2009**, *19*, 369–380. [[CrossRef](#)] [[PubMed](#)]
51. Eden, E.; Lipson, D.; Yogev, S.; Yakhini, Z. Discovering Motifs in Ranked Lists of DNA Sequences. *PLoS Comput. Biol.* **2007**, *3*, e39. [[CrossRef](#)] [[PubMed](#)]
52. Eden, E.; Navon, R.; Steinfeld, I.; Lipson, D.; Yakhini, Z. GOrilla: A tool for discovery and visualization of enriched GO terms in ranked gene lists. *BMC Bioinform.* **2009**, *10*, 48. [[CrossRef](#)] [[PubMed](#)]
53. Motlík, J.; Sutovský, P.; Kalous, J.; Kubelka, M.; Moos, J.; Schultz, R.M. Co-culture with pig membrana granulosa cells modulates the activity of cdc2 and MAP kinase in maturing cattle oocytes. *Zygote* **1996**, *4*, 247–256. [[CrossRef](#)] [[PubMed](#)]
54. Laemmli, U.K. Cleavage of structural proteins during the assembly of the head of bacteriophage T4. *Nature* **1970**, *227*, 680–685. [[CrossRef](#)] [[PubMed](#)]





Article

# Identifying the Translatome of Mouse NEBD-Stage Oocytes via SSP-Profilig; A Novel Polysome Fractionation Method

Tomas Masek <sup>1,\*</sup>, Edgar del Llano <sup>1,2</sup>, Lenka Gahurova <sup>2,3</sup>, Michal Kubelka <sup>2</sup>, Andrej Susor <sup>2,\*</sup>, Kristina Roucova <sup>1</sup>, Chih-Jen Lin <sup>4</sup>, Alexander W. Bruce <sup>3</sup> and Martin Pospisek <sup>1,\*</sup>

<sup>1</sup> Laboratory of RNA Biochemistry, Department of Genetics and Microbiology, Faculty of Science, Charles University, Viničná 5, 128 44 Prague 2, Czech Republic; Llano@iapg.cas.cz (E.d.L.); Ronea@seznam.cz (K.R.)

<sup>2</sup> Laboratory of Biochemistry and Molecular Biology of Germ Cells, Institute of Animal Physiology and Genetics, CAS, Rumburská 89, 277 21 Liběchov, Czech Republic; lveselovska@prf.jcu.cz (L.G.); Kubelka@iapg.cas.cz (M.K.)

<sup>3</sup> Laboratory of Early Mammalian Developmental Biology (LEMDB), Department of Molecular Biology and Genetics, Faculty of Science, University of South Bohemia, 370 05 České Budějovice, Czech Republic; awbruce@prf.jcu.cz

<sup>4</sup> Queen's Medical Research Institute, MRC Centre for Reproductive Health, The University of Edinburgh, 47 Little France Crescent, Edinburgh EH16 4TJ, UK; Chih-Jen.Lin@ed.ac.uk

\* Correspondence: masek@natur.cuni.cz (T.M.); susor@iapg.cas.cz (A.S.); martin@natur.cuni.cz (M.P.)

Received: 7 January 2020; Accepted: 10 February 2020; Published: 13 February 2020



**Abstract:** Meiotic maturation of oocyte relies on pre-synthesised maternal mRNA, the translation of which is highly coordinated in space and time. Here, we provide a detailed polysome profiling protocol that demonstrates a combination of the sucrose gradient ultracentrifugation in small SW55Ti tubes with the qRT-PCR-based quantification of 18S and 28S rRNAs in fractionated polysome profile. This newly optimised method, named Scarce Sample Polysome Profiling (SSP-profiling), is suitable for both scarce and conventional sample sizes and is compatible with downstream RNA-seq to identify polysome associated transcripts. Utilising SSP-profiling we have assayed the translatome of mouse oocytes at the onset of nuclear envelope breakdown (NEBD)—a developmental point, the study of which is important for furthering our understanding of the molecular mechanisms leading to oocyte aneuploidy. Our analyses identified 1847 transcripts with moderate to strong polysome occupancy, including abundantly represented mRNAs encoding mitochondrial and ribosomal proteins, proteasomal components, glycolytic and amino acids synthetic enzymes, proteins involved in cytoskeleton organization plus RNA-binding and translation initiation factors. In addition to transcripts encoding known players of meiotic progression, we also identified several mRNAs encoding proteins of unknown function. Polysome profiles generated using SSP-profiling were more than comparable to those developed using existing conventional approaches, being demonstrably superior in their resolution, reproducibility, versatility, speed of derivation and downstream protocol applicability.

**Keywords:** polysome profiling; polysome fractionation; translatome; mouse oocyte; mouse zygote; mouse early embryo; SW55Ti rotor; RNA-seq

## 1. Introduction

Protein synthesis is not solely dependent on the steady state level of transcript abundance caused by the trade-off between mRNA transcription and degradation but also upon the dedicated regulation of specific mRNA translation. Indeed, it has already been demonstrated that this level of gene expression



is exhaustively regulated and is centrally important in many physiological situations, including stress and during development [1–4].

For almost 50 years, polysome profiling has provided a gold-standard method to precisely assay functional genome readout at a given time point [5]. Indeed, it has for many years been widely applied to assess translational fitness under various physiological conditions relating to cellular stress [6–9], as well as being applied to study ribosome biogenesis and the functional roles of proteins involved in translation, regulation of mRNA stability and miRNA-mediated silencing [10–13]. Although, originally established in yeast, polysome profiling has been successfully introduced in mammalian cell, plant, bacteria and translation competent cell-free model systems [14–17]. In contrast to ribosome profiling, which determines the position of ribosomes within mRNA coding sequence, polysome profiling enables the analysis of entire mRNA transcripts. Consequently, this permits the study of individual transcript isoforms with particular resonance for the identification of conserved *cis*-acting sequences and structural motifs that can participate in transcript-specific translational regulation [18–21]. Furthermore, polysome profiling is readily combinable with several downstream applications, including microarrays and next generation sequencing (NGS) techniques, to identify polysome-bound mRNAs [16,20,21]. Alternatively, Western blot, proteomic and affinity capture methods can be applied to research proteins specifically associated with ribosomes/polysomes and to study the function of translation initiation factors [22–24]. Importantly, the identification of mRNAs engaged in active translation has the inherent potential to aid our understanding of the long-standing observations relating to intra-cellular discrepancies in transcriptome and proteome composition [25,26].

The wide-spread utilisation of polysome profiling has nevertheless been historically hindered by its intrinsic complexity, time-consuming nature, limited capacity for high throughput adaptation and its requirement for relatively large initial sample sizes [27]. The most commonly applied protocols utilise sucrose gradients, of varying concentrations, with volumes of ~12 mL, most frequently in the Beckman SW41Ti rotor [7,9,13,28], and the technique has been successfully scaled up using SW28Ti rotor tubes (with 38 mL gradients) to accommodate up to 45 OD<sub>260 nm</sub> units of cell extract [10,29]. However, efforts to reduce sample size and sucrose gradient volume, more applicable to biological specimens of initial scarcity, have provided limited success [30–32].

An appropriate progression through meiotic maturation in female germ cells (oocytes) is essential for successful fertilisation and the birth of healthy offspring. Mammalian oocytes undergo two successive cell divisions without an intermediate replicative phase during their maturation. At the onset of meiosis I, the nuclear lamina is phosphorylated and disassembled, leading to nuclear envelope breakdown (NEBD). Concomitantly, the chromosomes condense, and progressive reorganisation of microtubules into a bipolar spindle occurs [33], culminating in the first asymmetric cell division (generating the first polar body), the separation of homologous chromosome bivalents at the end of meiosis I and the generation of a fertilisable egg. However, developing oocytes only actively transcribe their genome during their growth phase, within the ovarian follicles, and store such mRNAs in ribonucleoprotein particles for subsequent translation after the resumption of meiosis and into early embryonic development [4]. Thus, following prolonged arrest in the prophase of meiosis I, there is a unique absence of *de novo* transcription that means oocytes uniquely and solely rely on the spatial and temporal regulation of mRNA stability and translation for their maturation, thus, making oogenesis a very attractive model system to study RNA related biology. The meiotic maturation of oocytes, within this context, requires a tightly coordinated array of cellular and metabolic processes that includes the inhibition of cell death, remodelling of chromatin and preparation for the metabolic demands connected with the first mitotic division and subsequent fertilisation [34,35]. Accordingly, such processes are largely mediated by the pre-synthesised maternal mRNA stored in translationally-inactive ribonucleoprotein particles [36]. The ribosomal recruitment of specific and required mRNAs during oocyte maturation is controlled by a complex regulatory network involving a central role for the cytoplasmic polyadenylation of targeted transcripts at their 3'-end [37–40], leading to



the creation of translational hotspots (under the influence of the mTOR-eIF4E signalling axis) essential for meiotic maturation [41].

During the past two decades, there has been a shift from the study of individual post-transcriptional mRNAs populations towards high throughput and multiplexed analyses of global mRNA abundance [42]. There are numerous comprehensive studies, from various species including human, reporting temporal patterns of transcriptome composition at various stages of the oocyte development, in zygotes and during early embryogenesis [43–46]. These experiments have provided valuable insight but have not been able to distinguish stored and translationally active mRNA populations. Therefore, various microarray-based approaches (themselves limited to, and thus biased by, the composite probe features on the array) have been developed to assay polysome-bound mRNAs from limiting numbers of oocytes [30,31,47]. These have latterly been supplemented by RNA-seq based approaches restricted to organisms, where only large number of eggs are accessible, such as the sea urchin and the zebrafish [48,49]. Thus, there exists a requirement for the development and refinement of novel techniques that can both comprehensively assay polysome associated mRNAs and be applied to limiting/scarce amounts of starting material, such as mammalian oocytes [27].

Here we provide a detailed protocol, that we have specifically optimised for polysome profiling of a low number of mammalian oocytes (but is adaptable to other experimental paradigms necessitating the use of scarce starting material) and which is compatible with RNA-seq analysis of polysome-bound mRNAs (we have named it “Scarce Sample Polysome Profiling”, SSP-profiling). Our approach is founded on the utilisation of reduced-volume ultra-centrifugation tubes for sucrose gradient preparation, using the Beckman SW55Ti rotor, and the omission of heterologous cell lysate during the velocity sedimentation procedure. Additionally, we demonstrate the reconstruction of oocyte polysomal profiles by qRT-PCR, as a reliable approach for the visualization of the actual state of translation. As a proof of concept to demonstrate the suitability of SSP-profiling for downstream RNA-seq analysis, we have determined the translome of mouse oocytes at NEBD.

## 2. Results

### 2.1. Optimisation of Polysome Profiling in SW55Ti Tubes

Our aim was to conduct a RNA-seq analysis of polysome-bound mRNAs from NEBD-stage oocytes. Therefore, given the comparative scarcity of our oocyte sample and to counter the potential loss of valuable polysomal RNA, we sought to minimise the polysome profiling protocol volumes involved. Conventional polysome profiling protocols typically employ sucrose gradients established in tubes with a size of 14 × 89 mm and a volume of 12.1 mL, compatible with Beckman SW41Ti ultra-centrifugation rotor. However, we optimised ultra-centrifugation conditions to produce high-quality polysome profiles in tubes with a size of 13 × 51 mm and the volume of 5.5 mL (compatible with Beckman SW55Ti rotor), that resulted in a 2.2-fold decrease in gradient volume. During our initial optimisation experiments, carried out using 8 OD<sub>260 nm</sub> units of HEK-293 cell line lysate as a common type of conventional sample, and employing centrifugal conditions of 47,500 RPM (274,180× g) for 75 min, we discovered that high-molecular weight polysomes were lost from the profile (Figure S1). Following further optimisations, that are also included in Figure S1, we established the most suitable centrifugation conditions producing complete polysome profiles, as being 45,000 RPM (246,078× g) for 65 min.

We next sought to test whether the profiles obtained using the reduced volume protocol in the SW55Ti centrifugation tubes were comparable, in terms of peak resolution and amplitude, to those obtained using the conventional SW41Ti method. Moreover, we also wanted to determine whether the SW55Ti-derived profiles exhibited an equal dependency on sedimentation velocity coefficient (S). Accordingly, we employed cell lysates of the yeast strain W303 *ceg1<sup>ts</sup>*, that carries a thermosensitive allele of the guanylyltransferase gene [50]. When grown at the restrictive temperature (37 °C), the W303 *ceg1<sup>ts</sup>* strain is unable add 5'-methyl-guanosine caps to newly synthesised mRNAs leading to an accumulation of uncapped transcripts that inhibits translation initiation and triggers mRNA

degradation. This is reflected in a diminution in polysomal peaks in any derived polysome profile. We therefore performed ultra-centrifugation for each lysate variant - HEK-293 cells and the W303 *ceg1<sup>ts</sup>* yeast strain cultivated at either permissive (24 °C) or restrictive (37 °C) temperatures, using both the newly developed SW55Ti-derived (8 OD<sub>260 nm</sub> units of lysates) and the original SW41Ti-dependent (20 OD<sub>260 nm</sub> units of lysates) protocols.

Figure 1 shows the position, number and amplitude of the corresponding peaks agreed well between each pairwise comparison of equivalent lysate. Please note that yeast and human large ribosomal subunits (LSU) have different sedimentation velocity coefficients (25S and 28S, respectively) leading to a comparative shift of the human LSU peak position versus that derived from the yeast LSU and a consequent shift in the comparative positions of the monosomal and polysomal peaks in the polysome profile. Importantly, this shift was clearly visible and highly similar between the profiles obtained using either the SW41Ti- or SW55Ti-based protocols, demonstrating the comparability of the sucrose concentration gradients prepared in both ultra-centrifugation tube variants. The diminution of polysomes in the W303 *ceg1<sup>ts</sup>* lysate obtained from yeast cultured at the restrictive temperature was also similar in both derived polysome profiles, providing extra confidence in the reliability of the newly developed SW55Ti protocol.

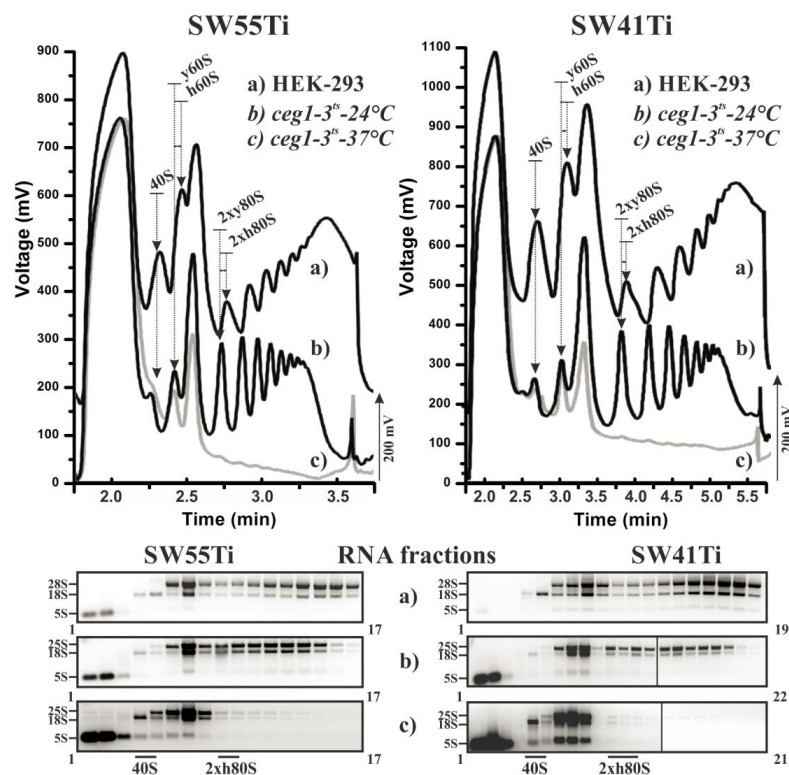


**Figure 1.** Performance of polysomal profiling in SW55Ti centrifugation tubes. Identical cell lysates from HEK-293 cells (a) and yeast strain W303 *ceg1<sup>ts</sup>* cultivated either at 24 °C (b) or 37 °C (c) were loaded on 10%–50% sucrose gradients prepared either in SW55Ti tubes (left panels) or SW41Ti tubes (right panels). RNA was isolated from equal fractions of the respective profiles and loaded on agarose gel (lower panels). Individual fraction numbers are indicated next to each electrophoretogram. Note in upper polysome profiles the obtained HEK-293 curves are shifted up by 200 mV to prevent overlapping with the yeast derived data curves. Arrows indicate the position of specific peaks within the profiles: i.e., 40S, small ribosomal subunits; 60S, large ribosomal subunits; and 2 × 80S, low molecular weight polysomes consisting of two ribosomes; h denotes human and y signifies yeast ribosomal subunits/polysomes. To the left of each electrophoretogram are denoted the positions of rRNAs in corresponding gels (note, the 5S rRNA label denotes the collective positions of 5.8S rRNA, 5S rRNA and tRNAs in gels).

We next isolated RNA from the collected fractions (of equal volume) corresponding to the three lysate variants profiled using either protocol. As can be observed, after agarose gel electrophoresis, the presence and relative abundance of either 18S, 28S (25S in yeast lysates) or both rRNA species corresponded well with the position and the amplitude of the corresponding peak in any one particular polysome profile. Moreover, such visualised and fractionated rRNA gel profiles were highly similar for equivalent lysates polysome profiled using the newly developed and low volume (SW55Ti) or the original (SW41Ti) assays (Figure 1 and Figure S2). Therefore, we conclude that polysome profiles obtained in the SW55Ti centrifugation tubes are equivalent to those profiles obtained by the commonly utilised SW41Ti tube-based protocol, thus validating our newly developed low volume polysome profiling assay.

## 2.2. Scarce Sample Polysome Profiling (SSP-Profiling) in SW55Ti-Based Format

To test our Scarce Sample Polysome profiling (SSP-profiling) protocol against scarce biological samples, we disrupted 200 NEBD-stage oocytes in 350  $\mu$ L of lysis buffer and loaded the obtained lysate onto a 10%–50% sucrose gradient prepared in SW55Ti tubes. Ultra-centrifugation was performed for 65 min at 45,000 RPM at 4 °C. However, Figure 2b details that we did not record any peaks in the derived polysome profile. In parallel, we processed 200 NEBD-stage oocyte lysates that had been treated with 0.5 M EDTA, to induce polysome disassembly into free ribosomal subunits, and although the overall absorbance was higher (due EDTA specific absorbance at 280 nm), we were still unable to detect any polysome profile peaks (Figure 2b). Furthermore, as a centrifugation quality control, we co-processed HEK-293 cell lysates (8 OD<sub>260 nm</sub> units) as described in Figure 2a. Accordingly, we did obtain a good quality polysome profile that could be disassembled if the lysates were treated with EDTA, as evidenced by the disappearance of polysomal specific peaks and the shift towards individual ribosomal subunits (at positions within the gradient typical for 40S, 60S and 80S peaks). Collectively, these results suggest that it is not possible to record absorbance to generate polysome profiles from a limited number of cells, such as 200 mouse oocytes, even in smaller SW55Ti centrifugation tube sucrose gradients.

However, the inclusion of the centrifugation control HEK-293 samples is not in itself a fully conclusive quality check. Therefore, to test the veracity of the polysomal fractionation directly, we compared levels of 18S and 28S rRNAs in 10 equal fractions from each HEK-293 or NEBD oocyte obtained profile ( $\pm$ EDTA) by qRT-PCR (Figure 2a,b). Thus, quantification of the 18S and 28S rRNA levels served as an indicator of the positions of the 40S small ribosomal subunit (high 18S rRNA, low 28S rRNA), the 60S large subunit (low 18S rRNA, high 28S rRNA) and the 80S monosome (high both), plus polysomes (characterised by alternating high and low levels of both rRNAs reflecting the increasing number of ribosomes in the polysomal fractions) in the obtained polysome profiles. Importantly, we also generated standard curves (derived after cloning the mouse 18S and the 28S rRNA qRT-PCR amplicons into pCR<sup>TM</sup>4-Topo<sup>TM</sup> plasmids, note that qPCR primers can detect also human rRNA) to permit absolute copy number calculations in each analysed fraction. A comparison of the obtained HEK-293 polysome profile with the result of the rRNA qRT-PCR fraction screening, indicated a good level of concurrence in the polysome profile readout (Figure 2a), typified by detection of the 40S and the 60S subunits within the third and fourth fractions, respectively. In the case of EDTA-treated HEK-293 cells, we observed maximal abundance of 18S and 28S rRNAs in fractions 2 and 3, respectively, indicating a shift in position of the 40S and 60S peaks by one fraction back in the polysome profile. Crucially, similar qRT-PCR analyses enabled the visualization of the otherwise undetectable absorbance peaks of oocyte polysome profiles (Figure 2b). The maximal rRNA abundances characteristic of the 40S and 60S subunits, were again resident in the fractions 2 and 3, respectively, but this was irrespective of whether NEBD-stage oocyte lysates had been treated with EDTA indicating very low concentration of ribosomal complexes in the oocyte lysate.

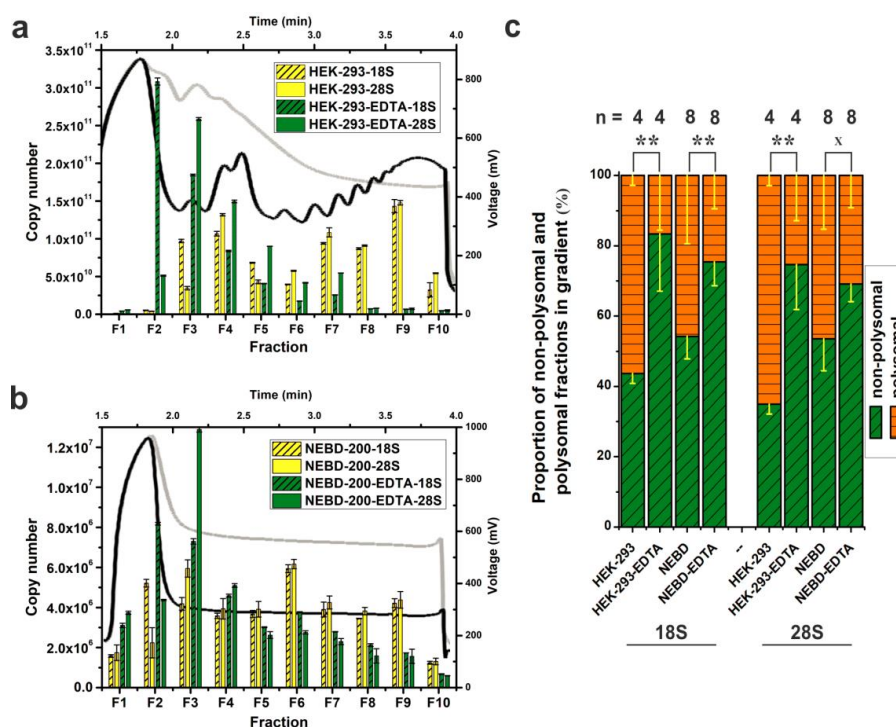


**Figure 2.** qRT-PCR-based visualization of polysome profiles from scarce samples using SW55Ti tubes. Comparison of polysome profiles of HEK-293 cells (a) and 200 NEBD-stage oocytes (b). Black curves and yellow columns in each chart indicate untreated lysates; EDTA-treated polysome profiles are traced in light grey and green columns. Absolute copy number of 18S and 28S rRNA was determined in fractions F1–F10 and error bars display  $\pm$ SD of qPCR technical triplicates. (c) Proportion of the non-polysomal (NP, fractions F2–F5, in green) and polysomal (P, fractions F6–F10, in orange) parts of profiles from untreated and EDTA-treated HEK-293 cells and NEBD-stage oocytes; error bars,  $\pm$ SD; *n*, number of independent biological replicates; \*\* *p* < 0.001; x signifies a lack of significance; only non-treated and EDTA-treated pairs from Dunn’s multiple comparison are displayed.

qRT-PCR-based absolute quantification allowed the calculation of 18S rRNA copy number in the used lysates. We loaded 190  $\mu$ L of the HEK-293 lysate with RNA concentration of 1.435  $\mu$ g/ $\mu$ L. Loaded lysate volume corresponded to  $2.8 \times 10^7$  cells approximately. The sum of 18S rRNA copies in all 10 fractions was  $6.74 \times 10^{11}$  (Figure 2a). In the case of NEBD-stage oocytes, a lysate of 200 cells was loaded in a volume of 300  $\mu$ L. The 18S rRNA copy number was  $3.7 \times 10^7$  (Figure 2b). Thus, the copy number of 18S rRNA was  $1.82 \times 10^4$  higher in HEK-293 sample compared to NEBD-stage oocytes.

We noticed a considerable amount of detected rRNA in the first fraction of the NEBD-stage oocyte polysome profile that contrasted with a significantly lower amount in fraction 1 of the HEK-293 cell line. We therefore decided to test to what extent the NEBD-stage oocyte sample might be contaminated with DNA. We repeated the polysomal fractionation of NEBD-stage oocytes and performed reverse transcription, on RNA isolated from individual fractions reactions, with or without added reverse transcriptase enzyme in parallel, followed by qPCR (Figure S3d,e). Accordingly, we calculated only a minimal copy number of contaminating DNA in the oocyte derived profile, that could not account for amount of 18S/28S rRNAs detected in fraction 1 (detected DNA was more than ten thousand times less abundant than RNA, as calculated for the sum of all 10 fractions). We performed an additional parallel experiment using HEK-293 lysate, with an initial RNA concentration of 1.470  $\mu$ g/ $\mu$ L that we diluted ten thousand times before performing polysome fractionation. Again, we only detected trace amounts of DNA throughout the whole HEK-293 polysome profile (Figure S3b,c). As we utilised qPCR primer pairs producing only short amplicons, we thus concluded that NEBD-stage oocytes contained a detectable level of rRNA degradation products, which then accumulated at the top of the



gradient (fraction 1). Additionally, we discovered that ten thousand times diluted HEK-293 lysate produced polysome profiles with a similar quality to the HEK-293 profiles obtained after application of concentrated lysate on sucrose gradients, as determined by qRT-PCR. Additionally, Figure S3a includes the cell numbers and the yields of RNA isolated from the diluted HEK-293 and NEBD-stage oocyte lysates, to assist other researchers with optimisation of the starting number of cells for their own adopted SSP-profiling, when different cell types will be applied.

Additionally, we measured extra and independent biological replicates in order to evaluate the effect of EDTA treatment on the disassembly of polysomes in NEBD-stage oocyte and control HEK-293 cell samples (Figure 2c). Thus, by assaying the abundance of 18S and 28S rRNAs within the obtained fractions we were able to calculate the polysome/non-polysomal ratio (P/NP, i.e., polysomal part; fractions 6–10 versus non-polysomal part; fractions 2–5) of the associated detected rRNAs. The P/NP ratio serves as approximate correlate of the translational activity of the sampled cells. In the rapidly dividing HEK-293 cell line, the calculated P/NP ratios of 18S rRNA and 28S rRNA were equal to 1.29 and 1.87, respectively, indicative of highly active translation, but upon addition of EDTA, the ratio reduced, as anticipated, to 0.2 for 18S rRNA and 0.35 for 28S rRNA. For NEBD-stage oocytes, we calculated the P/NP ratio as 0.85/0.87 (18S rRNA/28S rRNA), indicative of less active translation compared to the HEK-293 cell line, and this reduced in the EDTA-treated control sample to a value of 0.33 and 0.45 (18S rRNA/28S rRNA).

Lastly, we prepared four independent NEBD mouse oocyte derived biological replicates of SW55Ti tube-based polysomal profiles for RNA-seq and analysed them for 18S and 28S rRNA abundance by qRT-PCR (Figure 3b). The 18S and 28S rRNA contents of each individual fraction were plotted as an average and recalculated as a percentage of the given total rRNA abundance in the entire gradient. For comparison, Figure 3a demonstrates a typical qRT-PCR-based polysome profile readout of HEK-293 samples. Figure 3c,d illustrate the results obtained using the same approach applied to 200 mouse zygotes and two hundred two-cell stage embryos, respectively.

The polysome profiles of the NEBD-stage oocytes, zygotes, and two-cell stage embryos were broadly similar, with the 40S and the 60S peak maxima in fractions F2–F3 and F3–F4, respectively, and similar quantities of polysomes as evident from the qRT-PCR-visualised polysome profiles. In HEK-293 cells, the 40S and the 60S peak maxima were shifted to fractions F3–F4 and F4–F5 (as in Figure 2a), probably due to incomparably higher concentration of lysates that were loaded on the gradients. When we calculated P/NP ratios of zygotes and two-cell stage embryos samples and compared them to the P/NP ratio of NEBD-stage oocytes (Figure 2c), we observed a mild continuum in the decrease of detected polysomes from the NEBD, through zygote, to two-cell embryo stages (NEBD P/NP (18S rRNA/28S rRNA) = 0.85/0.87; zygote P/NP (18S rRNA/28S rRNA) = 0.46/0.61; two-cell stage embryo P/NP (18S rRNA/28S rRNA) = 0.39/0.52). However, the observed decrease of P/NP ratios cannot itself serve as a reliable indicator of an overall decrease in total protein synthesis throughout the development. In summary, the important overall conclusion of these experiments, including the three developmental mouse oocyte/embryo stages, was to confirm the applicability of the low volume SW55Ti tube-derived protocol to reliably visualise polysome profiles (using a qRT-PCR based readout) from samples of significant biological scarcity.



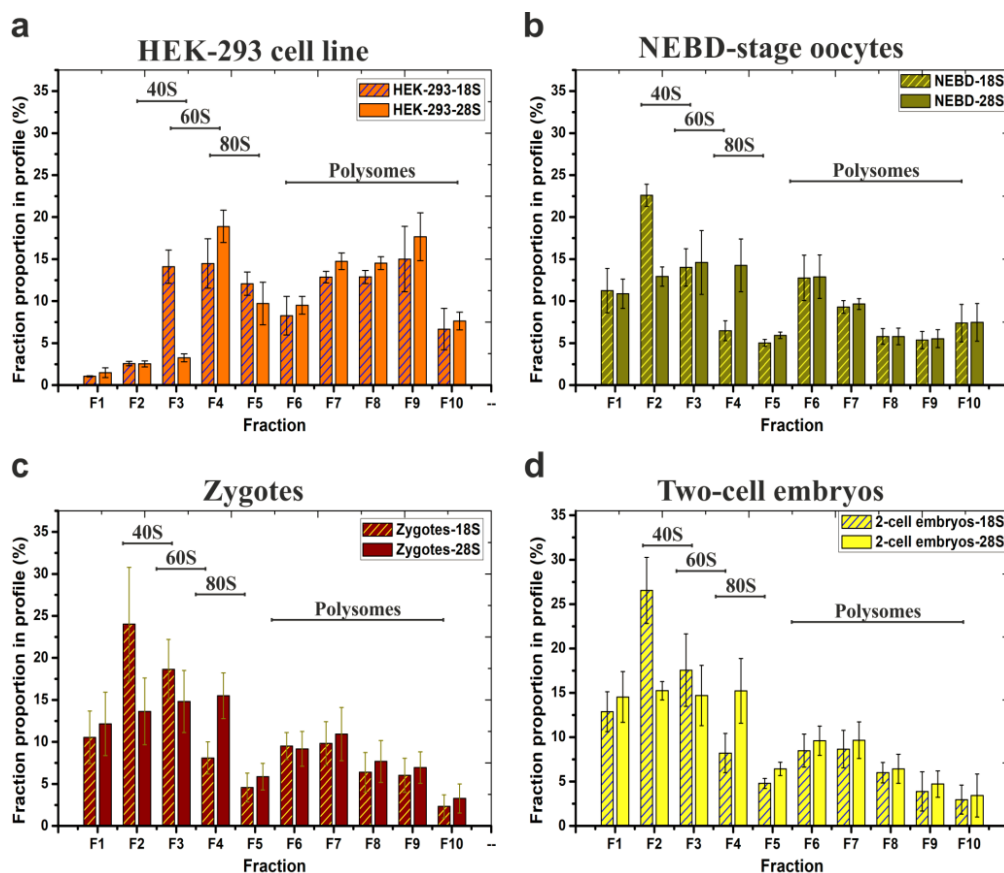


**Figure 3.** Typical distribution and abundance of ribosome- and polysome-ribonucleoprotein complexes in polysome profiles as determined by qRT-PCR analysis. Data are derived from four biological replicates of: (a) HEK-293 cell line (note, the same samples were analysed in Figure 2c); (b) 200 mouse NEBD-stage oocytes used for RNA-seq; (c) 200 zygotes and (d) 200 two-cell embryos. 18S and 28S contents in each fraction are displayed as percentages of the respective fraction compared to the whole polysome profile; error bars indicate  $\pm$ SD of biological replicates. Note, qRT-PCR-based visualization of individual replicate/source polysome profiles are included in Figure S4.

### 2.3. RNA-Seq Analysis to Reveal the Transcriptome of NEBD-Stage Oocytes

The fractionated polysome profiles obtained from NEBD-stage mouse oocytes, represented in Figure 3b, were employed in a RNA-seq analysis of polysome-bound (P) and non-polysome-bound (NP) mRNAs. In this particular RNA-seq experiment, we did not employ normalisation to total RNA since there is no transcription at the NEBD stage [4,51] and also maternal mRNA clearance occurs later in the development [52]. The NP region of the polysome profile, besides ribosomal complexes, contains maternally-stored mRNPs. Thus, comparison of the polysomal and the non-polysomal regions that indeed both contain intact mRNAs protected by proteins (and therefore display higher sedimentation coefficients) provides information about the degree of translation activation/repression of individual mRNA transcripts in oocytes. We excluded fraction 1 of the polysome profile because it contains 1% Triton-X100 that has the potential to influence RNA recovery (thus, being technically distinguished from fraction 2–5). Indeed, RNA degradation products have been reported to accumulate at the top of gradients [53,54]. Consistently, we also detected 18S- and 28S rRNA derived amplicons in the equivalent fraction of NEBD-oocyte polysome profiles (Figures 2b and 3b). Such fractions are also known to be highly enriched with RNPs consisting of short non-coding RNAs with lengths approximating 200 bp ([53]; e.g., tRNAs, as can be seen in the gels in Figure 1, fractions 1–2). For these stated reasons and because the RNA-seq library generation protocol we employed did not recover protein-coding RNAs shorter than 200 bp, the inclusion of fraction 1, provided no technical advantage

and it was excluded. However, we acknowledge we cannot completely exclude the possibility that fraction 1 may have contained a small fraction of stored RNPs, that we did not characterise in this study.

Accordingly, we pooled the RNA fractions representing the NP- (fractions 2–5) and P-populations (fractions 6–10) and subjected them to RNA-seq according to protocols described in the “Methods” section. A principal component analysis (PCA) of the RNA-seq data (Figure 4a) revealed that the component 1 (PC1; 28%) clustered the NP and P samples and that the NP samples were less variable in both components (PC2; 21%). Although a correlation of gene expression values showed that there was no profoundly obvious global difference between NP and P datasets (Figure 4b). Out of all 25,574 mRNAs transcribed from autosomes and chromosome X; 11,511 transcripts (with a value of fragments per kilobase per million reads mapped (FPKM) > 0.1) were detected in both NP and P datasets, and further 2152 mRNAs were detected only in the NP with 625 displaying expression unique to the P dataset (Table S1). 1847 transcripts with FPKM > 50 were found in the P dataset. Furthermore, from the 14,288 mRNAs with FPKM > 0.1 in at least one dataset, 5803 transcripts displayed more than 2-fold enrichment in the NP (NP/P > 2) and 2414 transcripts in the P (P/NP > 2, Figure 4b, Table S1). When we focused on the 2-fold enrichment of transcripts with FPKM > 1, the numbers changed to 4067 mRNAs enriched in the NP dataset and 1778 mRNAs in the P dataset.

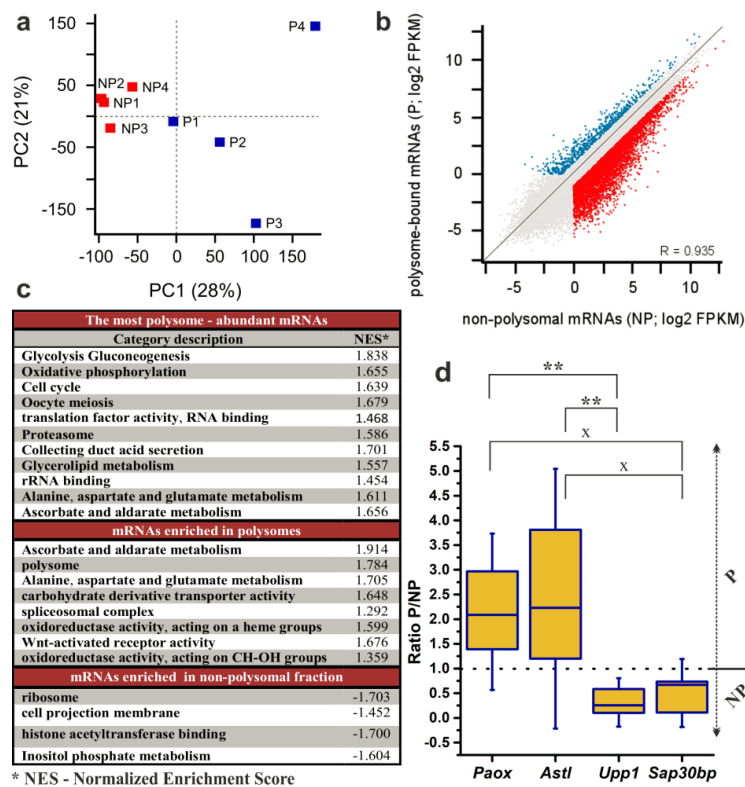


**Figure 4.** Analysis of RNA-seq results of 200 NEBD-stage oocytes. Non-polysomal (NP) and polysomal (P) RNAs were sequenced in four biological replicates. (a) Principal Component Analysis was applied to demonstrate variability among biological replicates. (b) Scatter plot highlighting genes with FPKM > 1 (fragments per kilobase per million reads mapped > 1) and > 2-fold enrichment in the NP (blue) and in the P (red). (c) Enriched gene categories according to GO (Gene Ontology) and KEGG (Kyoto Encyclopedia of Genes and Genomes) terms in dataset of all expressed genes with cut-off score of FPKM > 1. (d) qRT-PCR determination of the P/NP ratio for selected transcripts in three additional biological replicates. Box plot displays mean, 25th and 75th percentile and  $\pm$ SD; dotted line indicates no fold change; \*\*  $p < 0.01$ ; x signifies a lack of significance; Dunn’s multiple comparison is displayed only for pairs of transcripts that have been originally selected to be preferentially enriched in either the P or the NP dataset according to DeSeq2.

We next employed a ‘Gene Set Enrichment Analysis’ with the aim of gaining a complete overview of the global trends in gene expression in NEBD-stage oocytes. Thus, we utilised mean FPKM values of the P and the NP datasets from all four replicates and surveyed them in respect to their enrichment in either Gene Ontology (‘molecular function’ and ‘biological process’) or KEGG metabolic pathways databases (Figure 4c, full version is provided in Table S2). We were first interested in the enriched gene categories of the most abundant polysome-bound mRNAs. Furthermore, we determined which gene categories were significantly enriched according to their P/NP ratio, thus giving information about actively translated mRNAs in the NEBD-stage oocytes (Figure 4c). The obtained results from both analyses are thoroughly described in the Discussion section of the article.

We additionally performed DeSeq2 analysis of the NP and the P datasets and obtained a list of 355 transcripts identified as significantly and differentially enriched between NP and P datasets at the level of statistical significance  $p < 0.01$  (with  $\log_2$  of FPKM fold changes ranging from  $-9.11$  to  $7.93$ ; Figure 5; Table S3). To validate the results of the RNA-seq analysis, we selected four genes from this list for qRT-PCR analysis using three additional independent biological replicates of P and NP samples. The selected genes enriched in P fractions according to the RNA-seq data were *Paox* and *Astl* (with P/NP ratios of 7.17 and 5.88, respectively), and the genes enriched in NP fractions were *Upp1* and *Sap30bp* (with P/NP ratios of 0.19 and 0.23, respectively). qRT-PCR results confirmed the direction of enrichment in all four genes, however, the strength of the enrichment was weaker compared to the RNA-seq (Figure 4d, Table S3). Additionally, to confirm applicability of SSP-profiling to other similarly scarce samples, Figure S5b includes a result of a qRT-PCR validation of several zygotic genes that have been selected according to the RNA-seq analysis of 200 zygotes of three independent biological replicates (Figure S5a), sequenced by Dr. Ch.-J. Lin, Figure 3c provides qRT-PCR visualisation of the corresponding zygotic polysome profiles).

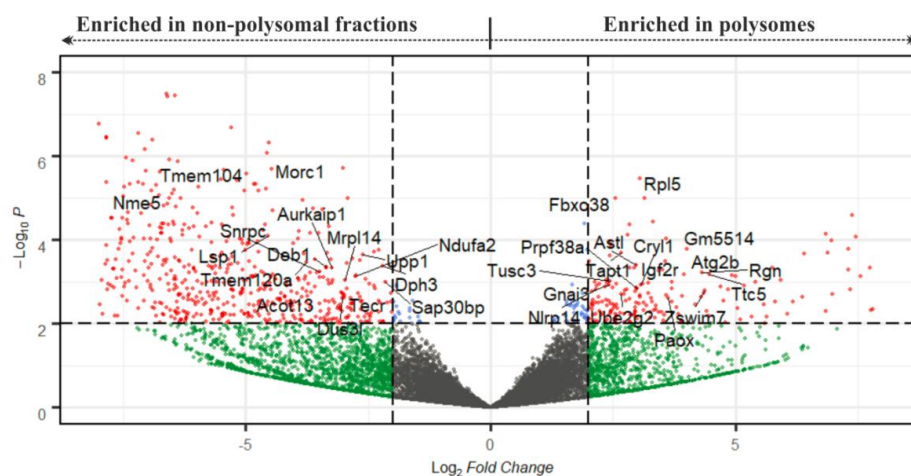


**Figure 5.** Volcano plot depicting transcripts according to their P/NP ratio after DeSeq2 analysis. The cut-off scores for the P/NP ratio (displayed as  $\log_2$  Fold Change) and the adjusted  $p$ -value ( $P_{adj}$ , displayed as  $-\log_{10}P$ ) were set to 4 and 0.01, respectively. Red spots denote mRNAs that are significant in both parameters; cut-off scores are marked with dotted lines. Gene names highlight mRNAs with strong expression (with FPKM > 80 in at least one from P and NP datasets, Table S3).

#### 2.4. Sensitivity and Versatility of SSP-Profiling for Conventional Sample Sizes and Compatibility with Downstream Methods

Conventional polysome profiling almost exclusively utilises a SW41Ti rotor-based format. The quality of the polysome profiles prepared using our novel low volume SW55Ti tube mediated methodology (SSP-profiling, Figure 1) convinced us that this approach has the potential to fully replace the traditional SW41Ti format. Therefore, we systematically tested our novel approach in polysome profiling of conventional samples, without a limiting number of cells, to provide experimental guidance

for other researchers working with conventional sample sizes. We first focused on determining the sensitivity threshold of SW55Ti-based polysome profiling (Figure 6a). Thus, we utilised a common HEK-293 cell lysate (with an RNA concentration  $0.87 \mu\text{g}/\mu\text{L}$ ) and prepared a series of 10%–50% sucrose gradients loaded with lysate volumes ranging from 1 to 8  $\text{OD}_{260 \text{ nm}}$  units that were ultra-centrifuged for 65 min at 45,000 RPM. In parallel, we constructed control polysome profiles in SW41Ti tubes, where 5–20  $\text{OD}_{260 \text{ nm}}$  units of the HEK-293 lysate were applied ( $1.249 \mu\text{g}/\mu\text{L}$ ). These samples were centrifuged in SW41Ti rotor for 3 h at 35,000 RPM (as per conventionally accepted protocols). The result presented in Figure 6a indicates that the application of just one  $\text{OD}_{260 \text{ nm}}$  unit to the novel low-volume-based approach produced a polysome profile with well-defined peaks that enabled the detection of polysomes. Furthermore, based on comparisons with the conventionally derived polysome profiles (obtained using the SW41Ti rotor-based system), we estimated that one  $\text{OD}_{260 \text{ nm}}$  unit loaded on in our newly developed approach (utilising SW55Ti rotor compatible tubes) corresponds roughly to 2.5  $\text{OD}_{260 \text{ nm}}$  units applied using the conventional method. These results suggest the novel SW55Ti-based methodology of generating polysome profiles is approximately 2.5 times more sensitive, compared to the established method, when actively translating, fast-growing cells are used.

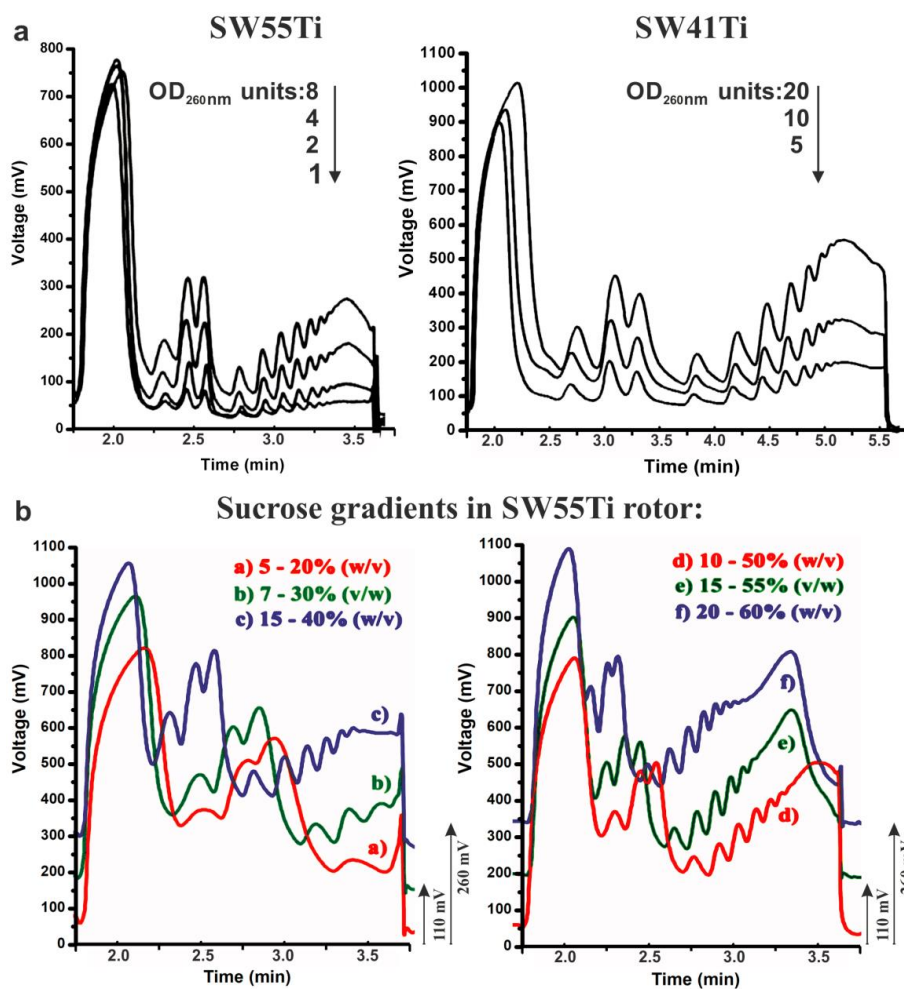


**Figure 6.** Sensitivity limit and versatility of polysome profiling in SW55Ti tubes. (a) 1–8  $\text{OD}_{260 \text{ nm}}$  of HEK-293 lysates were loaded onto 10%–50% sucrose gradients (in SW55Ti specific tubes) and centrifuged at 45,000 RPM for 65 min at  $4^\circ\text{C}$  (left). Peak readability was compared to the one of conventional polysome profiles made in SW41Ti tubes, where 5–20  $\text{OD}_{260 \text{ nm}}$  were loaded onto 10%–50% gradients which were centrifuged at 35,000 RPM for 3 h at  $4^\circ\text{C}$  (right). (b) Sucrose gradients of varying sucrose concentration ranges were prepared in SW55Ti tubes (a–f). Profiles in b + e and c + f were shifted up by 110 and 200 mV, respectively, to prevent overlapping of curve traces (to aid interpretation).



The application of gradients of varying sucrose concentration is commonly used in cases where enhanced resolution of macromolecular complexes within a specific range of sedimentation velocity coefficients is required (e.g., 40S–80S, polysomes). Therefore, we tested whether SW55Ti rotor compatible tubes, characterised by reduced gradient volume, are suitable for such high-resolution separation. Accordingly, we applied different volumes of HEK-293 cell lysate (RNA concentration=1.435 µg/µL) on the following series of sucrose gradients: 5%–20% (515 µL), 7%–30% (350 µL), 15%–40% (300 µL), 10%–50% (206 µL), 15%–55% (206 µL) and 20%–60% (206 µL). Note that differing volumes of identical lysate sample were loaded onto individual sucrose gradients (of differing concentrations) to ensure an approximately equal amount of material would be retained within the gradient after centrifugation. This is because complexes with higher sedimentation velocity are naturally spun to the bottom of the tube (e.g., polysomes in 7%–30% gradient). Ultra-centrifugation was then performed at 45,000 RPM for 65 min at 4 °C, before 65%-sucrose was used to push gradients into the detector cell. We observed clearly distinguishable polysome peaks and high-quality curves in all the tested gradient variants (Figure 6b). Indeed, the gradient of 5%–20% sucrose separated well the region just before the 40S peak to the first polysome; the 7%–30% gradient the region from the 40S peak to the polysomes containing three ribosomes; the 15%–40% gradient seemed to be suitable for good visualization of the region from the 40S peak to middle-molecular weight polysomes. The most common 10%–50% concentration range provided good resolution from the 40S peak to heavy polysomes. However, the 15%–55% gradient proved to be the most optimal for the separation of very heavy polysomes without any considerable loss of resolution in the region around the 40S peak. The gradient 20%–60% also produced very similar profile, but with reduced resolution in the region between the 40S and the 80S peaks. Overall, we concluded that the novel low volume SW55Ti rotor tube-based protocol is able to readily accommodate various sucrose gradients without compromising the quality of polysome separation.

Many studies aim to confirm the association of proteins of interest with ribosomes and/or polysomes by utilising western blot analysis of fractionated polysome profiles. In Figure S7, we demonstrate the reduced volume SW51Ti tube specific protocol can accommodate enough cell lysate to detect any moderately abundant protein and, in parallel, the KCl concentration used in sucrose gradient ultimately affects the western blot result.

### 3. Discussion

High throughput techniques are widely applied to understand time-dependent global changes in gene expression during oocyte maturation, oocyte-to-embryo transition and early embryonic development, often with special attention to human infertility [42]. Even though, methodical improvements of NGS methods have led to the establishment of suitable protocols for transcriptomic studies of mammalian oocytes, no such approach is available for deep-sequencing of polysome-bound mRNAs [55,56]. High quality polysome profiling has conventionally required large number of cells to obtain well-defined and interpretable peaks (e.g., for HeLa cells approximately  $2\text{--}4 \times 10^7$ ). However, such amount of material is not available from specific and scarce cell types, such as mammalian oocytes. Several modified polysome profiling methods have been presented in previous studies, all utilizing DNA microarrays, aiming to circumvent this problem. Potireddy and colleagues [30] described an approach for 160–200 MII-stage mouse oocytes and early embryos, that included pelleting translating polyribosomes through a sucrose cushion in 200 µL-centrifugation tubes, two rounds of cDNA amplification, and subsequent microarray analysis. Another approach, optimised for polysome fractionation of 75 bovine oocytes, entailed the application of incompletely crosslinked heterologous carrier polysomes (prepared from *Drosophila* SL2 cell line), centrifugation in small, SW60Ti centrifugation tubes, two rounds of cDNA amplification and microarray analysis [31]. The final published setup, that was applied to analyse groups of 500–600 mouse oocytes in various developmental stages, is based upon more conventional polysome profiling in 12 mL-, 15%–50%-sucrose gradients, cDNA amplification and microarray hybridisation [47]. Here, we report a protocol comprising centrifugation



in small SW55Ti tubes, quantification of 18S and 28S rRNA in each fraction of the derived polysome profile, cDNA amplification and RNA-seq analysis of polysome-bound and non-polysomal bound mRNA populations. We have optimised this approach for a sample size of 200 mouse NEBD stage oocytes (Figures 2b and 3b). Previously, published reports have provided a lot of valuable information concerning the specific recruitment of mRNAs to polyribosomes and have highlighted the irreplaceable role of specific translation to support proper developmental competence of maturing oocytes. However, in SSP-profiling, we have included several methodical improvements, including a reduced sample size (i.e., 200 oocytes) and compatibility with subsequent RNA-seq analyses. Moreover, the omission of heterologous cell derived carriers also prevents contamination of resultant NGS libraries by reads of non-mouse origin and thus sustains sequencing depth. As demonstrated our protocol is functional starting with 200 mouse oocytes, reflecting a reduction of the input material in comparative studies [47] or those utilising larger bovine oocytes [31], but we anticipate that with finer optimisation we may be able to feasibly reduce this number to only 100 oocytes (based on preliminary data).

When employing SWTi55 centrifugation tubes, we focused on adjusting the ultra-centrifugation conditions and checking every step of polysome profiling (Figures 1, 2 and 6 and Figures S1 and S2). We suggest that a reconstruction of each individual polysome profile using qRT-PCR of 18S and 28S rRNAs is one of the main methodical improvements for profiling samples of biological scarcity (Figures 2 and 3). In comparison to other published protocols, SSP-profiling allows the determination of the actual rate of translation in each individual profile by rough estimation of the area of the derived polysomal peaks, as well as visualizing the amplitude and positions of peaks corresponding to the 40S and the 60S ribosomal subunits and the 80S monosome. The quantification of absolute rRNA copy number also facilitates the quality control of any derived polysome profiles, in addition to estimating the RNA amount in applied oocyte lysate (Figure 2). Using such methodology, we were able to calculate that the copy number of 18S rRNA was  $1.82 \times 10^4$  higher in HEK-293 samples as compared to NEBD-stage oocytes (Figure 2). We thus estimate that at least 10,000 oocytes would be required to obtain readable peaks in any oocyte derived polysome profile using the ISCO detector (at its given sensitivity). Clearly, such estimates exclude the possibility of using a conventional, non-qRT-PCR based, method as a huge number of animals would need to be sacrificed in one experiment (given the fact that 20–40 developmentally competent oocytes could be obtained from one female mouse). Taken together, the above stated observations highlight the attractiveness of SSP-profiling protocol, given we can reliably detect polysome profiles from only 200 oocytes.

The combined use of at least four biological replicates of NEBD-stage oocytes, zygotes and two-cell embryos allowed us to validate the reproducibility of the described qRT-PCR-based polysome profiles in other types of scarce/limiting sample (Figure 3). We also investigated NEBD-stage oocyte polysome profiles with and without EDTA treatment (Figure 2c). EDTA disassembles elongating ribosomes and is thus commonly applied for verification of the absence of other complexes containing joined ribosomal subunits in the polysomal regions of the obtained profile. The NEBD-stage oocytes showed a more equal ratio of polysomal and non-polysomal rRNA associated regions of the profile (18S rRNA P/NP = 0.85; 28S rRNA P/NP = 0.87) than HEK-293 cells, demonstrating more moderate levels of translation (Figure 2c). The P/NP ratio of EDTA-treated oocytes decreased to 0.33 and 0.45 for 18S rRNA and 28S rRNA, respectively, indicating that the vast majority of the detected 18S and 28S rRNAs represented polysomes. However, according to the P/NP ratio of EDTA-treated NEBD-stage oocyte, we could not confirm or exclude the possibility that there were no high-molecular-weight stored ribonucleoprotein particles (RNP) that co-sedimented with polysomes and thus contained both rRNA species. It has been shown that maternal RNPs are stored in distinct sub-cellular regions in the oocyte [36]. Indeed, microscopic studies have revealed RNP aggregates at the cortex and in fibrillar cytoplasmic lattices and the latter of which also contains inactive ribosomes [36,57]. However, very little is known about their physical properties, complete protein composition nor their velocity sedimentation coefficients. It is noteworthy that no direct experiments have been reported to exclude the presence of high-weight, yet inactive, ribosome complexes in the fractionated polysomal regions of oocytes so far. EDTA-treatment

has been only applied to assess the quality of polysome profiling in oocytes, but only when detecting protein-coding transcripts [31]. Contrarily, we have focused on the simultaneous detection of 18S and 28S rRNAs, an approach that we argue, better reflects the presence of RNP containing inactive ribosomes or their subunits, although we acknowledge a more direct method to assess this would be preferable.

Existing microarray-based studies have focused on the differences in mRNA polysome recruitment during mammalian oocyte maturation [30,31,47]. With the aim of providing new insight into the mechanisms regulating meiosis progression, we applied our own polysomal fractionation method, followed by RNA-seq analysis of polysome-bound and polysome-unbound mRNAs (also containing stored mRNPs) on oocytes at the NEBD-stage. This specific developmental time-point was deliberately chosen as the earliest recognizable developmental point indicative of the end of prolonged meiotic prophase I arrest. Moreover, it is also associated with breakdown of the nuclear lamina, chromosomal condensation and the initiation of meiotic spindle assembly [36]. Maturing oocytes exhibit a high rate of aneuploidy that is associated with increased maternal age and atypically short NEBD-stage duration [58,59]. Indeed, following NEBD, a strong poly(A) signal is known to be present in the vicinity of chromosomes where the meiotic spindle is assembled and certain transcripts exhibit specific nuclear/chromatin localisation [36]. Furthermore, it is speculated that such cellular mRNA localisation might serve as a means to ensure the precise timing of translation of specific proteins needed for meiosis progression [41]. Therefore, revealing the actively translated mRNAs at the NEBD stage has the potential to shed extra light upon such mechanisms related to oocyte aneuploidy and NEBD, that have until now been largely overlooked.

We performed RNA-seq of polysomal and non-polysomal mRNAs in four biological replicates (Figure 3b). Our Principal Component Analysis confirmed polysomal and non-polysome-bound mRNAs clustered away from each other, confirming their heterogenous nature (Figure 4a). In agreement, the conducted Gene Set Enrichment Analysis revealed polysomal enrichment of certain mRNAs, which encoded proteins implicated in an increase of total translation or translation initiation rate, with the potential to contribute to increased polysome formation (GO:0005844, category “polysome”, Figure 4c). We also attempted to confirm that we did not lose some portion of detectable and stored mRNPs by the technically required exclusion of fraction 1 of the fractionated polysome profiles. However, since fraction 1 may only contain mRNPs with a maximum sedimentation coefficient of about 20S, it can be theorised that these mRNPs will preferentially contain only short transcripts of some protein-coding genes. Nevertheless, we assayed for any correlation between transcript length and their calculated P/NP ratio, or any correlation between transcript length and their expression levels, in our derived NP- and P datasets (Figure S6). These analyses did not yield any correlation between these parameters, suggesting no significant bias in the derived data. However, we still cannot be completely sure that we did not lose some mRNPs in the initially excluded fraction 1, but it seems unlikely.

Our study extends the knowledge of gene expression changes during oocyte maturation by focusing on a still unexplored stage of oocyte maturation by polysome profiling. As a result, we found some abundant polysome-associated mRNAs that encode proteins with unspecified function in oocyte maturation, e.g., TAPT1, TUSC3, FBXO38, ZSWIM7 and DPCD (Table S3). Conversely, when we investigated the overexpressed gene categories, we found our data agrees well with many studies describing the overall metabolic status of the maturing oocyte and in many ways complements the current theories relating to the actual synthesis of regulatory proteins and enzymes [34,60]. For example, from the most abundant polysome-bound mRNAs we identified (Figure 4c, Table S2), we observed an enrichment of gene categories for pyruvate, glutamine, aspartate, alanine, glycerolipid and L-ascorbate metabolic pathways, and an enrichment of mRNAs for many glycolytic/gluconeogenic enzymes (e.g., glucose-6-phosphate dehydrogenase). Furthermore, mRNAs encoding subunits of mitochondrial and lysosomal ATPases demonstrated the same trend. These findings agree with the well-documented metabolic status of the maturing oocyte [34]. The main source of energy required for oocyte maturation and resumption of meiosis is known to be pyruvate and glutamine, which are

metabolised by the TCA (tricarboxylic acid) cycle and oxidative phosphorylation in mitochondria [61]. Moreover, gluconeogenesis is preferred to glycolysis and the expression of glucose-6-phosphate dehydrogenase is increased along with the activity of the pentose phosphate pathway, which produces pentose bodies for the synthesis of nucleosides [34]. Tubulins and tubulin-associated proteins were also amongst another enriched gene category and it is evident that their synthesis supports correct meiotic spindle formation. Additionally, we observed abundant polysome-bound mRNAs coding for translation initiation factors, rRNA binding proteins (including ribosomal proteins) and number of proteins with a well-established role in meiosis (e.g., DAZL, MOS, Cyclins B1 and B2 and AURKA) in enriched gene categories. It is proposed that active translation in oocytes is partially sustained by amino acids generated by protein degradation, in the context where only six amino acid transport system has been identified [62]. Consistently, we identified proteasome subunit mRNAs to be abundantly enriched in polysomes. Indeed, the ubiquitin-proteasome system is also implicated in the regulation of meiotic progression, fertilisation and zygotic genome activation [63]. Lastly, we observed very high level translation of mRNAs encoding oocyte membrane-associated proteins, which play roles in sperm recognition and the regulation of fertilization; e.g., ZP2, ZP3, Ovastacin and several CCT chaperonins [64].

In the second component of our Gene Set Enrichment Analysis (Figure 4c, Table S2), we were interested in comparing particular mRNA abundancies in the non-polysomal and polysomal regions of the derived polysome profiles. This comparison permitted the degree of translational activation for individual mRNAs to be determined regardless of their relative abundance because the non-polysomal pool also contains stored mRNPs. Similar results, focusing on the most abundant polysomal transcripts, were observed. However, we discovered that some of the highly translated mRNAs were in fact still more abundant in the stored mRNA pool. This finding applied particularly to mRNAs for both cytosolic and mitochondrial ribosomal proteins, ATPase subunits and some glycolytic enzymes, indicating that only the minority of these mRNA molecules were translated and that the majority still remained pre-synthesised for later translation. The same trend was also evident for many mRNAs coding for protein regulators of meiotic progression. During oocyte growth and maturation, mitochondria replicate up to numbers between 300,000–400,000 [65]. We found that mRNAs for the mitochondrial cytochrome C oxidase subunits were enriched in polysomes, while mRNAs for the NADH:ubiquinone oxidoreductase subunits were more abundant in the non-polysomal mRNA pool. We observed translational activation of mRNAs for resident endoplasmic reticulum proteins and many proteins with antioxidant activity, such as superoxide dismutase, thioredoxin reductase, glutathione peroxidase, glutathione dehydrogenase and peroxiredoxin. We also detected mRNA encoding lactate dehydrogenase to be abundant in polysomes. Taken together, these facts demonstrate that active translation of such proteins, which are significant for the maintenance of the redox state in the oocyte and buffering mitochondria respiratory activity, occur in the NEBD-stage oocytes [66]. mRNAs for two UDP-galactose and one nucleotide solute carrier transporters were additionally found to be also enriched in polysomes, demonstrating that their active synthesis supports galactose, pyrimidine and adenine-containing base import to NEBD-stage oocytes. Intriguingly, several mRNAs of the spliceosomal complex were enriched in polysomes, whereas mRNAs for several basal transcription factors were enriched in the non-translated mRNA pool. We found Prpf38A mRNA that encodes the spliceosome protein PRP38 and SRSF1 splicing factor encoding mRNA to be enriched in polysomes (Table S3). This suggests that transcriptionally silent NEBD-stage oocytes contain pre-synthesised mRNAs for proteins involved in both transcriptional initiation and splicing, but the splicing related mRNAs are translated earlier in development.

During the optimization of this novel SSP-profiling protocol, we also used HEK-293 cell line and W303 yeast strain lysates as controls (Figure 1). The performance of SSP-profiling in regard to these conventional samples, in the SW55Ti rotor, was very favourable (Figures 1, 2a and 6). This SW55Ti rotor is occasionally applied in plant science protocols where polysome profiles are often obtained from crude ribosome pellets after centrifugation of lysates over a sucrose cushion in a Type70Ti rotor [67,68].

The SW55Ti rotor, or the even smaller SW60Ti rotor, have been utilised for polysome profiling in a couple of previous studies but either the relevant authors did not provide evidence of the obtained curves or the profiles were obtained from specialised material and/or by different sucrose gradient mediated methods [69–72]. Owing to these facts and the general sparsity of SW55Ti-derived polysome profile experiments, we decided to carefully compare polysome profiling in SW55Ti and conventional SW41Ti rotors (SW41Ti represents the most often used rotor size format, but sometimes similar SW40Ti is used). Accordingly, for this comparison, we applied the most often studied biological materials; i.e., mammalian cell lines and yeast cells. The results in Figure 1, Figure 6 and Figure S7 suggest that the SW55Ti-based polysome profiles are fully comparable to those conventionally obtained with SW41Ti rotors and that this SSP-profiling protocol is fully compatible with downstream methods. Importantly, the usage of smaller tubes offers economic benefits to the whole polysome profiling methodology, as it not only directly saves on required chemicals (to the extent of ~2.2-fold), but also reduces consumable usage, in terms of the material required for cell growth. We also predict that the three times reduction in centrifugation time, plus the additional shortening of gradient analysis time, will be very attractive for a large number of researchers.

#### 4. Materials and Methods

##### 4.1. Human Cell Line, Yeast Strains and Mouse Oocyte, Zygotes and 2C-Embryos Isolation and Culture

The human embryonic kidney 293 (HEK-293) cell line was maintained in Dulbecco's Modified Eagle Medium (DMEM, Gibco, Gaithersburg, MD, USA) supplemented with 10% FBS and 2 mM L-glutamine at 37 °C in humidified atmosphere containing 5% CO<sub>2</sub>. Cells were grown to 60%–70% confluency in 150 mm diameter dishes. Cycloheximide was added to medium at final concentration of 0.1 mg/mL. After 10 min, cells were washed with ice-cold PBS supplemented with cycloheximide (0.1 mg/mL) and then scraped in the presence of 800 µL of Polysome Extraction Buffer (PEB; 10 mM HEPES, pH 7.5; 62.5 mM KCl; 5 mM MgCl<sub>2</sub>; 2 mM Dithiothreitol (DTT); 1% Triton X-100; 100 µg/mL cycloheximide; complete EDTA-free (Roche, Basel, Switzerland, 1 tablet/10 mL); and 40 U/mL Ribolock (Thermo Fisher Scientific, Waltham, MA, USA) and collected in 1.5 mL tubes.

Fifty milliliters of the *Saccharomyces cerevisiae* strain W303 bearing a temperature-sensitive mutation in guanylyltransferase (*ceg1-3<sup>ts</sup>*, [50]) gene were cultivated in YPD medium at 24 °C with shaking. The culture was split into two parts at an OD<sub>660 nm</sub> of 0.6. The first half was immediately harvested, the second one was mixed with pre-warmed, 52 °C-hot medium and cultivated for 12 h at 37 °C. At the time of harvesting, cycloheximide was added to the medium at final concentration 0.1 mg/mL. After 10 min, the cells were pelleted by centrifugation and washed three times with ice-cold water with cycloheximide (0.1 mg/mL). Dry cell pellets were kept at –80 °C for later use.

Germinal vesicle (GV) oocytes were obtained from 8 weeks old CD1 mice, 46 h after injection with 5 IU pregnant mare serum gonadotropin (PMSG, ProSpec, Rehovot, Israel). Oocytes were isolated at the GV stage (0 h) in M16 medium (Sigma-Aldrich, Darmstadt, Germany) [73], supplemented with 100 µM 3-isobutyl-1-methylxanthine (IBMX, Sigma-Aldrich, Darmstadt, Germany) to prevent nuclear envelope breakdown (NEBD). Selected oocytes were denuded and cultured in M16 medium (Sigma-Aldrich, Darmstadt, Germany) without IBMX at 37 °C in 5% CO<sub>2</sub>. After 80 min of culture, those oocytes that underwent NEBD were selected. Finally, after 3 h post-IBMX, cycloheximide at final concentration 0.1 mg/mL was added to medium and oocytes were cultured for 10 further minutes. NEBD oocytes were then transferred to polyvinyl alcohol (PVA) supplemented with cycloheximide (0.1 mg/mL) and stored at –80 °C in a low-binding retention tubes.

In the case of zygotes and two-cell embryos, 48 h post PMSG injection, mice were further injected with 5 IU of hCG (Pregnyl<sup>®</sup>, MSG, Merck Sharp & Dohme B.V, White House Station, NJ, USA) and placed with males for mating. Zygotes and embryos were collected 23 h and 35 h later, respectively, from oviducts, and moved into M2 medium (Sigma-Aldrich, Darmstadt, Germany), which was supplemented with cycloheximide (0.1 mg/mL). After 10 min of cultivation at 37 °C in atmosphere



containing 5% CO<sub>2</sub>, they were harvested and stored at −80 °C. All animal work was conducted according to Act No 246/1992 for the protection of animals against cruelty; issued by Ministry of Agriculture of the Czech Republic, 25.09.2014, number CZ02389.

#### 4.2. Preparation of Lysates and Polysomal Profiling

All cell types were lysed in PEB. HEK-293 cells were incubated in lysis buffer for 20 min on ice with occasional vortexing. Cell extracts were centrifuged at 8000× *g* for 5 min at 4 °C. Yeast cells were disrupted using acid-washed glass beads in a mixer mill apparatus MM301 (Retsch, GmbH, Haan, Germany), set at 30 shakes/second for 3 min, followed by immediate cooling on ice. To disrupt oocytes and their rigid zona pellucida (ZP), zirconia-silica beads were added to the tubes containing 200 NEBD-stage oocytes together with 350 µL of lysis buffer. Tubes were placed in MM301 and shaken in the frequency of 30 shakes/second for 1 min followed by immediate cooling on ice for 3 min. This step was repeated 3 times. Lysates were cleared by centrifugation at 10,000× *g* for 5 min at 4 °C and then cast on sucrose gradients, which were prepared in solution containing 10 mM HEPES, pH 7.5; 100 mM KCl; 5 mM MgCl<sub>2</sub>; 2 mM DTT; 100 µg/mL cycloheximide; Complete EDTA-free (1 tablet/100 mL); and 5 U/mL Ribolock (Thermo Scientific). For polysome dissociation experiments, 100 mM EDTA was added to lysis solution without MgCl<sub>2</sub> prior to disrupting the cells and the resulting lysate was loaded on sucrose gradients supplemented with the same concentration of EDTA. Sucrose gradients were prepared in Gradient Master™ 108 v5.3 (Biocomp, Fredericton, NB, Canada) with the following programs for SW55Ti tubes with long cap: 5%–20% (*w/v*), one-step; 7%–30% (*w/v*), one-step; 15%–40% (*w/v*), one-step; 10%–50% (*w/v*), twelve-step; 15%–55%, two-step; 20%–60% (*w/v*), two-step. SW41Ti long-cap 10%–50% (*w/v*) sucrose gradients were prepared using the eleven-step program. We adjusted the weights of SW55Ti and SW41Ti tubes with prepared gradients to 6.59 g (SW55Ti) and 15.19 g (SW41Ti), respectively, before loading lysates. This protocol improvement allowed us to load the identical volumes of samples and subsequently helped with fitting the position of the loading peak in the polysome profile curve. Meaning, the SW55Ti tube can accommodate 8 OD<sub>260 nm</sub> of lysate in maximal volume of 300 µL and SW41Ti tube 20 OD<sub>260 nm</sub> in volume 520 µL. Where lysate concentration is indicated, it corresponds to RNA concentration in the lysate as calculated. Velocity sedimentation was performed in Optima L-90 Ultracentrifuge (Beckman Coulter, Indianapolis, IN, USA) at 45,000 RPM (246,078× *g*) for 65 min at 4 °C in SW55Ti UltraClear™ tubes (Beckman Coulter) or at 35,000 RPM (210,053× *g*) for 180 min at 4 °C in SW41Ti UltraClear™ tubes (Beckman Coulter). Continuous absorbance monitoring at 280 nm was performed using an ISCO UA-5 detector and ISCO UV absorbance reader (Teledyne, ISCO, Lincoln, NE, USA). 60% sucrose solution was pumped into SW55Ti and SW41Ti tubes with the speed 1.8 mL/minute and 2.2 mL/minute, respectively, using NE-1000 syringe pump (New Era Pump Systems, Inc., Farmingdale, NY, USA). Polysome profile data were collected and processed using Clarity Lite software [29].

#### 4.3. RNA Isolation, RNA Electrophoresis and qRT-PCR

For coarse RNA isolation from human and yeast cells (Figure 1), we collected SW55Ti and SW41Ti polysome profiles into fractions of equal volume. One microliter of GeneElute™-LPA (linear polyacrylamide, Sigma Aldrich) was added to each fraction as a co-precipitant. After vortexing, equal volumes of 5.25 M guanidine thiocyanate and isopropanol were added. Samples were precipitated overnight and then RNA was spun at 19,000× *g* for 20 min at 4 °C. After two washes with 75% ethanol, pellets were air-dried and RNA corresponding to SW55Ti- and SW41Ti-derived fractions was dissolved in 20 µL and 30 µL of RNase-free H<sub>2</sub>O, respectively. RNA electrophoresis was performed according to [74] with the exception that loading dye was supplemented with 0.1% SDS. We loaded 15 µL (SW55Ti) and 10 µL (SW41Ti) of dissolved RNA. RNA concentration and yield were determined spectrophotometrically at 260 and 280 nm.

High quality RNA isolation from the HEK-293 cell line, mouse oocytes, zygotes and two-cell stage embryos was performed by collecting 10 fractions, of 0.5 mL each, of SW55Ti-derived polysome



profiles. Working on ice, 1  $\mu$ L of GeneElute<sup>TM</sup>-LPA was added, vortexed and immediately added 1 mL of TriReagent (Sigma Aldrich). After vortexing, 350  $\mu$ L of chloroform was added, again vortexed and centrifuged at 19,000 $\times$ g for 20 min at 4 °C. Equal volumes of isopropanol were added to RNA-containing phases. RNA isolation was then completed as described above in the case of the coarse RNA isolation.

4  $\mu$ L of RNA from each fraction were reverse-transcribed using 20 U of M-MuLV Reverse Transcriptase (Thermo Scientific) and 0.3  $\mu$ g of random hexamer primers in a reaction volume of 20  $\mu$ L. cDNA synthesis was performed at 25 °C for 10 min and then in 37 °C for 5 min followed by incubation at 42 °C for 1 h and subsequent inactivation at 70 °C for 10 min. qRT-PCR experiments were performed using a LightCycler480<sup>®</sup> (Roche, Basel, Switzerland) and LightCycler480<sup>®</sup> SYBR Green I Master mix (Roche). The 10- $\mu$ L reactions were performed in triplicates. Each reaction contained 2  $\mu$ L of cDNA and 500 nM gene-specific primers (list of used primers is provided in Table S4). The amplification protocol was 95 °C for 5 min; 44 cycles of 95 °C for 10 s, 58 °C for 15 s, 72 °C for 15 s; followed by melting curve determination. For absolute qRT-PCR quantification, we created recombinant pCR<sup>TM</sup>4-Topo<sup>TM</sup> plasmids (Invitrogen, Carlsbad, CA, USA) containing 18S and 28S rRNA PCR amplicons (Table S4). For qRT-PCR validation of selected transcripts, we took half of dissolved RNA in each collected fraction (10  $\mu$ L) and created two pools: non-polysomal sample (NP; corresponding to the 40S, the 60S and monosomal peaks, fractions 2–5) and polysomal associated one (P; polysomal region, fractions 6–10). Then, we performed reverse transcription reactions in the final volume 100  $\mu$ L containing 40  $\mu$ L of pooled RNA, 2.5  $\mu$ g of oligod(T<sub>18</sub>) and 1  $\mu$ g of random hexamer primer and 100 U of M-MuLV Reverse Transcriptase. RT reaction and qPCR conditions were identical as those described above. The relative quantification mode was applied and the mean of 18S and 28S RNA level was used for normalization of NP and P components of the polysome profiles.

#### 4.4. RNA-Seq Library Preparation

For RNA-seq, we measured 18S and 28S rRNA content in collected fractions derived from NEBD-stage oocyte polysome profiles and then we pooled fractions as described for the qRT-PCR validation. Pooled RNA was concentrated using RNA Clean & concentrator kit (ZYMO Research, Irvine, CA, USA) and rRNA depleted using Ribozero Gold rRNA Removal kit (Illumina, San Diego, CA, USA). Remaining RNA in each sample was DNase-treated, reverse transcribed and amplified using the Repli-G WTA single cell amplification kit (Qiagen, Hilden, Germany). cDNA synthesis was primed by a mixture of oligod (T<sub>18</sub>) and random hexamers primers. The amplified cDNA was then processed by the Nextera DNA library prep kit (Illumina) to generate sequencing libraries. Sequencing was performed on HiSeq 2500 (Illumina) with 150 bp paired-end reads.

#### 4.5. Bioinformatical and Statistical Analyses

Reads were trimmed using Trim Galore! v0.4.1, checked for sequencing quality using FastQC v0.11.5 and for contamination by mapping to genomes of several model organisms using FastQC Screen v0.11.1, and finally mapped to the mouse GRCm38 genome assembly using Hisat2 v2.0.5 [75]. Gene expression was quantified as fragments per kilobase per million (FPKM) values in Seqmonk v1.40.0 (Manufacturer name, city, state abbreviation if USA or Canada, country). Mapping of RNA-seq reads on mouse genome is accessible in UCSC Genome Browser ([https://genome.ucsc.edu/s/lenkagahurova/NAR\\_Masek\\_polysome\\_RNAseq](https://genome.ucsc.edu/s/lenkagahurova/NAR_Masek_polysome_RNAseq)). RNA-seq data have been deposited in Gene Expression Omnibus database under the accession: GSE121358. PCA for transcripts with FPKM >1 was performed using R function (R v3.4.0) within Seqmonk v1.40.0. DeSeq2 (R v3.4.0) was applied to analyse transcripts with differential abundance in the NP and the P samples. The R code for the translome analysis is available upon request. qRT-PCR data analyses were performed in the LightCycler 480 software (version 1.5, Roche, Basel, Switzerland) in absolute and relative quantification modes. Gene Set Enrichment analysis was performed by utilising the WEB-based GEne SeT AnaLysis Toolkit (<http://webgestalt.org/option.php>). Results in Figures 2c and 4d were statistically evaluated by Kruskal–Wallis ANOVA followed by post-hoc Dunn's multiple comparison test.

## 5. Conclusions

In summary, this study describes SSP-profiling as a novel protocol that is able generate high quality data with all the versatility of currently described and conventional methods. We have demonstrated the suitability of this novel polysome profiling technique by coupling it to RNA-seq screens of polysome associated transcripts from biologically scarce samples, as represented by 200 mouse NEBD-stage oocytes (in the process generating novel and biologically relevant data on a previously unexplored point in mouse oocyte maturation development). Lastly, we have also provided a detailed description of the SSP-profiling experimental technique that we anticipate will aid its adoption in the wider scientific community.

**Supplementary Materials:** Supplementary materials can be found at <http://www.mdpi.com/1422-0067/21/4/1254/s1>. Supplementary Materials include Figure S1. Influence of different centrifugation times and speeds on polysomal profile performance in SW55Ti centrifugation tubes and rotor; Figure S2. Spectrophotometric measurement of quantity and purity of isolated RNA obtained from polysome profile fractions of HEK-293 human cell line and W303 ceg1ts yeast strain; Figure S3. qRT-PCR analyses of HEK-293 cell and NEBD-stage oocyte polysome profiles including parallel measurements of DNA contamination and information about cell numbers and total RNA contents in input lysates; Figure S4. qRT-PCR-based visualizations of individual replicate/source polysome profiles used for Figures 2c and 3; Figure S5. Validation of the selected polysome-enriched zygotic mRNAs; Figure S6. Plots represent the P/NPs or FPKM values in the P and the NP datasets of individual transcripts according to their lengths. Figure S7. Reduced-sized-, 5-mL-SW55Ti ultracentrifugation tubes can accommodate enough cell lysate to detect moderately abundant protein in polysome profile fractions (contains the following references: [76–78]; Table S1. List of expressed genes with mean FPKM higher than 0.1 in at least one dataset; Table S2. Sheet S2-1: GSEA according to FPKM in P dataset, Sheet S2-2: GSEA according to P/NP ratio; Table S3. DeSeq2 analysis of polysome-bound mRNAs versus non-polysomal mRNAs; Table S4. List of used primers.

**Author Contributions:** Conceptualization, T.M., A.S., A.W.B. and M.P.; Data curation, L.G.; Formal analysis, L.G. and M.P.; Funding acquisition, T.M., M.K. and M.P.; Investigation, T.M., E.d.L. and C.-J.L.; Methodology, T.M.; Software, L.G., and K.R.; Visualization, T.M., and L.G.; Writing—original draft, T.M.; Writing—review and editing, A.W.B., and T.M. All authors have read and agreed to the published version of the manuscript.

**Funding:** This research was supported by The Czech Science Foundation (GACR, no. 19-13491S). L.G. was supported by MSC IF 708255.

**Acknowledgments:** Access to computing and storage facilities owned by parties and projects contributing to the National Grid Infrastructure MetaCentrum provided under the programme “Projects of Large Research, Development, and Innovations Infrastructures” (CESNET LM2015042), was greatly appreciated.

**Conflicts of Interest:** The authors declare no conflict of interest.

## References

1. Mathews, M.B.; Sonenberg, N.; Hershey, J.W. Origins and Principles of Translational control. In *Translational Control in Biology and Medicine*; Mathews, M.B., Sonenberg, N., Hershey, J.W., Eds.; Cold Spring Harb Lab. Press: New York, NY, USA, 2007; pp. 1–40.
2. Holcik, M.; Sonenberg, N. Translational control in stress and apoptosis. *Nat. Rev. Mol. Cell Biol.* **2005**, *6*, 318–327. [[CrossRef](#)] [[PubMed](#)]
3. Cnop, M.; Toivonen, S.; Igoillo-Esteve, M.; Salpea, P. Endoplasmic reticulum stress and eIF2alpha phosphorylation: The Achilles heel of pancreatic beta cells. *Mol. Metab.* **2017**, *6*, 1024–1039. [[CrossRef](#)] [[PubMed](#)]
4. Susor, A.; Jansova, D.; Anger, M.; Kubelka, M. Translation in the mammalian oocyte in space and time. *Cell Tissue Res.* **2016**, *363*, 69–84. [[CrossRef](#)] [[PubMed](#)]
5. Warner, J.R.; Knopf, P.M.; Rich, A. A multiple ribosomal structure in protein synthesis. *Proc. Natl. Acad. Sci. USA* **1963**, *49*, 122–129. [[CrossRef](#)]
6. Gamm, M.; Peviani, A.; Honsel, A.; Snel, B.; Smeekens, S.; Hanson, J. Increased sucrose levels mediate selective mRNA translation in Arabidopsis. *BMC Plant Biol.* **2014**, *14*, 306. [[CrossRef](#)]
7. Ashe, M.P.; De Long, S.K.; Sachs, A.B. Glucose depletion rapidly inhibits translation initiation in yeast. *Mol. Biol. Cell* **2000**, *11*, 833–848. [[CrossRef](#)]
8. Shalgi, R.; Hurt, J.A.; Krykbaeva, I.; Taipale, M.; Lindquist, S.; Burge, C.B. Widespread regulation of translation by elongation pausing in heat shock. *Mol. Cell* **2013**, *49*, 439–452. [[CrossRef](#)]

9. Swaminathan, S.; Masek, T.; Molin, C.; Pospisek, M.; Sunnerhagen, P. Rck2 is required for reprogramming of ribosomes during oxidative stress. *Mol. Biol. Cell* **2006**, *17*, 1472–1482. [[CrossRef](#)]
10. Sydorsky, Y.; Dilworth, D.J.; Halloran, B.; Yi, E.C.; Makhnevych, T.; Wozniak, R.W.; Aitchison, J.D. Nop53p is a novel nucleolar 60S ribosomal subunit biogenesis protein. *Biochem. J.* **2005**, *388*, 819–826. [[CrossRef](#)]
11. Choudhuri, A.; Maitra, U.; Evans, T. Translation initiation factor eIF3h targets specific transcripts to polysomes during embryogenesis. *Proc. Natl. Acad. Sci. USA* **2013**, *110*, 9818–9823. [[CrossRef](#)]
12. Martinez-Nunez, R.T.; Wallace, A.; Coyne, D.; Jansson, L.; Rush, M.; Ennajdaoui, H.; Katzman, S.; Bailey, J.; Deinhardt, K.; Sanchez-Elsner, T.; et al. Modulation of nonsense mediated decay by rapamycin. *Nucleic Acids Res.* **2017**, *45*, 3448–3459. [[CrossRef](#)] [[PubMed](#)]
13. Androsavich, J.R.; Sobczynski, D.J.; Liu, X.; Pandya, S.; Kaimal, V.; Owen, T.; Liu, K.; MacKenna, D.A.; Chau, B.N. Polysome shift assay for direct measurement of miRNA inhibition by anti-miRNA drugs. *Nucleic Acids Res.* **2016**, *44*, e13. [[CrossRef](#)] [[PubMed](#)]
14. Qin, D.; Fredrick, K. Analysis of polysomes from bacteria. *Methods Enzymol.* **2013**, *530*, 159–172. [[CrossRef](#)] [[PubMed](#)]
15. Seimetz, J.; Arif, W.; Bangru, S.; Hernaez, M.; Kalsotra, A. Cell-type specific polysome profiling from mammalian tissues. *Methods* **2018**, *155*, 131–139. [[CrossRef](#)]
16. Kawaguchi, R.; Bailey-Serres, J. mRNA sequence features that contribute to translational regulation in Arabidopsis. *Nucleic Acids Res.* **2005**, *33*, 955–965. [[CrossRef](#)]
17. Kopeina, G.S.; Afonina, Z.A.; Gromova, K.V.; Shirokov, V.A.; Vasiliev, V.D.; Spirin, A.S. Step-wise formation of eukaryotic double-row polyribosomes and circular translation of polysomal mRNA. *Nucleic Acids Res.* **2008**, *36*, 2476–2488. [[CrossRef](#)]
18. McGlincy, N.J.; Ingolia, N.T. Transcriptome-wide measurement of translation by ribosome profiling. *Methods* **2017**, *126*, 112–129. [[CrossRef](#)]
19. Fu, Y.; Chen, L.; Chen, C.; Ge, Y.; Kang, M.; Song, Z.; Li, J.; Feng, Y.; Huo, Z.; He, G.; et al. Crosstalk between alternative polyadenylation and miRNAs in the regulation of protein translational efficiency. *Genome Res.* **2018**, *28*, 1656–1663. [[CrossRef](#)]
20. Floor, S.N.; Doudna, J.A. Tunable protein synthesis by transcript isoforms in human cells. *eLife* **2016**, *5*. [[CrossRef](#)]
21. Sterne-Weiler, T.; Martinez-Nunez, R.T.; Howard, J.M.; Cvitovik, I.; Katzman, S.; Tariq, M.A.; Pourmand, N.; Sanford, J.R. Frac-seq reveals isoform-specific recruitment to polyribosomes. *Genome Res.* **2013**, *23*, 1615–1623. [[CrossRef](#)]
22. Peng, X.; Emiliani, F.; Smallwood, P.M.; Rattner, A.; Lei, H.; Sabbagh, M.F.; Nathans, J. Affinity capture of polyribosomes followed by RNAseq (ACAPseq), a discovery platform for protein-protein interactions. *eLife* **2018**, *7*. [[CrossRef](#)] [[PubMed](#)]
23. Aviner, R.; Hofmann, S.; Elman, T.; Shenoy, A.; Geiger, T.; Elkon, R.; Ehrlich, M.; Elroy-Stein, O. Proteomic analysis of polyribosomes identifies splicing factors as potential regulators of translation during mitosis. *Nucleic Acids Res.* **2017**, *45*, 5945–5957. [[CrossRef](#)] [[PubMed](#)]
24. Castelli, L.M.; Talavera, D.; Kershaw, C.J.; Mohammad-Qureshi, S.S.; Costello, J.L.; Rowe, W.; Sims, P.F.; Grant, C.M.; Hubbard, S.J.; Ashe, M.P.; et al. The 4E-BP Caf20p Mediates Both eIF4E-Dependent and Independent Repression of Translation. *PLoS Genet.* **2015**, *11*, e1005233. [[CrossRef](#)] [[PubMed](#)]
25. de Sousa Abreu, R.; Penalva, L.O.; Marcotte, E.M.; Vogel, C. Global signatures of protein and mRNA expression levels. *Mol. BioSyst.* **2009**, *5*, 1512–1526. [[CrossRef](#)]
26. Wang, T.; Cui, Y.; Jin, J.; Guo, J.; Wang, G.; Yin, X.; He, Q.Y.; Zhang, G. Translating mRNAs strongly correlate to proteins in a multivariate manner and their translation ratios are phenotype specific. *Nucleic Acids Res.* **2013**, *41*, 4743–4754. [[CrossRef](#)]
27. Zhao, J.; Qin, B.; Nikolay, R.; Spahn, C.M.T.; Zhang, G. Translatomics: The Global View of Translation. *Int. J. Mol. Sci.* **2019**, *20*, 212. [[CrossRef](#)]
28. Chasse, H.; Boulben, S.; Costache, V.; Cormier, P.; Morales, J. Analysis of translation using polysome profiling. *Nucleic Acids Res.* **2017**, *45*, e15. [[CrossRef](#)]
29. Masek, T.; Valasek, L.; Pospisek, M. Polysome analysis and RNA purification from sucrose gradients. *Methods Mol. Biol.* **2011**, *703*, 293–309. [[CrossRef](#)]

30. Potireddy, S.; Vassena, R.; Patel, B.G.; Latham, K.E. Analysis of polysomal mRNA populations of mouse oocytes and zygotes: Dynamic changes in maternal mRNA utilization and function. *Dev. Biol.* **2006**, *298*, 155–166. [[CrossRef](#)] [[PubMed](#)]
31. Scantland, S.; Grenon, J.P.; Desrochers, M.H.; Sirard, M.A.; Khandjian, E.W.; Robert, C. Method to isolate polyribosomal mRNA from scarce samples such as mammalian oocytes and early embryos. *BMC Dev. Biol.* **2011**, *11*, 8. [[CrossRef](#)]
32. Wang, Y.; Ringquist, S.; Cho, A.H.; Rondeau, G.; Welsh, J. High-throughput polyribosome fractionation. *Nucleic Acids Res.* **2004**, *32*, e79. [[CrossRef](#)] [[PubMed](#)]
33. Schuh, M.; Ellenberg, J. Self-organization of MTOCs replaces centrosome function during acentrosomal spindle assembly in live mouse oocytes. *Cell* **2007**, *130*, 484–498. [[CrossRef](#)] [[PubMed](#)]
34. Collado-Fernandez, E.; Picton, H.M.; Dumollard, R. Metabolism throughout follicle and oocyte development in mammals. *Int. J. Dev. Biol.* **2012**, *56*, 799–808. [[CrossRef](#)] [[PubMed](#)]
35. Gahurova, L.; Tomizawa, S.I.; Smallwood, S.A.; Stewart-Morgan, K.R.; Saadeh, H.; Kim, J.; Andrews, S.R.; Chen, T.; Kelsey, G. Transcription and chromatin determinants of de novo DNA methylation timing in oocytes. *Epigenetics Chromatin* **2017**, *10*, 25. [[CrossRef](#)] [[PubMed](#)]
36. Susor, A.; Kubelka, M. Translational Regulation in the Mammalian Oocyte. *Results Probl. Cell Differ.* **2017**, *63*, 257–295. [[CrossRef](#)]
37. Stebbins-Boaz, B.; Hake, L.E.; Richter, J.D. CPEB controls the cytoplasmic polyadenylation of cyclin, Cdk2 and c-mos mRNAs and is necessary for oocyte maturation in *Xenopus*. *EMBO J.* **1996**, *15*, 2582–2592. [[CrossRef](#)]
38. Igea, A.; Mendez, R. Meiosis requires a translational positive loop where CPEB1 ensues its replacement by CPEB4. *EMBO J.* **2010**, *29*, 2182–2193. [[CrossRef](#)]
39. Elisovich, C.; Peset, I.; Vernos, I.; Mendez, R. Spindle-localized CPE-mediated translation controls meiotic chromosome segregation. *Nat. Cell Biol.* **2008**, *10*, 858–865. [[CrossRef](#)]
40. Belloc, E.; Pique, M.; Mendez, R. Sequential waves of polyadenylation and deadenylation define a translation circuit that drives meiotic progression. *Biochem. Soc. Trans.* **2008**, *36*, 665–670. [[CrossRef](#)]
41. Susor, A.; Jansova, D.; Cerna, R.; Danylevska, A.; Anger, M.; Toralova, T.; Malik, R.; Supolikova, J.; Cook, M.S.; Oh, J.S.; et al. Temporal and spatial regulation of translation in the mammalian oocyte via the mTOR-eIF4F pathway. *Nat. Commun.* **2015**, *6*, 6078. [[CrossRef](#)]
42. Labrecque, R.; Sirard, M.A. The study of mammalian oocyte competence by transcriptome analysis: Progress and challenges. *Mol. Hum. Reprod.* **2014**, *20*, 103–116. [[CrossRef](#)] [[PubMed](#)]
43. Liu, Q.; Li, Y.; Feng, Y.; Liu, C.; Ma, J.; Li, Y.; Xiang, H.; Ji, Y.; Cao, Y.; Tong, X.; et al. Single-cell analysis of differences in transcriptomic profiles of oocytes and cumulus cells at GV, MI, MII stages from PCOS patients. *Sci. Rep.* **2016**, *6*, 39638. [[CrossRef](#)] [[PubMed](#)]
44. Suo, L.; Zhou, Y.X.; Jia, L.L.; Wu, H.B.; Zheng, J.; Lyu, Q.F.; Sun, L.H.; Sun, H.; Kuang, Y.P. Transcriptome profiling of human oocytes experiencing recurrent total fertilization failure. *Sci. Rep.* **2018**, *8*, 17890. [[CrossRef](#)] [[PubMed](#)]
45. Fragouli, E.; Bianchi, V.; Patrizio, P.; Obradors, A.; Huang, Z.; Borini, A.; Delhanty, J.D.; Wells, D. Transcriptomic profiling of human oocytes: Association of meiotic aneuploidy and altered oocyte gene expression. *Mol. Hum. Reprod.* **2010**, *16*, 570–582. [[CrossRef](#)] [[PubMed](#)]
46. Karlic, R.; Ganesh, S.; Franke, V.; Svobodova, E.; Urbanova, J.; Suzuki, Y.; Aoki, F.; Vlahovicek, K.; Svoboda, P. Long non-coding RNA exchange during the oocyte-to-embryo transition in mice. *Dna Res. Int. J. Rapid Publ. Rep. Genes Genomes* **2017**, *24*, 129–141. [[CrossRef](#)]
47. Chen, J.; Melton, C.; Suh, N.; Oh, J.S.; Horner, K.; Xie, F.; Sette, C.; Blelloch, R.; Conti, M. Genome-wide analysis of translation reveals a critical role for deleted in azoospermia-like (*Dazl*) at the oocyte-to-zygote transition. *Genes Dev.* **2011**, *25*, 755–766. [[CrossRef](#)]
48. Chasse, H.; Aubert, J.; Boulben, S.; Le Corguille, G.; Corre, E.; Cormier, P.; Morales, J. Transcriptome analysis at the egg-to-embryo transition in sea urchin. *Nucleic Acids Res.* **2018**, *46*, 4607–4621. [[CrossRef](#)]
49. Winata, C.L.; Lapinski, M.; Prysycz, L.; Vaz, C.; Bin Ismail, M.H.; Nama, S.; Hajan, H.S.; Lee, S.G.P.; Korzh, V.; Sampath, P.; et al. Cytoplasmic polyadenylation-mediated translational control of maternal mRNAs directs maternal-to-zygotic transition. *Development* **2018**, *145*. [[CrossRef](#)]
50. Schwer, B.; Shuman, S. Multicopy suppressors of temperature-sensitive mutations of yeast mRNA capping enzyme. *Gene Expr.* **1996**, *5*, 331–344.



51. De La Fuente, R.; Viveiros, M.M.; Burns, K.H.; Adashi, E.Y.; Matzuk, M.M.; Eppig, J.J. Major chromatin remodeling in the germinal vesicle (GV) of mammalian oocytes is dispensable for global transcriptional silencing but required for centromeric heterochromatin function. *Dev. Biol.* **2004**, *275*, 447–458. [[CrossRef](#)]
52. Svoboda, P.; Franke, V.; Schultz, R.M. Sculpting the Transcriptome During the Oocyte-to-Embryo Transition in Mouse. *Curr. Top. Dev. Biol.* **2015**, *113*, 305–349. [[CrossRef](#)] [[PubMed](#)]
53. Rederstorff, M.; Bernhart, S.H.; Tanzer, A.; Zywicki, M.; Perfler, K.; Lukasser, M.; Hofacker, I.L.; Huttenhofer, A. RNPomics: Defining the ncRNA transcriptome by cDNA library generation from ribonucleo-protein particles. *Nucleic Acids Res.* **2010**, *38*, e113. [[CrossRef](#)] [[PubMed](#)]
54. Mukherjee, C.; Patil, D.P.; Kennedy, B.A.; Bakthavachalu, B.; Bundschuh, R.; Schoenberg, D.R. Identification of cytoplasmic capping targets reveals a role for cap homeostasis in translation and mRNA stability. *Cell Rep.* **2012**, *2*, 674–684. [[CrossRef](#)]
55. Bouckenheimer, J.; Fauque, P.; Lecellier, C.H.; Bruno, C.; Commes, T.; Lemaitre, J.M.; De Vos, J.; Assou, S. Differential long non-coding RNA expression profiles in human oocytes and cumulus cells. *Sci. Rep.* **2018**, *8*, 2202. [[CrossRef](#)] [[PubMed](#)]
56. Reyes, J.M.; Silva, E.; Chitwood, J.L.; Schoolcraft, W.B.; Krisher, R.L.; Ross, P.J. Differing molecular response of young and advanced maternal age human oocytes to IVM. *Hum. Reprod.* **2017**, *32*, 2199–2208. [[CrossRef](#)]
57. Capco, D.G.; Gallicano, G.I.; McGaughey, R.W.; Downing, K.H.; Larabell, C.A. Cytoskeletal sheets of mammalian eggs and embryos: A lattice-like network of intermediate filaments. *Cell Motil. Cytoskelet.* **1993**, *24*, 85–99. [[CrossRef](#)]
58. Vogt, E.; Kirsch-Volders, M.; Parry, J.; Eichenlaub-Ritter, U. Spindle formation, chromosome segregation and the spindle checkpoint in mammalian oocytes and susceptibility to meiotic error. *Mutat. Res.* **2008**, *651*, 14–29. [[CrossRef](#)]
59. Duncan, F.E.; Chiang, T.; Schultz, R.M.; Lampson, M.A. Evidence that a defective spindle assembly checkpoint is not the primary cause of maternal age-associated aneuploidy in mouse eggs. *Biol. Reprod.* **2009**, *81*, 768–776. [[CrossRef](#)]
60. Ma, J.Y.; Li, M.; Luo, Y.B.; Song, S.; Tian, D.; Yang, J.; Zhang, B.; Hou, Y.; Schatten, H.; Liu, Z.; et al. Maternal factors required for oocyte developmental competence in mice: Transcriptome analysis of non-surrounded nucleolus (NSN) and surrounded nucleolus (SN) oocytes. *Cell Cycle* **2013**, *12*, 1928–1938. [[CrossRef](#)]
61. Harris, S.E.; Leese, H.J.; Gosden, R.G.; Picton, H.M. Pyruvate and oxygen consumption throughout the growth and development of murine oocytes. *Mol. Reprod. Dev.* **2009**, *76*, 231–238. [[CrossRef](#)]
62. Pelland, A.M.; Corbett, H.E.; Baltz, J.M. Amino Acid transport mechanisms in mouse oocytes during growth and meiotic maturation. *Biol. Reprod.* **2009**, *81*, 1041–1054. [[CrossRef](#)] [[PubMed](#)]
63. Huo, L.J.; Fan, H.Y.; Zhong, Z.S.; Chen, D.Y.; Schatten, H.; Sun, Q.Y. Ubiquitin-proteasome pathway modulates mouse oocyte meiotic maturation and fertilization via regulation of MAPK cascade and cyclin B1 degradation. *Mech. Dev.* **2004**, *121*, 1275–1287. [[CrossRef](#)] [[PubMed](#)]
64. Dun, M.D.; Smith, N.D.; Baker, M.A.; Lin, M.; Aitken, R.J.; Nixon, B. The chaperonin containing TCP1 complex (CCT/TRiC) is involved in mediating sperm-oocyte interaction. *J. Biol. Chem.* **2011**, *286*, 36875–36887. [[CrossRef](#)] [[PubMed](#)]
65. Jansen, R.P.; de Boer, K. The bottleneck: Mitochondrial imperatives in oogenesis and ovarian follicular fate. *Mol. Cell. Endocrinol.* **1998**, *145*, 81–88. [[CrossRef](#)]
66. Dumollard, R.; Ward, Z.; Carroll, J.; Duchen, M.R. Regulation of redox metabolism in the mouse oocyte and embryo. *Development* **2007**, *134*, 455–465. [[CrossRef](#)]
67. Bai, B.; Peviani, A.; van der Horst, S.; Gamm, M.; Snel, B.; Bentsink, L.; Hanson, J. Extensive translational regulation during seed germination revealed by polysomal profiling. *New Phytol.* **2017**, *214*, 233–244. [[CrossRef](#)]
68. Juntawong, P.; Bailey-Serres, J. Dynamic Light Regulation of Translation Status in *Arabidopsis thaliana*. *Front. Plant Sci.* **2012**, *3*, 66. [[CrossRef](#)]
69. Das, A.; Morales, R.; Banday, M.; Garcia, S.; Hao, L.; Cross, G.A.; Estevez, A.M.; Bellofatto, V. The essential polysome-associated RNA-binding protein RBP42 targets mRNAs involved in *Trypanosoma brucei* energy metabolism. *RNA* **2012**, *18*, 1968–1983. [[CrossRef](#)]
70. Bunnik, E.M.; Chung, D.W.; Hamilton, M.; Ponts, N.; Saraf, A.; Prudhomme, J.; Florens, L.; Le Roch, K.G. Polysome profiling reveals translational control of gene expression in the human malaria parasite *Plasmodium falciparum*. *Genome Biol.* **2013**, *14*, R128. [[CrossRef](#)]



71. Frey, S.; Pool, M.; Seedorf, M. Scp160p, an RNA-binding, polysome-associated protein, localizes to the endoplasmic reticulum of *Saccharomyces cerevisiae* in a microtubule-dependent manner. *J. Biol. Chem.* **2001**, *276*, 15905–15912. [[CrossRef](#)]
72. Minia, I.; Merce, C.; Terrao, M.; Clayton, C. Translation Regulation and RNA Granule Formation after Heat Shock of Procyclic Form *Trypanosoma brucei*: Many Heat-Induced mRNAs Are also Increased during Differentiation to Mammalian-Infective Forms. *PLoS Negl. Trop. Dis.* **2016**, *10*, e0004982. [[CrossRef](#)] [[PubMed](#)]
73. Tetkova, A.; Hancova, M. Mouse Oocyte Isolation, Cultivation and RNA Microinjection. *Bio-protocol* **2016**, *6*, e1729. [[CrossRef](#)]
74. Masek, T.; Vopalensky, V.; Suchomelova, P.; Pospisek, M. Denaturing RNA electrophoresis in TAE agarose gels. *Anal. Biochem.* **2005**, *336*, 46–50. [[CrossRef](#)] [[PubMed](#)]
75. Kim, D.; Paggi, J.M.; Park, C.; Bennett, C.; Salzberg, S.L. Graph-based genome alignment and genotyping with HISAT2 and HISAT-genotype. *Nat. Biotechnol.* **2019**, *37*, 907–915. [[CrossRef](#)]
76. Sivan, G.; Kedersha, N.; Elroy-Stein, O. Ribosomal slowdown mediates translational arrest during cellular division. *Mol. Cell. Biol.* **2007**, *27*, 6639–6646. [[CrossRef](#)]
77. Frydryskova, K.; Masek, T.; Borcin, K.; Mrvova, S.; Venturi, V.; Pospisek, M. Distinct recruitment of human eIF4E isoforms to processing bodies and stress granules. *BMC Mol. Biol.* **2016**, *17*, 21. [[CrossRef](#)]
78. Zamostna, B.; Novak, J.; Vopalensky, V.; Masek, T.; Burysek, L.; Pospisek, M. N-terminal domain of nuclear IL-1alpha shows structural similarity to the C-terminal domain of Snf1 and binds to the HAT/core module of the SAGA complex. *PLoS ONE* **2012**, *7*, e41801. [[CrossRef](#)]



© 2020 by the authors. Licensee MDPI, Basel, Switzerland. This article is an open access article distributed under the terms and conditions of the Creative Commons Attribution (CC BY) license (<http://creativecommons.org/licenses/by/4.0/>).

# Age-related differences in the translational landscape of mammalian oocytes

Edgar del Llano<sup>1,2\*</sup>, Tomas Masek<sup>2</sup>, Lenka Gahurova<sup>1,3</sup>, Martin Pospisek<sup>2</sup>, Marketa Koncicka<sup>1</sup>, Anna Jindrova<sup>1</sup>, Denisa Jansova<sup>1</sup>, Rajan Iappan<sup>1</sup>, Kristina Roucova<sup>2</sup>, Alexander W. Bruce<sup>3</sup>, Michal Kubelka<sup>1</sup> and Andrej Susor<sup>1\*</sup>

<sup>1</sup> Laboratory of Biochemistry and Molecular Biology of Germ Cells, Institute of Animal Physiology and Genetics, CAS, Rumburska 89, 277 21 Libechov, Czech Republic.

<sup>2</sup> Laboratory of RNA Biochemistry, Department of Genetics and Microbiology, Faculty of Science, Charles University in Prague, Albertov 6, 128 43 Prague, Czech Republic.

<sup>3</sup> Laboratory of Early Mammalian Developmental Biology, Department of Molecular Biology and Genetics, Faculty of Science, University of South Bohemia, Branisovska 1760, 370 05 Ceske Budejovice, Czech Republic.

Correspondence: [susor@iapg.cas.cz](mailto:susor@iapg.cas.cz); [llano@iapg.cas.cz](mailto:llano@iapg.cas.cz)

## Abstract

Increasing maternal age in mammals is associated with poorer oocyte quality, involving higher aneuploidy rates and decreased developmental competence. Prior to resumption of meiosis, fully developed mammalian oocytes become transcriptionally silent until the onset of zygotic genome activation. Therefore, meiotic progression and early embryogenesis are driven largely by translational utilization of previously synthesized mRNAs. We report that genome-wide translome profiling reveals considerable numbers of transcripts that are differentially translated in oocytes obtained from aged compared to young females. Additionally, we show that a number of aberrantly translated mRNAs in oocytes from aged females have roles associated with cell cycle regulation. Indeed, we demonstrate the differential translation rates of four specific maternal age related transcripts (*Sgk1*, *Castor1*, *Aire* and *Eg5*) are associated with distinct localization patterns at the newly forming meiotic spindle. Moreover, we report substantial defects in chromosome alignment and cytokinesis in the oocytes of young females, in which candidate CASTOR1 and SGK1 protein levels or activity are experimentally altered. Our findings indicate that improper translation of specific proteins at the onset of meiosis contributes to increased chromosome segregation problems associated with female aging.

## Introduction

The quality of oocytes (female germ cells) is an essential factor for successful sexual reproduction. Mammalian oocyte development is a complex and long process beginning during embryogenesis and then arresting in the first meiotic prophase. It is not until puberty that oocytes can finally be recruited for ovulation, by reinitiating meiosis and culminating in eventual fertilization. It is accepted that chromosomal aneuploidy, a consequence of chromosomal segregation errors during meiosis, is one of the most common causes of poor oocyte quality, leading to embryo lethality or severe developmental disabilities (Savva et al., 2010). Importantly, it has been reported that most chromosomal segregation aberrations take place during the first meiotic division, occurring after meiotic resumption and Nuclear Envelope Break Down (NEBD) (Hassold and Hunt, 2001). Precisely, it is shortly after NEBD when chromosome condensation and assembly take place at the newly forming meiotic spindle (Schuh and Ellenberg, 2007). Chromosomal aneuploidy in human oocytes is not a rare event, exemplified by a 20% incidence in 32 year old women that further increases with age, reaching 60-80% in women aged 42 (Kuliev et al., 2011; Jones and Lane, 2013a; Capalbo et al., 2017). This so called 'age-related aneuploidy' in oocytes has long been a focus in the study of human reproduction, as women in economically advanced societies are trending to delay their pregnancies (Molina-García et al., 2019). However, we are still far from fully understanding the mechanisms underlying this phenomenon. In order to provide enhanced insight into the dysfunctional molecular mechanisms behind age-related aneuploidy, the transcriptomes of oocytes from young and advanced aged females have been compared, using various animal models (Labrecque and Sirard, 2014), of which mouse has proven to be a suitable one (Sebestova et al., 2012; Jones and Lane, 2013b). These studies have revealed that there are actual significant differences in the transcriptomes of oocytes from

aged females, mainly associated with decreased levels of gene transcripts involved in managing oxidative stress, chromatin structure, genome stability and spindle structure. Nonetheless, another crucial feature of oocyte development must be taken into account. Namely, that oocytes proceed through meiotic maturation and to the post-fertilization zygote stage in the absence of *de novo* transcription (De La Fuente et al., 2004; Hamatani et al., 2004a). Accordingly, growing oocytes that become arrested at prophase I, synthesise large amounts of RNA that is stored for future use during the transcriptionally silent period after meiotic resumption (Fulka et al., 1998). Precisely, chromosome condensation and segregation take place in an environment where regulation of translation is a paramount gene expression control mechanism. As such, conventional transcriptome analysis, although undoubtedly useful, might not offer a sufficiently accurate picture of oocyte gene expression on the protein level, as the whole transcriptome includes large pools of stored RNAs not undergoing active translation. To overcome this limitation, polysomal fractionation of oocyte samples can be performed in order to isolate those RNAs which are bound to ribosomes and hence are more likely to be translated into proteins with functional roles during specific stages of meiosis. However, mammalian oocytes are a scarce source of material, which is a big limiting factor to such classical fractionation techniques that typically require millions of cells (Mašek et al., 2011). Thus, unsurprisingly, only a few experiments of this kind have been reported (Potireddy et al., 2006; Scantland et al., 2011; Chen et al., 2011). For this purpose we recently developed a Scarce Sample Polysomal-profiling (SSP-profiling) method, which allows the obtaining of polysomal RNAs with high reliability from as little as 200 oocytes (Masek et al., 2020). In this study, we present what to our knowledge is the first thorough analysis of ribosome bound mRNAs in mouse oocytes at the post-NEBD stage within the context of maternal age. Moreover, we validate several candidate mRNAs exhibiting altered translation in the oocytes of more advanced age females and identify novel gene transcripts and proteins related to mammalian oocyte development and aneuploidy.

## Results

### Genome wide analysis reveals differential translation of cell cycle players in oocytes from aged females.

To provide improved mechanistic insight into the increased aneuploidy rate of oocytes from aged females, we compared the polysome bound mRNAs of oocytes from young (6 week old, YF) and aged (58 weeks old, AF) female mice. Most of oocyte meiotic errors from aged females occur in meiosis I (Hassold and Hunt, 2001), therefore we performed the translome comparison on oocytes after they underwent NEBD (3h after 3-Isobutyl-1-methylxanthine (IBMX) removal); when chromosomes condense, the new meiotic spindle is forming and transcription is absent. Taking into account that transcriptionally silent oocyte and the transcriptome of GV oocytes does not significantly vary with maternal age (Pan et al., 2008) we analysed oocyte's ribosomal RNA content to unveil the translome in relation to maternal age. Four individual replicates were used for YF samples and three for AF (200 post-NEBD oocytes/sample). Using the SSP-profiling method (Masek et al., 2020) combined with RNA-Seq method, we analysed mRNA content in polysomal and non-polysomal fractions from oocytes of the two different female groups. Analyses of the YF and AF derived fractions did not reveal any significant differences between the two age groups regarding polysomal distribution (Fig. 1A). Significant decrease of ribosomal subunits in polysomal fractions was induced pre-treatment with Ethylenediaminetetraacetic acid (EDTA) compared to both the YF and AF samples (Fig. 1A). As EDTA sequesters magnesium ions to disrupt ribosomal subunit assembly (Scantland et al., 2011), thus reducing polysome levels, this important technical control provides confidence that the RNAs in polysomal fractions of untreated YF and AF oocytes are indeed bound to ribosomes.

Next, for each sample, we pooled the collected fractions into either non-polysomal (NP, fractions containing free RNAs or RNAs bound to monosomes) or polysomal fractions (P; fractions containing polysome bound RNAs). This was followed by ribodepleted RNA-Seq of NP and P fractions to detect genome wide translational differences between the two age groups.

Based on the RNA-Seq data output we were able to identify differentially translated mRNAs (Fig. 1B). Analysis of P fractions with transcripts with at least FPKM>1 in one group revealed 3589 (35.06 %) mRNAs with more than a five-fold comparative difference in enrichment between YF and AF oocytes ( $FC > 5$ ) and 1006 (9.83 %) mRNAs with an enrichment fold change above 10 ( $FC > 10$ ) (Fig. 1B and Supplementary Table 1). From those mRNAs with  $FC > 10$ , 623 mRNAs were more abundant in the P fractions of YF oocytes and 383 in P fractions of AF samples. In addition, 37 polysomal differentially enriched mRNAs were statistically significant between the two groups, as calculated by DESeq2 (Fig. 1B and Supplementary Table 1). Over-Representation Analysis (ORA) was performed on the polysomal differentially enriched transcripts exhibiting  $FC > 10$  between the two oocyte groups (Fig. 1C and Supplementary Table

2). Interestingly, among the significantly enriched categories were those related to cell division, microtubule cytoskeleton (e.g. *Cdk10*, *Cep63*, *Chek2*, *Nde1*, *Spice1* and kinesins: *Kif11*, *Kif3b*, *Kif18a*) and to the mRNA metabolism (e.g. *Eif3a*, *Prkra*, *Rpl38*; RNA methyltransferases: *Tfb2m*, *Trmt61a*, *Nsun2*, *Nsun3*), substantiating a possible link between increased aneuploidy in AF oocytes and the transcript specific translational alterations. Moreover, those gene transcripts that were differentially enriched between the P fractions of the two oocyte age groups (FC > 10) showed seven hierarchical clusters based on their observed enrichments in non-polysomal and polysomal fractions (Fig. S1 and Supplementary Table 3). Clusters 2, 5, 6 and 7 appear to comprise gene transcripts with differential translation regulation between the YF and AF groups, as despite having similar abundancies in non-polysomal (NP) fractions they exhibit opposing enrichment trends in the corresponding polysomal (P) fractions.

In summary, we used genome wide analysis to generate a comprehensive datasets of specific mRNAs with differential polysomal abundance in oocytes from different maternal age related oocytes that resumed meiosis.

### **Specific genes transcripts with different polysomal occupancy between YF and AF oocytes positively correlates with protein expression.**

To identify candidate genes potentially functionally involved in age-related aneuploidy, we selected 10 gene transcripts with different polysomal occupancy between YF and AF datasets (Deseq2,  $P < 0.1$  and/or  $FC > 10$ ). We primarily focused on transcripts that might have a potential direct/indirect effect on meiosis, cell division, G2/M phase transition or spindle localization according to the current literature (Fig. 1B,D). *Actb* mRNA was selected as a control due to similar polysomal occupancy in both oocyte groups.

In order to validate the observed differences in polysome association of selected transcripts, each specific mRNA was analysed by Digital Droplet PCR (ddPCR) from newly prepared and pooled YF and AF oocyte polysomal fractions. Due to the inherent scarcity of oocyte samples and the intrinsic difficulty to obtain enough replicates (especially from the limiting numbers of mice and oocytes in the AF group), it was challenging to retrieve flawlessly consistent qPCR results for all assayed transcripts. Nonetheless, we were able to moderately correlate the RNA-Seq data with the results of ddPCR (Fig. 1B,D) for a selected candidate mRNAs: Serum/Glucocorticoid Regulated Kinase 1 (*Sgk1*), Cytosolic Arginine Sensor For mTORC1 Subunit 1 (*Castor1*) and Kinesin-5 protein (*Eg5*, *Kif11*) (Fig. 2A). In our sequencing datasets; *Sgk1* mRNA was less abundant in the polysomal RNA of AF oocytes, while *Castor1* and *Eg5* mRNA levels were enriched. These relative oocyte age related polysome enrichment differences were reflected by ddPCR (Fig. 2A). However, despite the robust differences of Autoimmune Regulator (*Aire*) mRNA in polysomal occupancy observed in our RNA seq datasets (strongly favouring the AF group), we were not able to detect significant differences by ddPCR between the two groups. Moreover, we did speculate whether the levels of these transcripts would vary not only in the polysomal fractions but throughout the whole transcriptome as a potential consequence of an age-related differential transcription during the previous oocyte growth period (rather than a differential translation at post-NEBD stage). We therefore extracted total RNA (without polysomal fractionation) from freshly collected YF and AF post-NEBD oocytes and assayed the general expression levels of the same transcripts by qRT-PCR (Fig. S2). However, no significant differences in transcript levels were detected, indicating YF and AF oocytes contain similar amounts of *Sgk1*, *Castor1*, *Aire* and *Eg5* transcripts in their total RNA.

Higher polysomal occupancy by specific mRNAs is very likely to correlate with increased synthesis of the corresponding protein. After assaying the differences in *Sgk1*, *Castor1*, *Aire* and *Eg5* mRNA enrichment in the respective oocyte polysomal RNA pools (Fig. 2A), we asked if these differences (as originally identified by RNA-Seq – Fig. 1D) were also reflected at the protein levels. In order to elucidate this, we performed western blots (WB) from post-NEBD oocyte samples, from YF and AF groups. We found that SGK1 protein expression positively correlated with (Fig. 2B,C) RNA-seq results (Fig. 1B,D). Conversely, the levels of CASTOR1 and EG5 protein, the mRNAs of which were enriched in AF polysomes, were significantly increased in AF derived oocytes compared to the YF group (Fig. 2BC). Interestingly, despite not being able to clearly validate different levels in polysome associated transcripts of *Aire* by ddPCR, the expression of its protein was extremely increased (up to 10 fold) in the AF group (Fig. 2B,C); a result in strong accord with the original RNA-Seq polysome profiling results (Fig. 1D). Control, ACTB expression in oocyte from YF and AF, showed similar level (Fig. 2B). Therefore, the validation of significant differences in protein levels of selected genes correlated positively with those inferred from the RNA-Seq polysome association analysis. This difference in protein expression between YF and AF, regardless of similar transcript levels in total RNA, indicate that the differential occupation within polysomal fractions for the selected transcripts is directly related to their protein expression.

### **Selected differentially expressed proteins are localized at the newly forming spindle.**

Most proteins have functional roles within the specific sub-cellular regions they are localized (Femino et al., 1998; Jansova et al., 2018). Therefore, to better understand their role in meiosis resumption, we detected localization of selected differentially translated genes from YF and AF oocytes by immunocytochemistry (ICC). Interestingly, we found all four candidate proteins localized in the area of the newly forming spindle but in distinct patterns (Fig. 3A). SGK1 and EG5 were found in patches at the multipolar spindle and CASTOR1 and AIRE were both localized in a similar pattern to tubulin (Fig. 3A). Moreover, we quantified the fluorescence of individual proteins from ICC and found a positive correlation with our RNA-Seq (Fig. 1B,D) and WB (Fig. 2BC) results. Namely, there was a significant decrease of SGK1 protein fluorescence in AF oocytes compared to YF and significant increase in the protein expression of CASTOR1, AIRE and EG5 (Fig. 3B).

Previously, we reported that the timing of meiotic progression of AF derived oocytes is faster than in their younger counterparts by about 30 minutes (Koncicka et al., 2018). Therefore, we asked if such meiotic progression timing differences may promote translational differences between age groups. We analysed the expression of AIRE and EG5 proteins (by WB and ICC, respectively) in YF oocytes collected 30 minutes later than the conventional assay time (3h post IBMX removal) for YF and AF oocytes. We found that additional cultivation did not significantly alter the protein expression to levels previously detected in the AF group (Fig. S3). This indicates that the observed translational differences are inherent to translation of selected transcripts in AF oocytes and not due to timing differences.

Collectively, these results confirm the spindle localization of selected candidate proteins and that their differential expression in AF derived oocytes (versus YF counterparts), may play a role in spindle assembly, chromosome alignment and cytokinesis.

### **Perturbation of CASTOR1 and SGK1 protein levels/activity leads to meiotic abnormalities.**

The sum of the described results indicates that at the post-NEBD stage, there is a number of mRNAs that exhibit differential polysomal occupancy and consequently altered protein expression levels in AF oocytes compared to YF derived counterparts. We decided to experimentally perturb the protein levels of two selected candidates with opposing differential polysomal occupancy in AF oocytes (CASTOR1 and SGK1, Fig. 1B and 3B). As CASTOR1 protein has higher expression levels in AF oocytes, we performed overexpression of the protein in YF oocytes, by microinjection of *Castor1* mRNA (Fig. 4A) and consequently analysed their maturation rate and morphology (Fig. 4B,C). We found that the rate of progression to the MII stage occurred without major differences in PB extrusion between control (*H2b:gfp* mRNA microinjection) and CASTOR1 overexpressed groups (*Castor1:Ha* + *H2b:gfp* mRNA microinjection) (61±15% and 61±10%, n=31 and n=18, respectively;  $P<0.05$ ). However, we did find that 43% of CASTOR1 overexpressing oocytes which reached MII displayed significant abnormalities; namely chromosome misalignment in M-phase (MI) and/or extrusion of full DNA content into two polar bodies (Fig. 4B,C). Although these abnormalities did not affect PB extrusion rates, it is clear that full extrusion of DNA content is deleterious for the further oocyte quality as well as chromosome misalignment might be. On the other hand, translation of *Sgk1* mRNA was significantly decreased in AF oocytes (Fig. 1B and 3B), we decided to suppress SGK1 protein kinase activity in YF oocytes using the specific SGK1-inhibitor (GSK-650394; 10µM.) SGK1 affects CDK1 activity (Hiraoka et al., 2019), thus we validated successful SGK1 inhibition via decrease of CDK1 (Thr161) phosphorylation in YF oocytes (3h post IBMX removal in the presence of the inhibitor) (Fig. 4D and Fig. S4). Subsequently, we assayed meiotic progression of YF oocytes treated with vehicle or SGK1-inhibitor. We found that the inhibitor-treated group had significantly lower numbers of oocytes reaching the MII stage (40±18%;  $P<0.05$ ; n=75) compared with control vehicle treatment (93±7%;  $P<0.05$ ; n=75). Moreover, after PB extrusion, 83% of the oocytes treated with SGK1-inhibitor showed two abnormal phenotypes, including symmetric division (10% of MII oocytes) and tubulin non-disjunction with chromatin decondensation (73% of MII) (Fig. 4E,F and 4F).

In summary, by perturbing YF oocytes to mimic the protein expression or activity of CASTOR1 and SGK1 of AF oocytes, we have shown that these proteins play roles involved in meiosis I chromosome alignment and cytokinesis, which are intrinsically impaired in AF derived oocytes.

## **Discussion**

Although several models have been proposed to explain how the age-associated increase in aneuploidy could occur, further investigation is needed, considering the medical relevance of maternal age-related aneuploidy. Previous results (Sebestova et al., 2012; Jones and Lane, 2013b) have shown that mouse is a suitable model system to assess



the molecular basis for human age-associated increase in aneuploidy. A general view is that the quality of the cytoplasm, which includes the transcriptome, is compromised in aged oocytes. However, Pan et al. (2008) have shown that perturbations in the global transcriptome of GV oocytes from females of advanced age are actually minimal. In this study, we have tackled the old problem of oocyte age-related aneuploidy from a new perspective. We contribute to this field with novel genome wide analysis of the translation of maternal mRNAs in two different oocyte age groups. While there have been several studies comparing oocyte transcriptomes from young and aged females (Hamatani et al., 2004b; Pan et al., 2008; Grøndahl et al., 2010), actual translatoome has until now remained unanalyzed. Nonetheless, translation is particularly relevant as the fully grown mammalian oocyte is known to be transcriptionally silent and relies on large amounts of stored RNAs that utilizes when progressing through meiosis. In fact, stored mRNAs can be several times more abundant than those ongoing actual translation at any given point. In order to identify polysome-bound mRNAs in mouse oocytes, we previously developed a method that enables isolation of very small amounts of polyribosomal bound RNA for a subsequent genome wide analysis (Ganesh et al., 2020; Masek et al., 2020). To date, there have been very few experiments applying polysome profiling techniques on oocytes (Potireddy et al., 2006; Scantland et al., 2011; Chen et al., 2011) and to our knowledge we are the first to use it to interrogate the whole translatoome in oocytes of different maternal ages.

Research in this study was performed using oocytes at the post-NEBD stage. This specific meiotic time-point was deliberately selected, since the first meiotic division is ongoing: meiotic arrest at prophase I is over, chromosomes have recently condensed, the new spindle has begun to assemble (Schuh and Ellenberg, 2007) and translational reprogramming is occurring (Susor et al., 2015; Jansova et al., 2018). Additionally and importantly, chromosomal mis-segregation is reported to preferentially occur during the first meiotic division. Therefore, uncovering translational differences at this stage between YF and AF oocytes harbours a high potential to better understand age-related aneuploidy (Ottolini et al., 2015). Earlier studies dealing with whole oocyte transcriptome analysis in correlation with maternal age have focused mainly on the GV and/or MII stages as they represent the two meiotic arrest points of maturing oocytes. For example, Pan et al (2008) performed microarray analysis in order to obtain the whole transcriptome of oocytes from young and aged mice females at the GV and MII stages, and reported very little differences in transcriptome between the age groups at the GV stage (5% with FC >2) while the transcriptome of MII stage oocytes differed more significantly in correlation with maternal age (33% with FC >2). A similar trend was observed by Reyes et al. (2017) in a transcriptome study comparing human GV and MII oocytes. However, the transcriptome at the post-NEBD stage remains unstudied, possibly because whole transcriptome analysis would reveal few differences between the oocytes from different maternal ages, as it was previously reported in GV oocytes (Pan et al., 2008). Here, with the advantage of being able to reliably assay polysome bound mRNAs, we have been able to detect mRNAs that are actively translated. Thus, we have begun to unveil how specific oocyte translatoome changes, associated with maternal age, and how it affects the resulting proteome in the critical developmental window directly after meiotic resumption. For example, translatoome mRNA profiling of post-NEBD YF and AF oocytes has revealed differentially enriched and relevant ontology categories of mRNA transcripts related to cytokinesis and cell division processes. These ontological categories include specific transcripts with important roles in meiosis (e.g. *Cdk10*, *Cep63*, *Chek2*, *Nde1*, *Spice1* and various kinesins).

Derived from our polysome-associated mRNA-Seq screen, we have identified and validated four candidate transcripts that have significantly different polysome enrichment levels between YF and AF derived post-NEBD oocytes: *Sgk1*, *Castor1*, *Aire* and *Eg5*. Intriguingly, the respective proteins of all transcripts localize to the newly forming spindle, which is essential for chromosome alignment and cytokinesis. EG5 is involved in spindle bi-polarity establishment, microtubule sliding and has been thoroughly studied in mitosis and meiosis (Mann and Wadsworth, 2019). Despite previous whole transcriptome studies failing to report overt differences in *Eg5* mRNA expression between YF and AF oocytes (Hamatani et al., 2004b; Pan et al., 2008; Grøndahl et al., 2010; Reyes et al., 2017), our SSP-Profiling approach demonstrates a significant increase in *Eg5* transcript in polysomes of AF oocytes, that then translates to corresponding increased protein expression levels. Interestingly, Liu et al., (2010) and Castillo et al., (2007) have shown in other tissue models that overexpression of EG5 can induce aneuploidy and tumorigenesis. Therefore, alteration of EG5 levels in oocytes retains the potential to influence the spindle assembly process, leading to aberrant meiotic progression with abnormal chromosome segregation (Liu et al., 2010; Castillo et al., 2007; Kovacovicova et al., 2016).

AIRE is another interesting candidate with a possible role in age-related aneuploidy in mice. Although it has been mainly studied for its role as a transcription factor in immune tolerance control (Björnses et al., 1998), it is known *Aire* deficient female mice display infertility; albeit without a direct study of oocyte quality (Jasti et al., 2012). Furthermore, an interaction between AIRE and spindle-associated proteins has been reported to be essential for mitotic spindle

assembly in stem cells. In the same study, overexpression of a truncated version of AIRE leads to defective spindle in stem cells (Gu et al., 2017). Here, we also find AIRE is localized at the newly forming oocyte meiotic spindle and that *Aire* mRNA is highly translated in aged post-NEBD oocytes compared to their young counterpart. Due to AIRE's main studied role as a transcription factor, the presence of AIRE protein in transcriptionally silent oocytes is not entirely clear. However, as our data demonstrate, further research will explain its function in spindle assembly and cytokinesis, with particular emphasis on oocytes from aged females.

The third protein we have identified and validated as up-regulated in the AF oocytes is CASTOR1. In the presence of arginine, CASTOR1 binds to this amino acid, which prevents its inhibitory effect on GATOR2, ultimately allowing mTOR1 activation (Saxton et al., 2016). CASTOR1 localization to the spindle might be connected to mTOR1, which also accumulates to the spindle and its inhibition/downregulation leads to meiotic defects (Susor et al., 2015; Guo et al., 2018). Therefore, it is possible that localization of mTOR1 to the assembling spindle, under the control of a strong upstream regulator such as CASTOR1, might be important for its temporal and/or spatial regulation. Indeed, when we experimentally increased CASTOR1 levels in YF oocytes, in order to mimic the increased protein expression as detected in AF oocytes, the most frequently observed anomaly was chromosomal misalignment but also few cytokinesis errors, resulting in oocytes devoid of DNA. While the latter phenotype is obviously incompatible with further development, chromosome misalignment can be considered detrimental and can lead to aneuploidy (Liu and Keefe, 2008). Taken together, these results reveal CASTOR1 as a possible factor relevant to age-related chromosomal aneuploidy in oocytes.

In contrast to CASTOR1, SGK1 protein expression is lower in AF oocytes compared to YF oocytes. SGK1 is known to regulate the activity of ion channels, solute carriers, enzymes and transcription factors (Lang et al., 2018). SGK1 protein kinase activity can be triggered by insulin, follicle stimulation hormone (FSH), corticosterone and thrombin, and is mediated by several upstream kinases including PI3K, PDK1 and mTORC2 (Kobayashi and Cohen, 1999; Pearce et al., 2011). Surprisingly, despite its previously described localization in the plasma membrane, we observed it in the region of the post-NEBD forming oocyte spindle. Paralleling our results, SGK1 levels have also reported to decline with human aging (Harries et al., 2012). Moreover, we found that inhibition of SGK1 activity in YF oocytes visibly lead to cytokinetic errors.

Altogether, our study has generated a genome-wide database of mRNA transcripts that occupy post-NEBD oocyte polysomes in both young and aged mouse oocytes. Furthermore, we have demonstrated the existence of differential polysomal mRNA occupancy in young and aged oocytes, suggesting different translational program in post-NEBD oocytes dependent on maternal age, correlating with reduced quality of aged oocytes (see scheme in Fig. 5); a characteristic phenomenon of both mice and humans. Therefore, our data provides new information related to age related translational/proteome perturbation (including verified candidate gene mRNA/proteins) at the onset of meiosis, concomitant with spindle formation and resulting cytokinesis.

## Legends

### **Fig. 1 Genome wide analysis shows differential translation of cell cycle regulators in oocytes from aged females.**

**A)** qRT-PCR analysis of distribution of 18S rRNA between non-polysomal (NP) and polysomal (P) fractions in oocytes of young female (YF), aged female (AF) mice and in oocytes with disrupted polysomes (YF+EDTA). Data are represented as the mean  $\pm$  s.e.m, \* $P < 0.05$ ; ns, non-significant; according to Student's *t*-test.

**B)** Volcano plot displaying gene transcripts differentially enriched in P fractions of oocytes from YF and AF groups; highlighting those with FC >10 and adjusted- $P < 0.1$  (red), with only FC >10 (green) and the rest (grey). Data points with gene names refer to the selected target genes with possible function in female meiosis. See also Supplementary Table 1.

**C)** Top enriched ORA categories in differentially enriched genes (FC >10) from associated polysomal fractions. Categories related to cell division are highlighted in blue. NoG, Number of Genes that belong the category; ER, Enrichment Ratio. See also Supplementary Table 2.

**D)** FPKM values for selected target transcripts differentially enriched between YF and AF polysomal fractions that are potentially related to female meiosis. See also Supplementary Table 1.

**Fig. 2 Validation of specific genes with different polysomal mRNA occupancy; positive correlation with protein expression between YF and AF oocytes.**

**A)** ddPCR validation of selected mRNAs in polysomal fractions from YF and AF oocytes (200 oocytes per sample after SSP-profiling). Values obtained were normalized to ACTB and YF group was set as reference (100%). Data represented as the mean  $\pm$  s.e.m. of three independent experiments.

**B)** Western Blot analysis of protein abundance of mRNAs coding for selected genes from RNA-Seq datasets in the two groups of oocytes. ACTB was used as loading control. See also Supplementary Table 4 for the list of antibodies.

**C)** Western Blot quantification of protein expression for selected genes. Values obtained were normalized to ACTB and YF group was set as reference (100%). Data are represented as the mean  $\pm$  s.e.m. of at least three independent experiments;  $n \geq 20$  per sample;  $*P < 0.05$ , according to Student's *t*-test. See also Supplementary Table 4 for the list of antibodies.

**Fig. 3 Differentially expressed proteins are localized at newly forming oocyte spindles.**

**A)** Immunocytochemistry shows localization of SGK1, CASTOR1, AIRE and EG5 proteins at newly forming spindles in the post-NEBD oocytes (YF – left, AF – right). Protein in grey and green scales, DNA (DAPI) in blue. Dashed line indicates oocyte cortex; representative images of at least three independent experiments are shown; scale bar 25  $\mu$ m. See also Supplementary Table 4 for the list of antibodies.

**B)** Immunocytochemistry quantification of protein fluorescence in oocytes from YF ( $n \geq 48$ ) and AF ( $n \geq 23$ ) oocytes in at least three independent experiments. Data are presented as the percentage of oocytes with a fluorescence intensity higher than the average in each experiment;  $*P < 0.05$ ,  $***P < 0.001$ ; according to Fisher's exact test, error bars represent 95% confidence intervals by the adjusted Wald method.

**Fig. 4 Experimental manipulation of CASTOR1 and SGK1 protein levels/activity causes meiotic abnormalities.**

**A)** Western blot analysis of YF oocytes microinjected with RNA coding for H2B:GFP (Control) or CASTOR1 tagged with HA. ACTB was used as loading control. Representative images from three individual replicates;  $n \geq 20$  per sample.

**B)** Quantification of MII oocytes that displayed phenotype with overexpressed CASTOR1 protein from three independent experiments. Data are presented as the percentage of oocytes ( $n \geq 18$ ) with abnormalities;  $*P < 0.05$ ; according to Fisher's exact test, error bars represent 95% confidence intervals by the adjusted Wald method.

**C)** Representative images of chromosome abnormalities in MI and MII oocytes with overexpression of CASTOR1. Bright field (BF, grey) and H2B:GFP (green); dashed line indicates oocyte and polar body cortex; arrow indicate a misaligned chromosome, asterisks denote polar bodies, scale bar 25  $\mu$ m.

**D)** Western Blot validation of SGK1 inhibition via CDK1 phosphorylation (Thr161). ACTB was used as a loading control. Representative images from three biological replicates,  $n \geq 20$  oocytes per sample;  $*P < 0.05$ ; according to Student's *t*-test. See also Supplementary Table 4 for the list of antibodies.

**E)** Quantification of MII oocytes that displayed phenotype in control (DMSO 0.02%) or SGK1 inhibitor (10 $\mu$ M) treatment. Data are presented as the percentage of oocytes with abnormalities in control ( $n=75$ ) and treated ( $n=75$ );  $*P < 0.05$ ; according to Fisher's exact test, error bars represent 95% confidence intervals by the adjusted Wald method.

**F)** Representative images of oocytes with SGK1 inhibition progressing through cytokinesis. From at least three independent experiments; Tubulin (green) and DNA (grey scale); dashed line indicates oocyte and polar body cortex; arrow indicate tubulin bridge; arrowheads indicate decondensed chromatin; asterisks denote polar bodies, scale bar 25  $\mu$ m.

**Fig. 5 Schematic model depicting that maternal age affects the translation of specific mRNAs in oocytes.**

Fully grown oocytes from different maternal age have similar transcriptomes at the GV stage. However, shortly after NEBD, some of these transcripts are not translated at the same level between YF and AF oocytes, such as *Sgk1*, *Aire*, *Castor1* and *Eg5*. These differences in translation result in different protein expression which in turn lead to chromosome misalignments and cytokinesis abnormalities in AF oocytes.

## Supplementary Figures

### Supplementary Fig. 1 Differential non-polysomal and polysomal occupancy categorized to different clusters.

Hierarchical clustering of differentially enriched genes in non-polysomal and polysomal fractions of oocytes from young and aged females and relative abundance patterns in seven clusters with at least 10 genes. In the brackets number of genes in the cluster.

### Supplementary Fig. 2 qPCR quantification of selected transcripts from total RNA of oocytes from YF and AF groups.

Data are represented as the mean  $\pm$  s.e.m. of three independent experiments; \* $P < 0.05$ ; according to Student's *t*-test. See Fig. 2A.

### Supplementary Fig. 3 Translation of selected proteins is not influenced by differential timing of meiotic progression.

**A)** Western blot of AIRE protein expression in oocytes from YF+30 min (progressing in meiosis for 30 longer) and AF (collected at same time as YF group). Representative images from three independent experiments and ACTB was used as a control.

**B)** Quantification of AIRE protein expression (WB derived) normalized to ACTB and to YF+30 min group (progressing in meiosis for 30 longer). Data are represented as the mean  $\pm$  s.e.m. of three independent experiments;  $n \geq 20$  per sample; \* $P < 0.05$ ; according to Student's *t*-test.

**C)** Immunocytochemistry of YF oocytes cultured for 30 minutes longer after IBMX removal (YF+30) and AF for EG5 (grey scale - left and green channel - right) and DNA (DAPI) (blue). From two independent experiments, dashedline depicts oocyte cortex; scale bar 25  $\mu$ m.

**D)** Quantification of EG5 protein fluorescence. Data are presented as the percentage of oocytes with a fluorescence higher than the average in YF ( $n=31$ ) and AF ( $n=24$ ); \* $P < 0.05$ ; according to Fisher's exact test, error bars represent 95% confidence intervals by the adjusted Wald method.

### Supplementary Fig. 4 Western Blot quantification of CDK1 protein phosphorylation (Thr161).

Values obtained were normalized to ACTB and Control (DMSO 0.02%) group was set as reference (100%). Data are represented as the mean  $\pm$  s.e.m. of three independent experiments;  $n \geq 20$  per sample; \* $P < 0.05$ ; according to Student's *t*-test. See Fig. 4D.

**Supplementary Table 1.** List of genes up/down regulated in AF compared to YF according to FC>5, FC>10 and FC>10 plus  $P < 0.1$ .

**Supplementary Table 2.** List of genes in each Gene Ontology categories as seen in Fig 1C.

**Supplementary Table 3.** List of genes from cluster 1,3,6,7 (increasing presence from YF-NP to YF-P, and vice versa in AF) and clusters 2,4,5 (increasing presence from increasing presence from AF-NP to AF-P, and vice versa in YF)(see Fig. S1).

**Supplementary Table 4.** Table of primers used for PCR (A) and (B) list of antibodies used for the study.

## Acknowledgments

We would like to thank Jaroslava Supolikova and Marketa Hancova for their valuable assistance with many experiments and Martin Anger for kindly providing the *H2B:gfp* plasmid.

We also acknowledge Simon Andrews for his help and valuable suggestions with bioinformatics analysis (Bioinformatics Group, Babraham Institute, Cambridge).

Computational resources were supplied by the project "e-Infrastruktura CZ" (e-INFRA LM2018140) provided within the program Projects of Large Research, Development and Innovations Infrastructures.

## Funding

The project was funded by The Czech Science Foundation (GACR, no. 19-13491S); Lenka Gahurova was supported by MSC IF 708255.

## Author contributions

A.S., E.L. designed the experiments and planned the project; M.K., T.M. and M.P. also contributed intellectually during the development of the project. E.L. was involved in all experiments and performed most of them. T.M. designed, performed and helped in all polysomal fractionation experiments. A.J. and D.J. performed live-cell imaging experiments, M.K. carried out micro-injection experiments, R.Y. performed IVT. L.G. performed and helped in producing sequencing libraries and carried out bioinformatics analysis. M.P. and K.R. also contributed to bioinformatics analysis. E.L. and A.S. wrote the manuscript, all authors edited manuscript, A.S. conceived and supervised the project.

## Conflict of interest

The authors certify that they have NO conflict of interest of any kind in the subject matter or materials discussed in this manuscript/article.

## Material and Methods

### Oocyte collection and culture

GV stage oocytes were collected from - ICR mice (bred in-house) at the age of 6 - 10 weeks (YF, Young Females group) and 58 weeks (AF, Aged Females group) old. Mice were injected 46 hours prior to oocyte collection with 5 IU pregnant mare serum gonadotropin (PMSG, HOR 272, ProSpec, Rehovot, Israel). Collection from the ovaries was done in the presence of transfer media (Tetkova and Hancova, 2016) supplemented with 100  $\mu$ M 3-isobutyl-1-methylxanthine (IBMX, Sigma-Aldrich, Darmstadt, Germany) to block meiosis resumption. Fully grown oocytes were selected, isolated and denuded by pipetting followed by culture in M16 media (Sigma-Aldrich, Darmstadt, Germany) without IBMX at 37°C, 5% CO<sub>2</sub> for 3 hours. Oocytes, that underwent NEBD, were collected for experiments. For obtaining MII oocytes, they were left in culture for additional 13-16 hours. For SSP-profiling, after the 3 h of culture, cycloheximide was added to the M16 media with oocytes at a final concentration of 0.1 mg/ml for 10 minutes. Oocytes in groups of 200 were transferred to low-binding retention tubes and frozen at -80 °C. In the case of SGK1 inhibition experiments, after IBMX removal GV oocytes were transferred to M16 media supplemented with 0,02% Dimethyl Sulfoxide (DMSO) for solvent vehicle control or 0.02% DMSO+10 $\mu$ M GSK-650394 (Merk, Darmstadt, Germany) for SGK1 inhibitor treatment. All animal work was conducted according to Act No 246/1992 for the protection of animals against cruelty; from 25.09.2014 number CZ02389, issued by Ministry of Agriculture.

### Cell lysis and SSP-profiling

All steps for this protocol were detailed in Masek et al. (2020). Briefly, 200 oocytes per sample were collected in the presence of cycloheximide. Oocytes were lysed by adding 350  $\mu$ l of lysis buffer and Zirconia-Silica beads followed by shaking at 30 shakes/second for 1 min and 1 min on ice. This step was repeated three times. Oocyte lysates were centrifuged at 10,000 x g for 5 min before being then applied to 10-50% sucrose gradients prepared in SW55Ti ultracentrifuge rotor (Beckman Coulter, Indianapolis, IN, USA). Samples loaded onto sucrose gradients were then centrifuged at 45,000 RPM (246,078 x g) for 63 min at 4°C. Polysome profiles were collected by pumping 60% sucrose into SW55Ti tubes at a speed of 1.8 mL/minute using NE-1000 syringe pump (New Era Pump Systems, Inc., Farmingdale, NY, USA). Ten equal-volume fractions, each of 0,5 ml. Absorbance monitoring at 280 nm was performed using an ISCO UA-5 detector and ISCO UV absorbance reader (Teledyne, ISCO, Lincoln, NE, USA) and profiles were recorded with Clarity Lite software. HEK-293 cell sample (8 OD<sub>260 nm</sub>) was included in each centrifugation run to monitor quality of separation and one technical negative control containing 200 NEBD+EDTA (100mM), to sequester magnesium ions and disrupt ribosomal subunits were added. Finally, polysome profiles of all oocyte samples and HEK-293 technical controls for fractionation were visualized by detecting 18S rRNA levels in collected fractions by qRT-PCR according to Masek et al. (2020).

### Library preparation, sequencing and bioinformatic analysis

From each sample, fractions were pooled together to create two groups: non-polysomal (NP) and polysomal (P) fractions. These fractions were concentrated by Clean & Concentrator-5 (Zymo Research, Irvine, CA, USA) and rRNA depleted by Ribozero-Gold (Illumina, San Diego, CA, USA). cDNA was produced and amplified with REPLI-g WTA Single Cell Kit (Qiagen, Hilden, Germany). Afterwards, the amplified cDNA was used to produce libraries using the Nextera



DNA Library Prep Kit (Illumina, San Diego, CA, USA) and sequencing performed in Centro Nacional de Analisis Genomico facility (CNAG, Barcelona, Spain) by HiSeq 2500 (Illumina). Sequenced reads were trimmed by Trim Galore! v0.4.1 and mapped to the mouse GRCm38 genome assembly using Hisat2 v2.0.5. Quantification of gene expression was done by fragments per kilobase per million (FPKM) values in Seqmonk v1.40.0. The FC cuff-off of differentially expressed genes was calculated from FPKM >1 values (either in YF or AF) as quantified by Seqmonk v1.40.0 and FC > 10 and FC > 5. Hierarchical clustering was performed and a heatmap was generated using differentially abundant genes (FC>10) using hierarchical clustering function within Seqmonk v1.40.0. For gene ontology analysis, we uploaded our datasets into Webgestalt (Liao et al., 2019). ORA analysis was performed on the 1006 genes which displayed FC>10 and FPKM>1 between polysomal fractions of YF and AF. The protocol was described in Masek et al. (2020) and YF samples served to prove validity of the method.

### **Digital Droplet PCR (ddPCR)**

Primer sequences of *Sgk1*, *Castor1*, *Aire* and *Eg5* are listed in Supplementary Table 4. ddPCR reaction was performed in the QX200™ Droplet Reader machine (Bio-Rad, Hercules, CA, USA) using the QX200™ ddPCR™ EvaGreen® Supermix (Bio-Rad, Hercules, CA, USA). Absolute quantification was calculated using QuantaSoft™ Software (Bio-Rad, Hercules, CA, USA).

### **Western Blot**

Samples of 20-35 oocytes were lysed in 10 µl of 1xReducing SDS Loading Buffer (lithium dodecyl sulfate sample buffer NP 0007 and reduction buffer NP 0004 (Thermo Fisher Scientific, Waltham, MA, USA) and heated at 100°C for 5 min. Proteins were separated in gradient precast 4–12% SDS–PAGE gels (NP 0323, Thermo Fisher Scientific) and transferred onto Immobilon P membrane (IPVD 00010, Millipore, Merck group, Darmstadt, Germany) using a semidry blotting system (Biometra GmbH, Analytik Jena, Jena, Germany) for 25 min at 5 mA/cm<sup>2</sup>. Blocking was done by 5% skimmed milk dissolved in 0.05% Tween-Tris buffer saline (TTBS) with pH 7.4 for 1 h. Then, membranes were washed shortly with TTBS and incubated with 1% milk/TTBS diluted primary antibodies (listed in Supplementary Table 4) at 4°C O/N (). Secondary antibodies, Peroxidase Anti-Rabbit Donkey and Peroxidase Anti-Mouse Donkey (711-035-152 and 715-035-151, Jackson ImmunoResearch, West Grove, PA, USA) were diluted 1:7500 in 1% milk/TTBS. The membranes were incubated with secondary antibodies for 1 h at room temperature. Protein visualization was performed using chemiluminescent detection ECL, (Amersham, GE Healthcare Life Sciences, Barcelona, Spain) and X-ray autoradiography. Finally, the films were scanned by a GS-800 calibrated densitometer (Bio-Rad Laboratories, CA, USA) and acquired signals were quantified using ImageJ (<http://rsbweb.nih.gov/ij/>).

### **Immunocytochemistry**

Oocytes were transferred from cultivation media to 4% paraformaldehyde (PFA, Alfa Aesar, Thermo Fisher Scientific, Waltham, MA, USA) in PBS/PVA and left for 15 minutes followed by permeabilization in 0.1% Triton (X-100, Sigma-Aldrich) PBS/PVA for 10 min. Fixed oocytes were then washed in PBS/PVA and incubated with primary antibodies (Supplementary Table 4) at 4°C O/N. The next day, oocytes were twice washed in PBS/PVA and then incubated with the corresponding secondary antibody that was conjugated with Alexa Fluor 488/594/647 (Invitrogen, Carlsbad, CA, USA) for 1 h at room temperature protected from light. Afterwards, oocytes were washed twice in PBS/PVA and mounted on a glass slide using ProLong™ Gold antifade reagent with DAPI (Invitrogen, Carlsbad, CA, USA). Images of samples were taken with Leica SP5 inverted confocal microscope (Leica Microsystems, Wetzlar, Germany). Images were assembled in software LAS X (Leica Microsystems) and signal intensity from spindle area was quantified with ImageJ. Afterwards, the mean fluorescence intensity of each experiment was calculated. Finally, the fluorescence intensity of each sample was categorized as lower as or higher than the mean.

### **RNA synthesis, microinjection and live-cell imaging**

*Castor1* and *H2b:gfp* RNA were in vitro transcribed (IVT) using corresponding source plasmids as templates (*Castor1*: Chantranupong et al. (2016); *H2b:gfp*: provided by Dr. Martin Anger, Laboratory of Cell Division Control, IAPG CAS) and mMESSAGING mMACHINE™ Transcription Kit (Invitrogen, Carlsbad, CA, USA). IVT RNA was injected in GV oocytes at a final concentration of 50ng/µl in the presence of transfer media with IBMX. Microinjection of GV oocytes was performed using FemtoJet (Eppendorf) and TransferMan NK2 (Eppendorf, Hamburg, Germany) on an inverted microscope Leica DMI 6000B (Leica Microsystems, Wetzlar, Germany). GV oocytes were then placed for 2 h, still in the presence of IBMX, at 37°C, 5% CO<sub>2</sub>. Afterwards, oocytes were removed from IBMX and placed into 4-well culture

chamber (Sarstedt, Prague, Czech Republic) in 15  $\mu$ L of M16 media covered with mineral oil (M8410; Sigma Aldrich) for further cultivation in the inverted microscope for live-cell monitoring under the same cultivation conditions (Tempcontroller 2000–2 Pecon, and a CO<sub>2</sub> controller, Pecon, Erbach, Germany). Time lapse images were taken using LAS X software (Leica microsystems, Wetzlar, Germany) every 10 min. Chromosome movement was also assessed by H2B:GFP marker.

### Statistical analysis

The tool used to determine if the differences between groups were statistically significant was either Student's t-test on the averages and s.e.m. or Fisher exact test with a 95% confidence interval using adjusted Wald method; \* $P < 0.05$  considered as statistically significant (labelled with a star), \*\*\* $P < 0.005$  was considered as highly statistically significant (labelled with three stars).

### Data access

RNA-Seq data regarding YF and AF oocytes is deposited in Gene Expression Omnibus database. AF data accession number: PENDING. YF accession number, as stated in (Masek et al., 2020): GSE121358.

## References

- Björnses, P., Aaltonen, J., Horelli-Kuitunen, N., Yaspo, M.-L., and Peltonen, L. (1998). Gene Defect behind APECED: A New Clue to Autoimmunity. *Hum. Mol. Genet.* 7, 1547–1553.
- Capalbo, A., Hoffmann, E.R., Cimadomo, D., Maria Ubaldi, F., and Rienzi, L. (2017). Human female meiosis revised: new insights into the mechanisms of chromosome segregation and aneuploidies from advanced genomics and time-lapse imaging. *Hum. Reprod. Update* 23, 706–722.
- Castillo, A., Morse, H.C., Godfrey, V.L., Naeem, R., and Justice, M.J. (2007). Overexpression of *Eg5* Causes Genomic Instability and Tumor Formation in Mice. *Cancer Res.* 67, 10138.
- Chantranupong, L., Scaria, S.M., Saxton, R.A., Gygi, M.P., Shen, K., Wyant, G.A., Wang, T., Harper, J.W., Gygi, S.P., and Sabatini, D.M. (2016). The CASTOR Proteins Are Arginine Sensors for the mTORC1 Pathway. *Cell* 165, 153–164.
- Chen, J., Melton, C., Suh, N., Oh, J.S., Horner, K., Xie, F., Sette, C., Blelloch, R., and Conti, M. (2011). Genome-wide analysis of translation reveals a critical role for deleted in azoospermia-like (*Dazl*) at the oocyte-to-zygote transition. *Genes Dev.* 25, 755–766.
- De La Fuente, R., Viveiros, M.M., Burns, K.H., Adashi, E.Y., Matzuk, M.M., and Eppig, J.J. (2004). Major chromatin remodeling in the germinal vesicle (GV) of mammalian oocytes is dispensable for global transcriptional silencing but required for centromeric heterochromatin function. *Dev. Biol.* 275, 447–458.
- Femino, A.M., Fay, F.S., Fogarty, K., and Singer, R.H. (1998). Visualization of Single RNA Transcripts in Situ. *Science* 280, 585.
- Fulka, J., Jr, First, N.L., and Moor, R.M. (1998). Nuclear and cytoplasmic determinants involved in the regulation of mammalian oocyte maturation. *Mol. Hum. Reprod.* 4, 41–49.
- Ganesh, S., Horvat, F., Drutovic, D., Efenberkova, M., Pinkas, D., Jindrova, A., Pasulka, J., Iyyappan, R., Malik, R., Susor, A., et al. (2020). The most abundant maternal lncRNA *Sirena1* acts post-transcriptionally and impacts mitochondrial distribution. *Nucleic Acids Res.* 48, 3211–3227.
- Grøndahl, M.L., Yding Andersen, C., Bogstad, J., Nielsen, F.C., Meinertz, H., and Borup, R. (2010). Gene expression profiles of single human mature oocytes in relation to age. *Hum. Reprod.* 25, 957–968.

- Gu, B., Lambert, J.-P., Cockburn, K., Gingras, A.-C., and Rossant, J. (2017). AIRE is a critical spindle-associated protein in embryonic stem cells. *ELife* 6, e28131.
- Guo, J., Zhang, T., Guo, Y., Sun, T., Li, H., Zhang, X., Yin, H., Cao, G., Yin, Y., Wang, H., et al. (2018). Oocyte stage-specific effects of MTOR determine granulosa cell fate and oocyte quality in mice. *Proc. Natl. Acad. Sci. U. S. A.* 115, E5326–E5333.
- Hamatani, T., Carter, M.G., Sharov, A.A., and Ko, M.S.H. (2004a). Dynamics of Global Gene Expression Changes during Mouse Preimplantation Development. *Dev. Cell* 6, 117–131.
- Hamatani, T., Falco, G., Carter, M.G., Akutsu, H., Stagg, C.A., Sharov, A.A., Dudekula, D.B., VanBuren, V., and Ko, M.S.H. (2004b). Age-associated alteration of gene expression patterns in mouse oocytes. *Hum. Mol. Genet.* 13, 2263–2278.
- Harries, L.W., Fellows, A.D., Pilling, L.C., Hernandez, D., Singleton, A., Bandinelli, S., Guralnik, J., Powell, J., Ferrucci, L., and Melzer, D. (2012). Advancing age is associated with gene expression changes resembling mTOR inhibition: evidence from two human populations. *Mech. Ageing Dev.* 133, 556–562.
- Hassold, T., and Hunt, P. (2001). To err (meiotically) is human: the genesis of human aneuploidy. *Nat. Rev. Genet.* 2, 280–291.
- Hiraoka, D., Hosoda, E., Chiba, K., and Kishimoto, T. (2019). SGK phosphorylates Cdc25 and Myt1 to trigger cyclin B–Cdk1 activation at the meiotic G2/M transition. *J. Cell Biol.* 218, 3597–3611.
- Jansova, D., Tetkova, A., Koncicka, M., Kubelka, M., and Susor, A. (2018). Localization of RNA and translation in the mammalian oocyte and embryo. *PLoS One* 13, e0192544–e0192544.
- Jasti, S., Warren, B.D., McGinnis, L.K., Kinsey, W.H., Petroff, B.K., and Petroff, M.G. (2012). The autoimmune regulator prevents premature reproductive senescence in female mice. *Biol. Reprod.* 86, 110–110.
- Jones, K.T., and Lane, S.I.R. (2013a). Molecular causes of aneuploidy in mammalian eggs. *Development* 140, 3719.
- Jones, K.T., and Lane, S.I.R. (2013b). Molecular causes of aneuploidy in mammalian eggs. *Development* 140, 3719.
- Kobayashi, T., and Cohen, P. (1999). Activation of serum- and glucocorticoid-regulated protein kinase by agonists that activate phosphatidylinositol 3-kinase is mediated by 3-phosphoinositide-dependent protein kinase-1 (PDK1) and PDK2. *Biochem. J.* 339 ( Pt 2), 319–328.
- Koncicka, M., Tetkova, A., Jansova, D., Del Llano, E., Gahurova, L., Kracmarova, J., Prokesova, S., Masek, T., Pospisek, M., Bruce, A.W., et al. (2018). Increased Expression of Maturation Promoting Factor Components Speeds Up Meiosis in Oocytes from Aged Females. *Int. J. Mol. Sci.* 19, 2841.
- Kovacovicova, K., Awadova, T., Mikel, P., and Anger, M. (2016). In Vitro Maturation of Mouse Oocytes Increases the Level of Kif11/Eg5 on Meiosis II Spindles1. *Biol. Reprod.* 95.
- Kuliev, A., Zlatopolsky, Z., Kirillova, I., Spivakova, J., and Cieslak Janzen, J. (2011). Meiosis errors in over 20,000 oocytes studied in the practice of preimplantation aneuploidy testing. *Reprod. Biomed. Online* 22, 2–8.
- Labrecque, R., and Sirard, M.-A. (2014). The study of mammalian oocyte competence by transcriptome analysis: progress and challenges. *MHR Basic Sci. Reprod. Med.* 20, 103–116.
- Lang, F., Stournaras, C., Zacharopoulou, N., Voelkl, J., and Alesutan, I. (2018). Serum- and glucocorticoid-inducible kinase 1 and the response to cell stress. *Cell Stress* 3, 1–8.

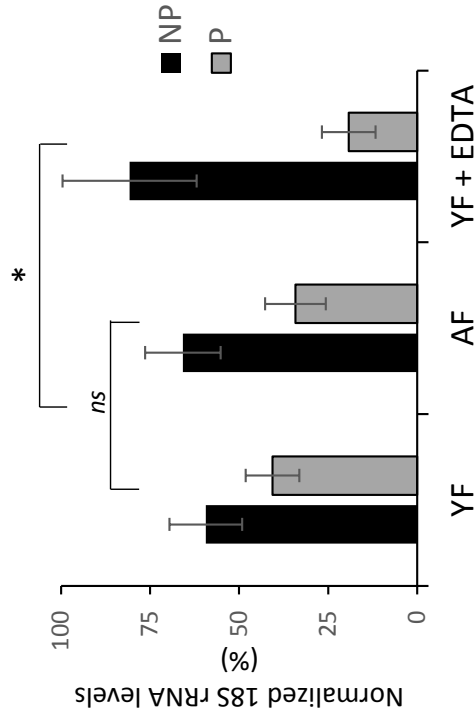
- Liao, Y., Wang, J., Jaehnig, E.J., Shi, Z., and Zhang, B. (2019). WebGestalt 2019: gene set analysis toolkit with revamped UIs and APIs. *Nucleic Acids Res.* *47*, W199–W205.
- Liu, L., and Keefe, D.L. (2008). Defective cohesin is associated with age-dependent misaligned chromosomes in oocytes. *Reprod. Biomed. Online* *16*, 103–112.
- Liu, M., Wang, X., Yang, Y., Li, D., Ren, H., Zhu, Q., Chen, Q., Han, S., Hao, J., and Zhou, J. (2010). Ectopic expression of the microtubule-dependent motor protein Eg5 promotes pancreatic tumorigenesis. *J. Pathol.* *221*, 221–228.
- Mann, B.J., and Wadsworth, P. (2019). Kinesin-5 Regulation and Function in Mitosis. *Trends Cell Biol.* *29*, 66–79.
- Mašek, T., Valášek, L., and Pospíšek, M. (2011). Polysome Analysis and RNA Purification from Sucrose Gradients. In *RNA: Methods and Protocols*, H. Nielsen, ed. (Totowa, NJ: Humana Press), pp. 293–309.
- Masek, T., del Llano, E., Gahurova, L., Kubelka, M., Susor, A., Roucova, K., Lin, C.-J., Bruce, A.W., and Pospisek, M. (2020). Identifying the Translatome of Mouse NEBD-Stage Oocytes via SSP-Profiling; A Novel Polysome Fractionation Method. *Int. J. Mol. Sci.* *21*, 1254.
- Molina-García, L., Hidalgo-Ruiz, M., Cocera-Ruiz, E.M., Conde-Puertas, E., Delgado-Rodríguez, M., and Martínez-Galiano, J.M. (2019). The delay of motherhood: Reasons, determinants, time used to achieve pregnancy, and maternal anxiety level. *PLoS One* *14*, e0227063–e0227063.
- Ottolini, C.S., Newnham, L., Capalbo, A., Natesan, S.A., Joshi, H.A., Cimadomo, D., Griffin, D.K., Sage, K., Summers, M.C., Thornhill, A.R., et al. (2015). Genome-wide maps of recombination and chromosome segregation in human oocytes and embryos show selection for maternal recombination rates. *Nat. Genet.* *47*, 727–735.
- Pan, H., Ma, P., Zhu, W., and Schultz, R.M. (2008). Age-associated increase in aneuploidy and changes in gene expression in mouse eggs. *Dev. Biol.* *316*, 397–407.
- Pearce, L.R., Sommer, E.M., Sakamoto, K., Wullschlegel, S., and Alessi, D.R. (2011). Protor-1 is required for efficient mTORC2-mediated activation of SGK1 in the kidney. *Biochem. J.* *436*, 169–179.
- Potireddy, S., Vassena, R., Patel, B.G., and Latham, K.E. (2006). Analysis of polysomal mRNA populations of mouse oocytes and zygotes: dynamic changes in maternal mRNA utilization and function. *Dev. Biol.* *298*, 155–166.
- Reyes, J.M., Silva, E., Chitwood, J.L., Schoolcraft, W.B., Krisher, R.L., and Ross, P.J. (2017). Differing molecular response of young and advanced maternal age human oocytes to IVM. *Hum. Reprod. Oxf. Engl.* *32*, 2199–2208.
- Savva, G.M., Walker, K., and Morris, J.K. (2010). The maternal age-specific live birth prevalence of trisomies 13 and 18 compared to trisomy 21 (Down syndrome). *Prenat. Diagn.* *30*, 57–64.
- Saxton, R.A., Chantranupong, L., Knockenhauer, K.E., Schwartz, T.U., and Sabatini, D.M. (2016). Mechanism of arginine sensing by CASTOR1 upstream of mTORC1. *Nature* *536*, 229–233.
- Scantland, S., Grenon, J.-P., Desrochers, M.-H., Sirard, M.-A., Khandjian, E.W., and Robert, C. (2011). Method to isolate polyribosomal mRNA from scarce samples such as mammalian oocytes and early embryos. *BMC Dev. Biol.* *11*, 8.
- Schuh, M., and Ellenberg, J. (2007). Self-Organization of MTOCs Replaces Centrosome Function during Acentrosomal Spindle Assembly in Live Mouse Oocytes. *Cell* *130*, 484–498.
- Sebestova, J., Danylevska, A., Dobrucka, L., Kubelka, M., and Anger, M. (2012). Lack of response to unaligned chromosomes in mammalian female gametes. *Cell Cycle* *11*, 3011–3018.

Susor, A., Jansova, D., Cerna, R., Danylevska, A., Anger, M., Toralova, T., Malik, R., Supolikova, J., Cook, M.S., Oh, J.S., et al. (2015). Temporal and spatial regulation of translation in the mammalian oocyte via the mTOR-eIF4F pathway. *Nat. Commun.* 6, 6078.

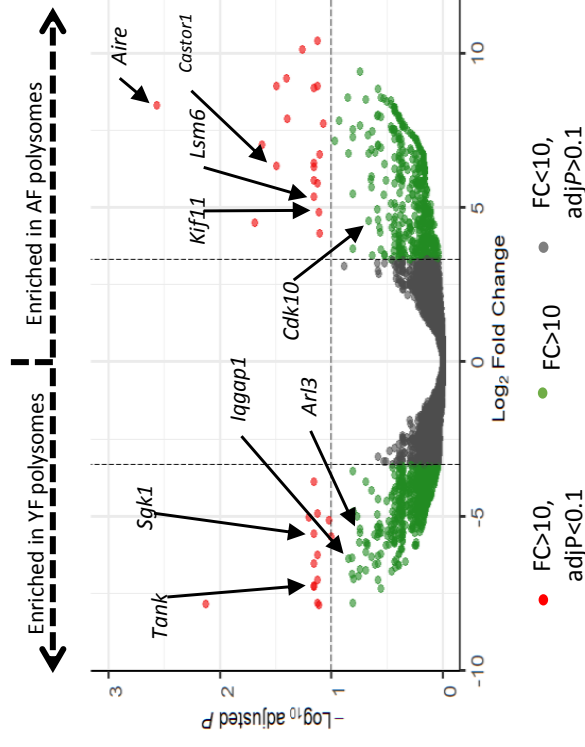


**Fig. 1**

**A**



**B**



**C**

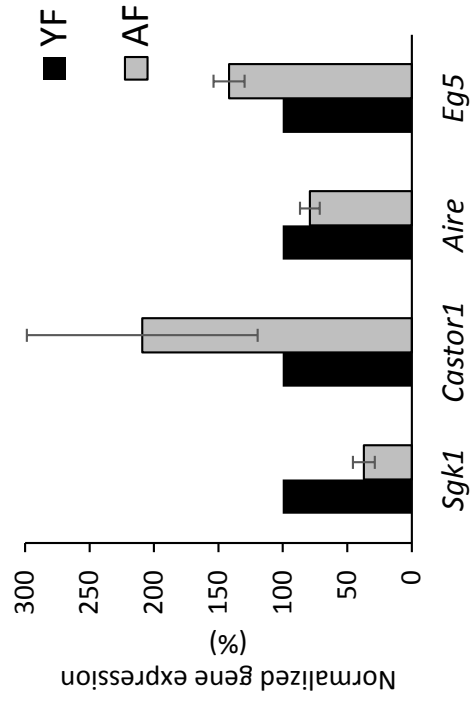
AF vs YF; FC>10			
Gene category description	NoG	ER	
mitotic spindle assembly	8	3.78	
centrosome duplication	9	3.82	
chromosome segregation	21	2.01	
negative regulation of cell cycle	29	1.85	
mRNA splicing, via spliceosome	21	2.43	
protein maturation	23	2.18	
methylation	25	2.34	
ribonucleoprotein complex biogenesis	27	1.85	
mRNA processing	29	1.89	
dephosphorylation	31	1.91	
negative regulation of intracellular signal transduction	35	1.90	
establishment of protein localization to plasma membrane	9	4.26	
cellular response to decreased oxygen levels	13	2.57	
negative regulation of protein serine/threonine kinase activity	13	2.93	

**D**

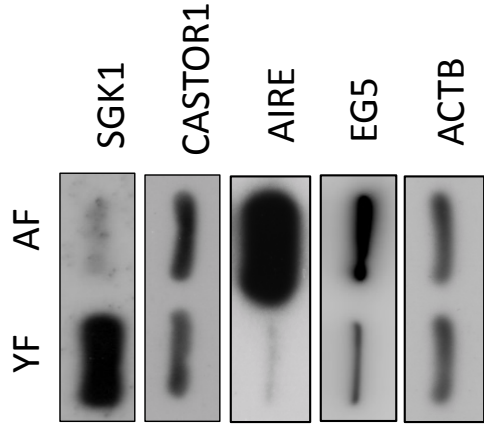
Polysomal occupancy (FPKM)			
Gene	YF	AF	
Actb	73.354	64.992	
Arl3	212.296	2.82	
Sgk1	59.269	1.097	
Tank	47.31	0.142	
lagap1	19.346	0.118	
Cdk10	4.177	52.277	
Lsm6	2.998	67.153	
Eg5	2.813	42.413	
Castor1	0.726	30.707	
Aire	0.244	36.82	

**Fig. 2**

**A**



**B**



**C**

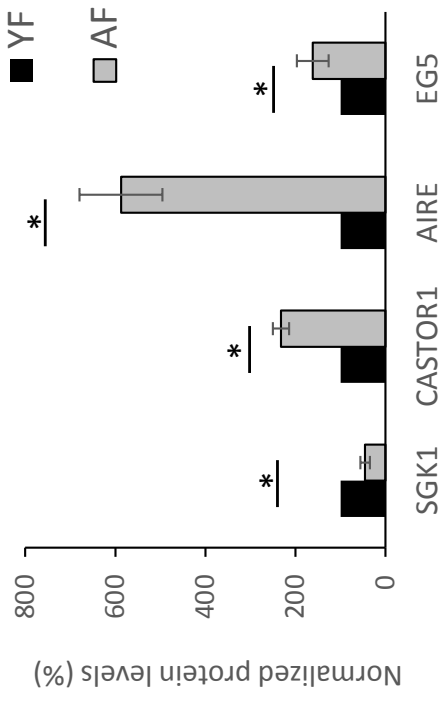


**Fig. 3**

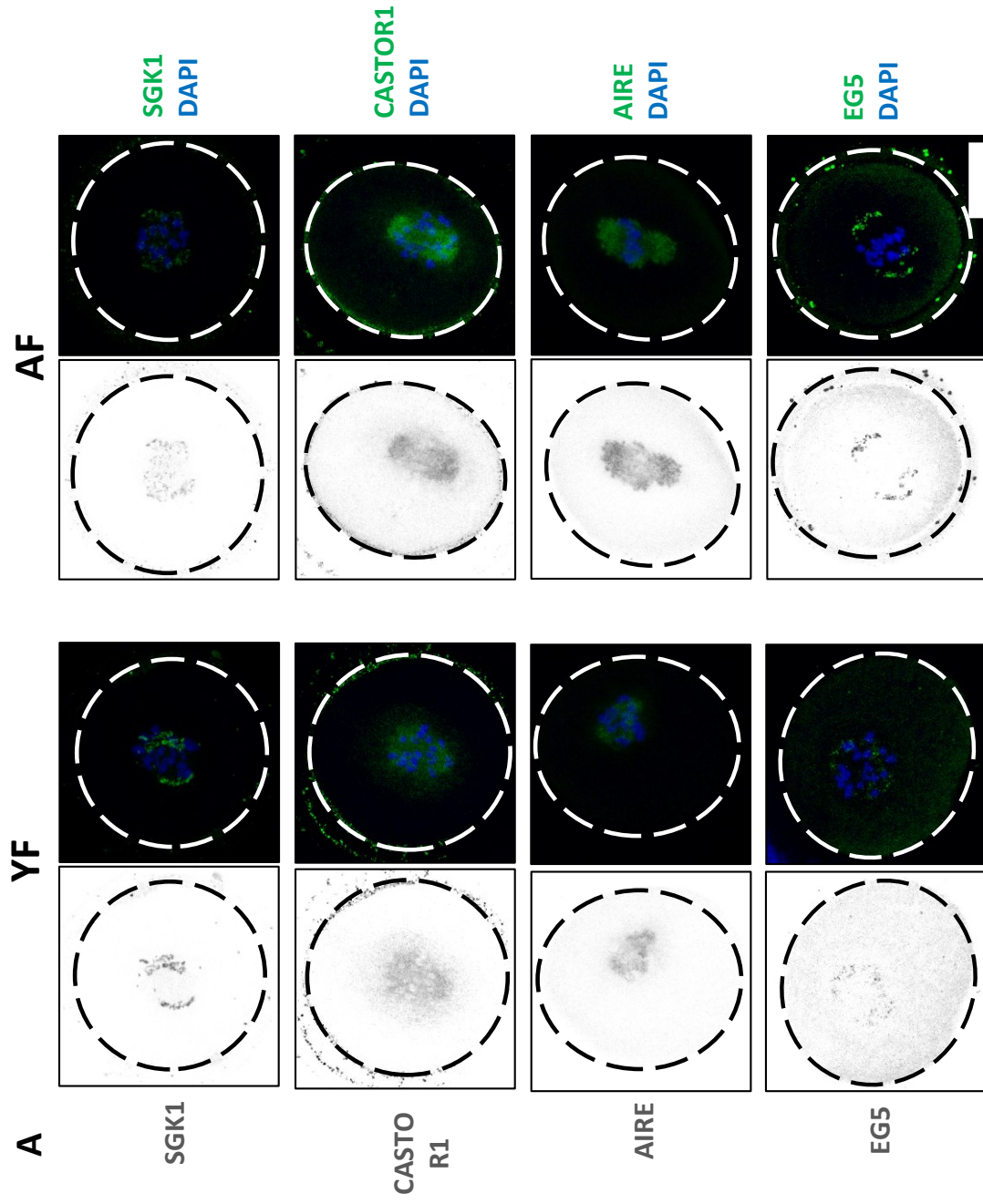


**Fig. 4**

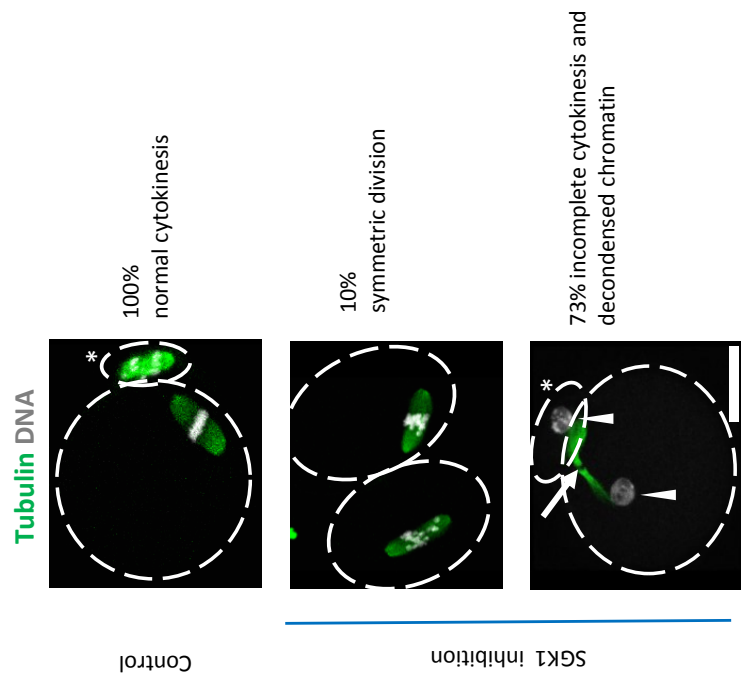
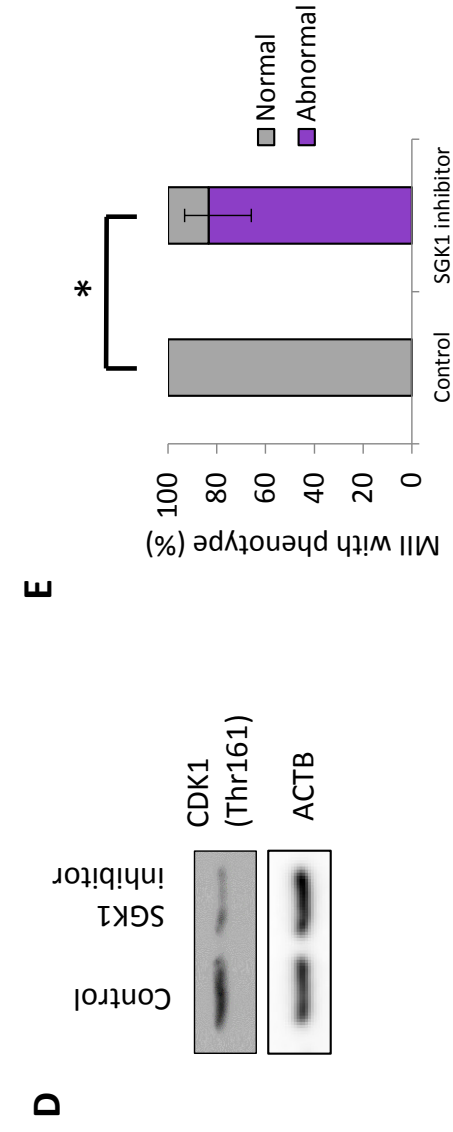
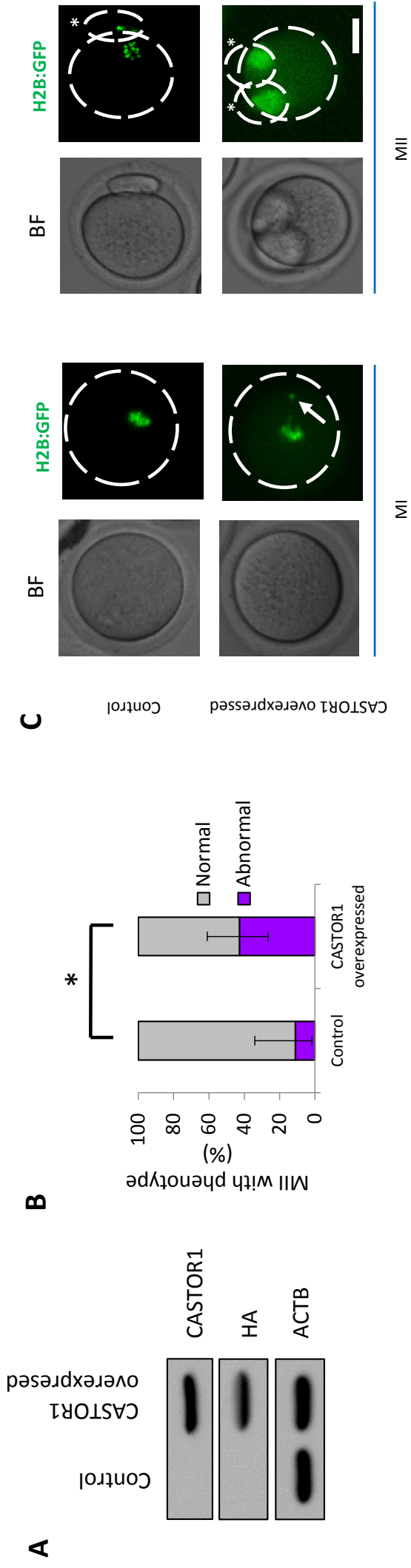
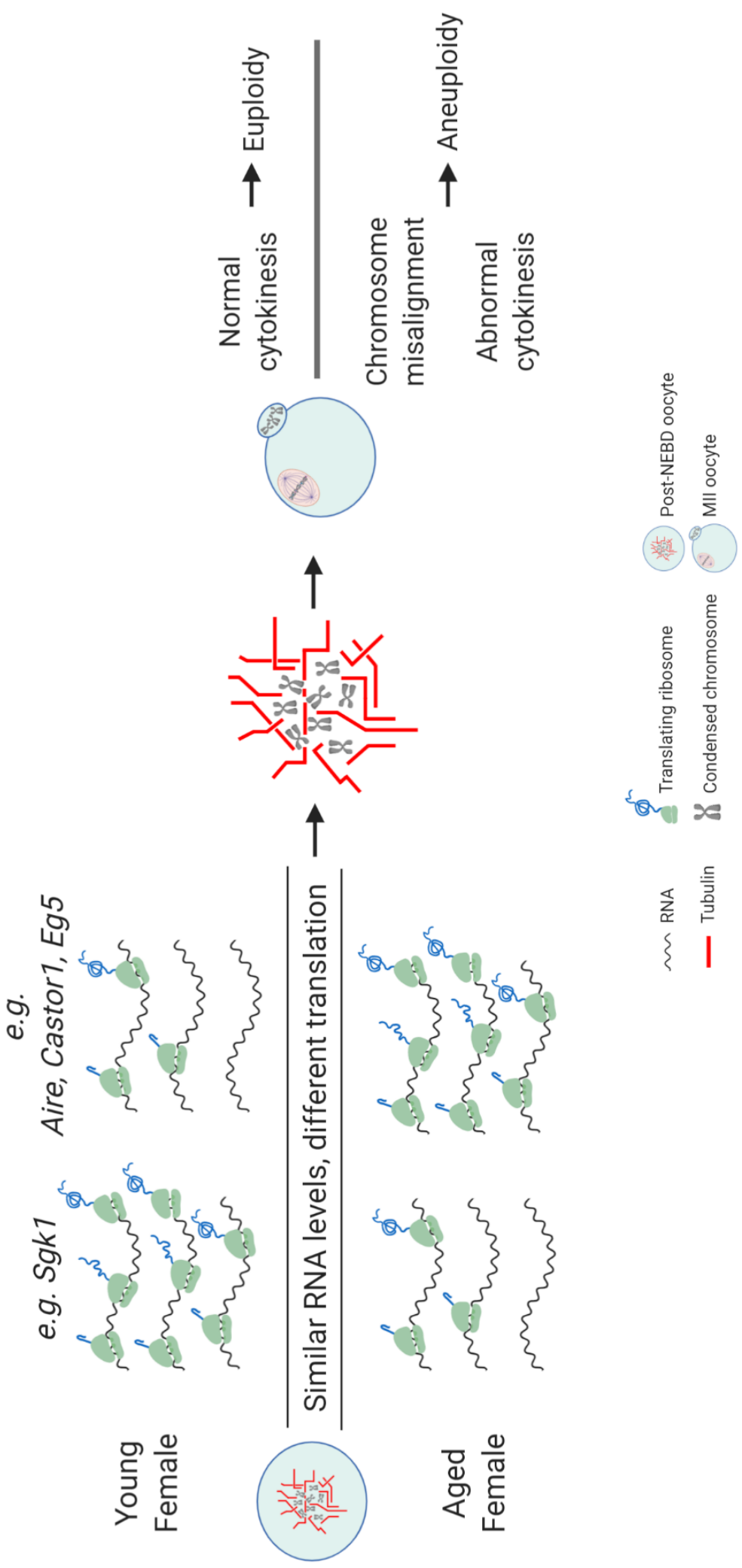


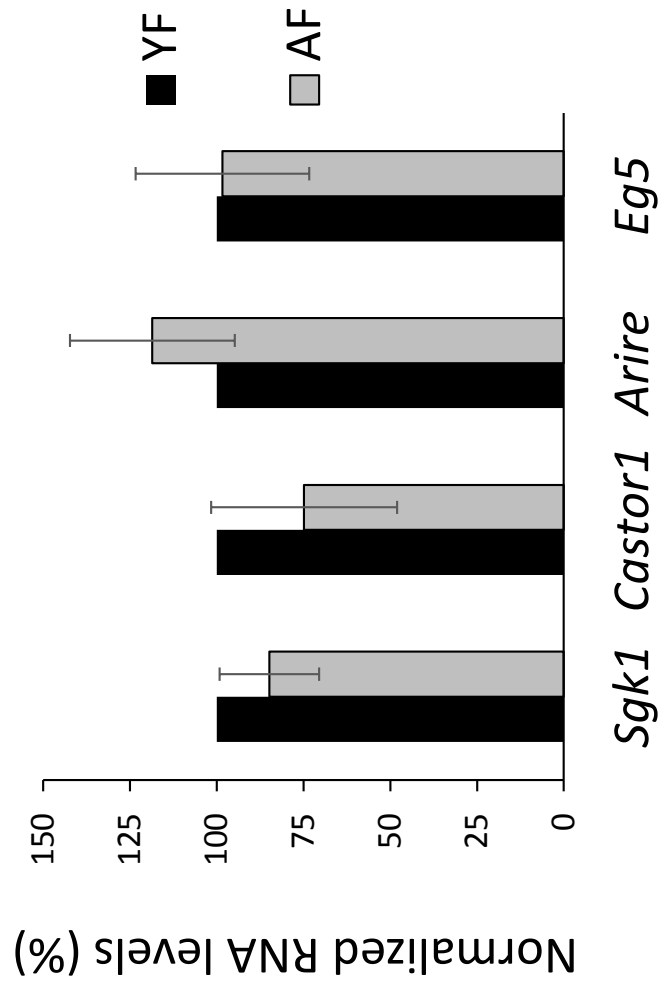
Fig. 5



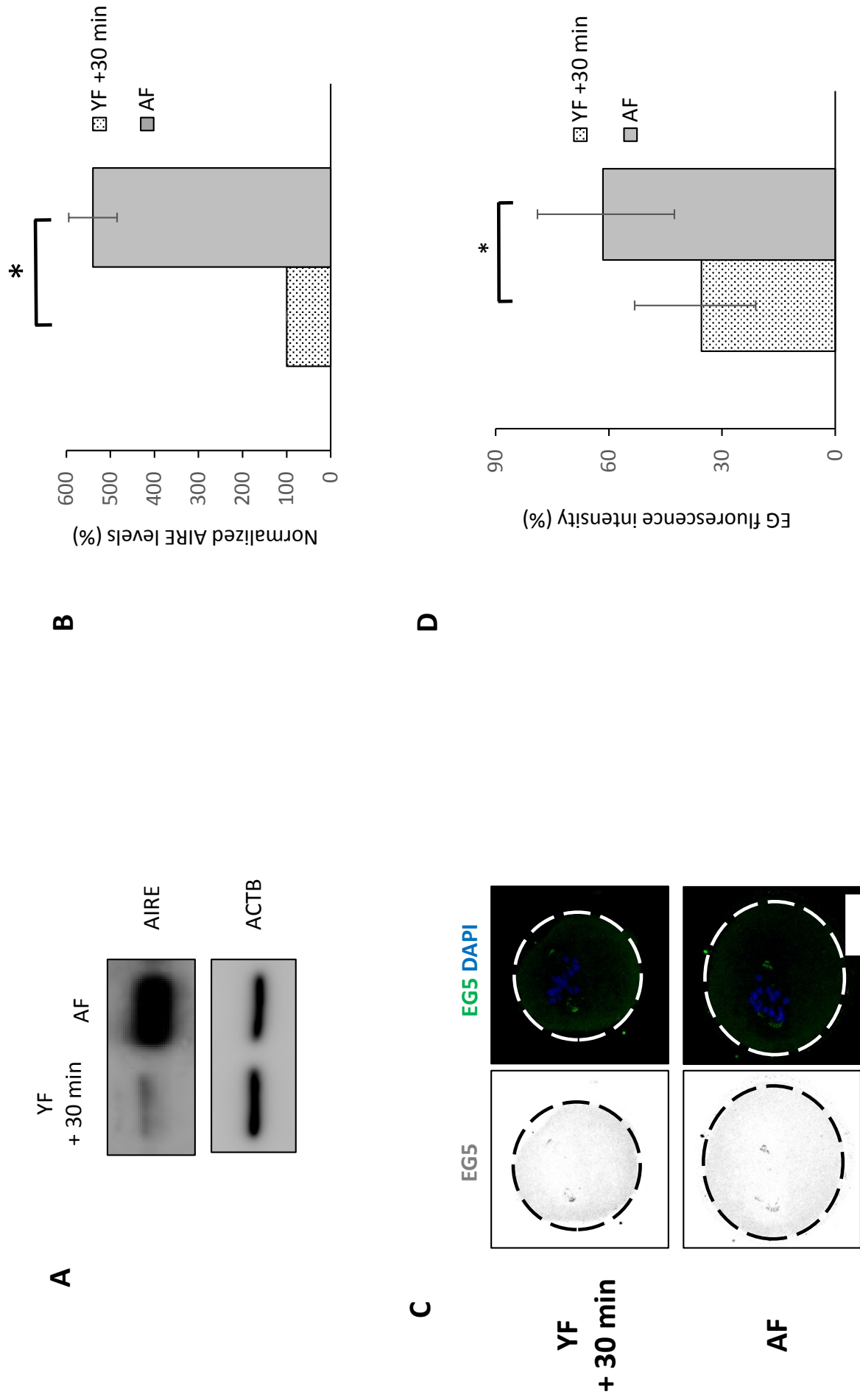




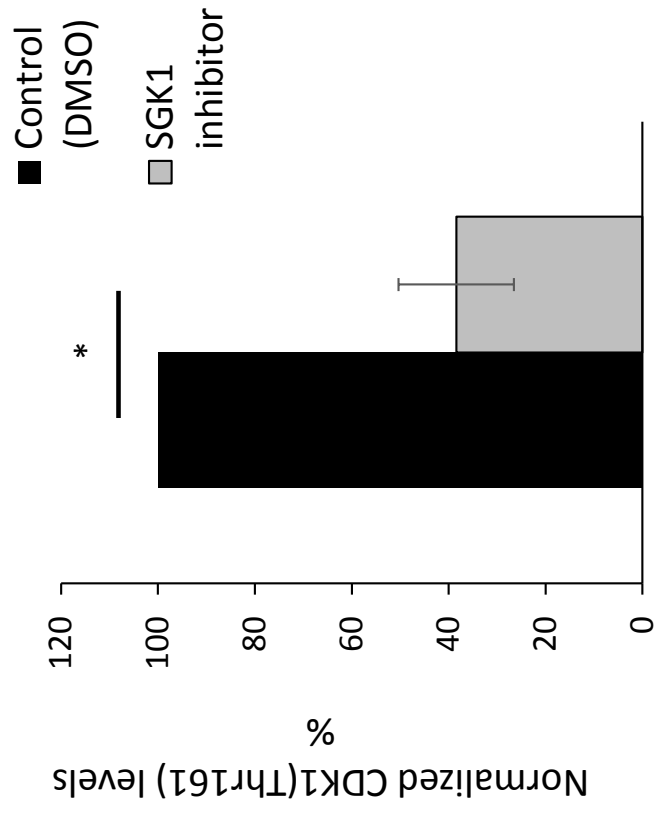
Supplementary Fig. 2



Supplementary Fig. 3



Supplementary Fig. 4



**Supplementary Table 1.** List of genes up/down regulated in AF compared to YF according to FC>5, FC>10 and FC>10 plus  $P<0.1$ .

**Supplementary Table 2.** List of genes in each Gene Ontology categories as seen in Fig. 1C.

**Supplementary Table 3.** List of genes from cluster 1,3,6,7 (increasing presence from YF-NP to YF-P, and vice versa in AF) and clusters 2,4,5 (increasing presence from increasing presence from AF-NP to AF-P, and vice versa in YF)(see Fig. S1).



**Supplementary Table 4.** Table of primers used for PCR (A) and (B) list of antibodies used for the study.

A

Primers		
Name	sequence	Accession num
18S-Forward	5'-CGCTCCACCAACTAAGAACG-3'	NR_003278
18S-Reverse	5'-CTCAACACGGGAAACCTCAC-3'	
28S-Forward	5'-CTAAATACCGCAGAGACC-3'	
28S-Reverse	5'-TTCACGCCCTTTGAACTCT-3'	
Sgk1-Forward	5'-GGTGCCAAGGATGACTTTATGG-3'	NM_001161845, NM_001161847, NM_001161848, NM_001161849, NM_001161850, NM_011361
Sgk1-Reverse	5'-GGATCGAAGTGCCGAAGGTC-3'	
Castor1-Forward	5'-AGTAACCAAGATTGCCCGGT-3'	NM_028022
Castor1-Reverse	5'-CCCGTACCAGGATGAAGTCTG-3'	
Aire-Forward	5'-ACTCTGCTAGTCACGACCCT-3'	NM_009646, NM_001271549, NM_001271551, NM_001271550, NM_001271552, NM_001271553, NM_001271554, NM_001271555, NM_001271556, NM_001271557, NM_001271558, NM_001271559, NR_073358
Aire-Reverse	5'-CTGCAGGATGCCGTCAAATG-3'	
Eg5-Forward	5'-ATGTGTCCGCTCGTGTCT-3'	
Eg5-Reverse	5'-GGTCGGTCACAAGTTCATCAATC-3'	
dsSgk1- Forward	5'- CTCATTCCAGACCGCTGACA- 3'	NM_001161845, NM_001161847, NM_001161848, NM_001161849, NM_001161850, NM_011361
dsSgk1- Reverse	5'- TTCCGGCTATAAAACGGGGG- 3'	

B

Antibodies		
Name and cat.#	Company	Experiment
SGK1 (H-4) - 28338	Santa Cruz Biotechnology	ICC
SGK1 - PA5-87746	Thermo Fisher Scientific	WB
GATSL3 (CASTOR1) (A-6) - 377114	Santa Cruz Biotechnology	ICC, WB
Aire 1 (C-2) - 373703	Santa Cruz Biotechnology	WB
AIRE Monoclonal Antibody (5H12), 14 5934 82	Thermo Fisher Scientific	ICC
EG5 (A-2) - 365593	Santa Cruz Biotechnology	ICC, WB
β Tubulin (9F3) - 2128	Cell Signalling Technology	ICC
HA-Tag(C29F4) - 3724	Cell Signalling Technology	ICC, WB
β Actin - 0061R	Biosusa	WB
Phospho-cdc2 (Thr161) - 9114	Cell Signalling Technology	WB